Title
A Spatiotemporal Study of Thymic Selection and Lineage Commitment

Author
Ross, Jenny Oriana

Publication Date
2013

Peer reviewed|Thesis/dissertation

A Spatiotemporal Study of Thymic Selection and Lineage Commitment

By

Jenny Oriana Ross

A dissertation submitted in the partial satisfaction of the

requirements for the degree of

Doctor of Philosophy

in

Molecular and Cell Biology

in the

Graduate Division

of the

University of California, Berkeley

Committee in charge:

Professor Ellen Robey, Chair
Professor Laurent Coscoy
Professor Daniel Fletcher
Professor David Raulet

Spring 2013

Abstract

A Spatiotemporal Study of Thymic Selection and Lineage Commitment

by

Jenny Oriana Ross

Doctor of Philosophy in Molecular and Cell Biology

University of California, Berkeley

Professor Ellen Robey, Chair

T cells are one of the main effectors of the adaptive immune response and as such, their development must be tightly regulated. Despite being well studied, the processes that produce mature T cells are not fully understood. The ultimate goal in T cell development biology is to understand the *in vivo* cues well enough to be able to recapitulate development *in vitro*. Such knowledge would unleash the therapeutic potential of stem cell biology. Although there are many gaps in our current knowledge, I have chosen to focus on two extreme ends of the developmental spectrum, from the earliest determinants in hematopoietic fate in human embryonic stem cells to the final processes of T cell development, positive and negative selection, which are ultimately responsible for the generation of a useful and self-tolerant T cell repertoire.

Although T cells can be derived *in vitro* from cord blood and fetal liver, a robust development from human embryonic stem cells into the T lineage has not yet been achieved *in vitro*. It's known that there are different developmental potentials among human embryonic stem cell lines. Therefore, we performed a comparison of the T lineage developmental potential of a panel of six independently derived human embryonic stem cell lines for their ability to differentiate into the known T lineage progenitors, CD34+ hemangioblasts or CD34+CD45+ hematopoietic precursors by embryoid body formation or OP9 co-cultures. Not only did we find indeed, there are differences in hematopoietic potentials among lines, but the passage conditions through which the stem cell lines were maintained also dramatically affected hematopoietic potential. None of the stem cell-derived progenitors could develop into T cells, unlike those found in cord blood. Differences between individual lines should allow for the future study of genetic or epigenetic factors that determine lineage commitment as a cell transitions from a stem cell to a T cell.

Second, I focused on the final stages of T cell development, specifically, the processes of positive and negative selection. Most of our current understanding of signaling behavior comes from *in vitro* studies that fail to fully recapitulate thymic selection events. Therefore, we expanded upon a relatively new model of selection, the thymic slice system, which supports positive selection and can be used to introduce a synchronized population of thymocytes. By adding a cognate peptide antigen or overlaying slices with peptide-loaded DCs, we were able to induce negative selection. Using the thymic slice system, we visualized the migration and

signaling behavior of thymocytes undergoing positive versus negative selection. Additionally, we characterized the effect of the affinity of the peptide-TCR interaction on migration, signaling, and developmental outcome. We found that thymocytes undergoing positive selection formed transient, serial interactions that lasted only a few minutes while thymocytes undergoing negative selection formed long lasting, monogamous contacts. The APC type plays an important role in selection outcome as dendritic cells and not epithelial cell cells presenting OVA most efficiently promoted negative selection and sustained calcium levels. Co-stimulatory and adhesion molecules did not appear to be required for selection outcome but contributed to sustained calcium signaling during negative selection and may therefore play a role in determining the threshold of affinity. We also found that thymocytes undergoing positive selection accumulate TCR signals over time, increase their speed, and appear to change their responsiveness to a TCR-induced stop signal over time.

Table of Contents

List of Figures

Acknowledgements

First and foremost, I would like to thank my mentor, Ellen Robey for all of her help and support throughout my graduate career. I would also like to thank the members of the Robey lab, both past and present. I would especially like to recognize Heather Melichar, who I worked with side-by-side in all the studies presented in this thesis. I also want to thank her for being an amazing friend, system of support, co-worker, mentor, and someone that I admire scientifically. I truly would not have survived graduate school without her.

Special thanks to my family and friends (both in and outside of graduate school), especially my parents for all of their love and support throughout the years as well as for being excellent role models in dedication and having the courage to follow your dreams.

Last but not least, I would also like to thank my committee for all of their support and guidance.

Chapter 1: Introduction

T and B cells are the main effectors of the adaptive immune system, and are responsible for clearing a wide variety of pathogens and infected or altered-self cells. A thorough understanding of their developmental process is important for several reasons. Hematopoiesis itself is an excellent model system for studying how cells make fate decisions and undergo lineage commitment, a question that is critically important to animal biology. Additionally, by understanding how these processes are dysregulated in disease allows for the better design therapeutic treatments. Finally, only once we understand the mechanism of development *in vivo* can we recapitulate them *in vitro.* With the development of stem cell technologies, understanding the entire T cell developmental program will allow us to generate tailored T cells that can potentially be used to treat any number of diseases from cancer to autoimmunity.

1.1 Hematopoiesis

All blood cells (including T cells) are derived from the hematopoietic stem cell (HSC). HSCs are rare, self-renewing, cells that are capable of multi-lineage differentiation (Figure 1.1). During ontogeny, the location of development changes. At first, stem cells develop in the yolk sac and ventral wall of dorsal aorta. In humans, they then move to fetal liver and spleen where they reside for the 6^{th} to the 22^{nd} weeks of gestation and ultimately home to the bone marrow where they are maintained for the remaining life of the individual (Tavian). Because of the high turnover of mature blood cells, HSCs continuously provide progenitors for differentiation to the required lineage while simultaneously self-renewing, thereby maintaining the stem cell population as well as meeting the demands of an ever-changing peripheral blood system. Progenitors destined to become T cells, must migrate to the thymus where they undergo a complex developmental program as they transition from lymphoid progenitor to a T cell progenitor, and finally an immature T cell that will be subject to the positive and negative selection processes.

The concept of "stem cell" was first proposed by Till and McCulloch during their investigations of regeneration of the blood system (Becker, Siminovitch, Till, Wu). Since then, the stem cell field has vastly expanded, including the discovery of embryonic stem cells (ESCs) that can give rise to any cell within the body (Martin, Evans). Because of their potential for self-renewal and total plasticity, ES cell therapies have been proposed as a form of regenerative medicine. Recently, with the advent of induced pluripotent stem cells (iPSCs) (Takahashi), stem cells can be derived from each patient, thereby providing a perfect immunological match, making stem cells an even more promising therapy. Indeed, it is now a goal to be able to differentiate stem cells into particular lineages relevant to the treatment of disease, such as T cells. Therefore, the establishment of robust *in vitro* systems of T cell development will be important going forward, and is the subject of the second chapter of this thesis.

Mouse embryonic stem cells can be directed to the T cell lineage *in vitro* (Schmitt). Human ES cells can become blood lineage cells *in vitro* as well (Kaufman), but, differentiation into the T cell lineage has proven to be more challenging, with the exception of one report of low efficiency conversion (Timmermans). The T lineage cells that are produced *in vitro* must be further differentiated if the ultimate goal is to develop mature T cells for therapeutic purposes.

Currently, the low efficiency of T lineage generation coupled with the fact that no *in vitro* system fully recapitulates the selection processes of the thymus presents a roadblock in the development of this potential therapeutic. As such, we must perform further characterization of stem cell lines, as it is possible that other independently derived human ES cells have reduced or enhanced hematopoietic potential. Ultimately though, we need to turn to *in vivo* systems to further our understanding of development of the later stages of T cell development within the thymus.

1.2 Selection and Lineage Commitment

Immature precursors destined to become T cells enter the thymus where they proliferate and rearrange antigen receptors (T cell receptor or TCR). Following expression of the newly rearranged receptor, they are positively selected to progress towards mature T cells if their TCR recognizes a self-peptide presented by a major histocompatibility complex (MHC). Thymocytes are concurrently screened for potential auto-reactivity, and if their TCR recognizes self-MHC with sufficient avidity, they are deleted. Ultimately, it is the processes of positive and negative selection that are responsible for shaping the repertoire of functional, self-tolerant T cells that will emerge from the thymus.

Progression through developmental stages from immature to a positively selected thymocyte is marked by changes in the expression of cell surface markers. Initially, thymocytes do not express either CD4 or CD8 and are known to be double negative (DN). As they move through the thymus and the respective developmental stages they express both CD4 and CD8 as double positive (DP) cells. DP thymocytes interact with the MHC on the cortical thymic epithelial cells (TECs) and either fail to interact with an MHC and die by neglect or they are able to interact with MHC and become single positive (SP) cells (CD8+CD4- or CD8-CD4+) in a process called positive selection (Figure 1.2). Those thymocytes that are positively selected undergo a lineage commitment to become either CD4 SP or CD8SP. One of the current models predicts that this decision is dependent on the strength of the signal through the TCR, with higher affinity interactions leading to CD4 SP development and weaker affinity interactions leading to CD8 SP development (Figure 1.3).

Development must be tightly regulated to ensure specificity against foreign invaders to clear infections while at the same time being tolerant to self to prevent autoimmunity. Thus, those thymocytes with a self-reactive TCR are also eliminated in the thymus during a process known as negative selection. Though negative selection is usually thought to act on the SP population, thymocytes with auto-reactive TCRs can be screened during several stages of development. First, at the DP stage within the cortex, and second at the SP stage post positive selection within the medulla. The type and avidity of self-antigen, type of APC (including TECs, DCs, and even other thymocytes), and general extracellular milieu can all potentially contribute to the developmental stage at which thymocytes are deleted. For example, ubiquitous self-antigens can promote deletion in the cortex. (McCaughtry, Baldwin, Stritesky, Daley).

The currently favored model for positive and negative selection is based on affinity of TCR for peptide/MHC. While the K_d for the peptide-MHC interaction can itself govern this decision, other factors that contribute to the avidity such as receptor level and presence or absence of co-stimulatory and adhesion molecules all potentially affect the strength of the signal delivered

(Figure 1.4). According to this model, positive selection is achieved through low avidity interactions while high avidity interactions result in negative selection (Reviewed, Palmer and Naeher, 2009). In this way, a threshold of signaling would determine the fate of the thymocyte (Hogquist, Daniels). However, it is still largely unknown how TCR induced stop signals, duration of contact with the antigen presenting cell (APC), and the kinetics of TCR signaling affect selection outcomes within the relevant environment.

1.3 TCR induced Stop Signals

In order to test its TCR, a thymocyte must contact MHC-bearing stromal cells within the thymus. From imaging studies on intact thymus, we know that thymocytes are highly motile throughout development (Figure 1.5). This forces us to consider how TCR signaling events are occurring *in vivo* as, for selection and lineage commitment, there needs to be intercellular contact and signaling. In mature T cells, binding to antigen presented by MHC on an APC results in stable interactions and TCR signaling that leads to the reorientation of T cell polarity, increased adhesiveness, and the formation of the immunological synapse, which results in the arrest of T cell motility (Dustin). Recently, T cells have also been found to integrate signaling information while migrating over an APC, a type of interaction coined by Dustin as "kinapse" for moving synapse. Such dynamic, transient interactions can occur while a T cell is in contact with one or multiple APCs (Friedl). These interactions lack stability and are usually maintained for a period of minutes as opposed to hours during synapse formation. Despite their instability and short duration, kinapses can result in a functional signaling event as short lived, dynamic interactions of naïve T cells exposed to their antigen presented by DCs within a collagen matrix trigger calcium influx, up-regulate activation markers, and proliferate (Gunzer, 2000). Although the *in vivo* role of synapses versus kinapse formation is currently unknown, it seems likely that triggering of the TCR and sustained signaling of a T cell may depend upon the nature of the interaction it experiences (Dustin). Thus, it seems likely that stable versus dynamic contacts could induce distinct developmental outcomes such as positive and negative selection. We would predict that stable interactions associated with synapse formation should promote sustained signaling and negative selection while transient, kinapse-type interactions might typify positive selection.

In 1996, Negulescu et. al. found that for T cell hybridomas, antigen recognition led to an intracellular calcium spike that was both necessary and sufficient to arrest migration. This calcium dependent stopping downstream the TCR signaling was later confirmed in naïve T cells responding to antigen in the lymph nodes (Skokos). Further studies by Bhakta et. al. demonstrated that, as is the case for mature T cells, rises in intracellular calcium were also necessary and sufficient to arrest motility of positively selecting thymocytes. Thus T cell motility and TCR signaling are inter-related and the dynamics of interactions with APCs likely helps to tune TCR signaling and determine the ultimate outcome of antigen recognition. Indeed, in mature T cells, the oscillation frequency of a calcium signal has been linked to the activation of distinct transcriptional programs (Lewis, Dolmetsch). Therefore, it is reasonable to think that differences selection and lineage commitment events may be reflected in calcium signaling and motility and ultimately, it remains to be shown how various types of intercellular interactions result in selection decisions or how thymocytes may be changing over time.

1.4 Chemokines, Adhesion Molecules, and Co-stimulatory Molecules

Chemokines and adhesion molecules direct the movement and activity of immune cells. Thymocytes bind to epithelial cells through LFA-1/ICAM-1 interactions (Lepesant, 1990). Additionally, LFA-1 is required for the recruitment and exclusion of various proteins to establish the SMACs associated with immunological synapse where it may enhance TCR signaling in mature T cells (Graf, 2007). In mature T cells, TCR signaling activates integrins, such as LFA-1, which increases adhesion strength (Ponti, 2004). The integrin, LFA-1, has also been shown to be important in negative selection, as treatment with a blocking antibody to LFA-1 results in an inability of antigen presenting cells (APCs) to eliminate antigen-specific thymocytes (Carlow, 1992). Treatment with LFA-1 antibody also interferes with positive selection (Revilla, 1997). However, while the LFA-1 deficient mouse has a defect in T cell activation no thymic developmental deficiency has been noted (Scharffetter-Kochanek). In addition to adhesion molecules, the small chemotaxic proteins known as chemokines can alter lymphocyte motility and activation. Specifically, the chemokines CCL19 and CCL21 that bind to the CCR7 receptor on T cells are capable of arresting thymocytes and sensitizing them to TCR signaling, essentially "priming" them for synapse formation (Friedman, 2006). Additionally, in mature T cells, gradients of CCR7 but not CXCR4 had an immunosuppressive function by preventing the formation of a synapse, thereby affecting activation (Bromley). Finally, a differential localization of chemokines within the thymus may lead to directed migration. The chemokine receptor CCR7 is expressed on SP thymocytes and is up-regulated on a subset of DP cells (Campbell, 1999, Yin, 2007) while the chemokine receptor CXCR4's ligand (CXCL12) is expressed in the outer cortex of the thymus. Chemokines such as CCRL ligands may direct migration of positively selected thymocytes from the cortex to the medulla where interactions with mTECs promote further screening for negative selection (Reviewed, Norment, 2000).

Another potential contributing factor to the selection of thymocytes is the presence or absence of co-stimulatory molecules on the APC. While the important activating role of the co-stimulatory B7 molecules is well defined for peripheral T cells, their role in selection of thymocytes remains unclear. Conflicting studies claim a role in positive selection (Vacchio), and negative selection (Buhlmann, Williams, Lucas, Amsen, Kishimoto) while others claim that loss of co-stimulation has no effect on selection (Walunas, Page, Jones, Tan). The et. al. and Aoki et. al. are likely correct in that co-stimulatory signals through the B7/CD28 interaction may tune TCR signaling and thus, it is possible that the dependency of selection on these molecules may be determined by the affinity of the TCR or concentration of antigen.

It is well known that intercellular contacts and the resulting downstream signaling are crucial for both thymocyte development and T cell function, it remains to be shown how different types of cell-cell interactions result in selection decisions. Additionally, it is unclear how a difference in the dynamics and quality of peptide-MHC recognition that induces positive selection differs from negative selection within the native, spatiotemporal context of the thymus. It seems likely that the spatial and temporal dynamics of migration and signaling as well as the overall intensity of TCR signaling are crucial factors in the outcome of selection and lineage commitment events where frequent and/or longer duration of signaling will correspond with stable interactions established during synapse formation, resulting in negative selection of thymocytes while a less stable, transient interaction via kinapse formation results in positive selection due to a shorter,

less frequent signals. Additionally, these types of interactions may be mediated by changes in chemokines and adhesion. Understanding the spatial and temporal relationships of a developing thymocyte within its 3D microenvironment will inform us about the dynamics of thymocyte interactions and further our understanding of T cell development.

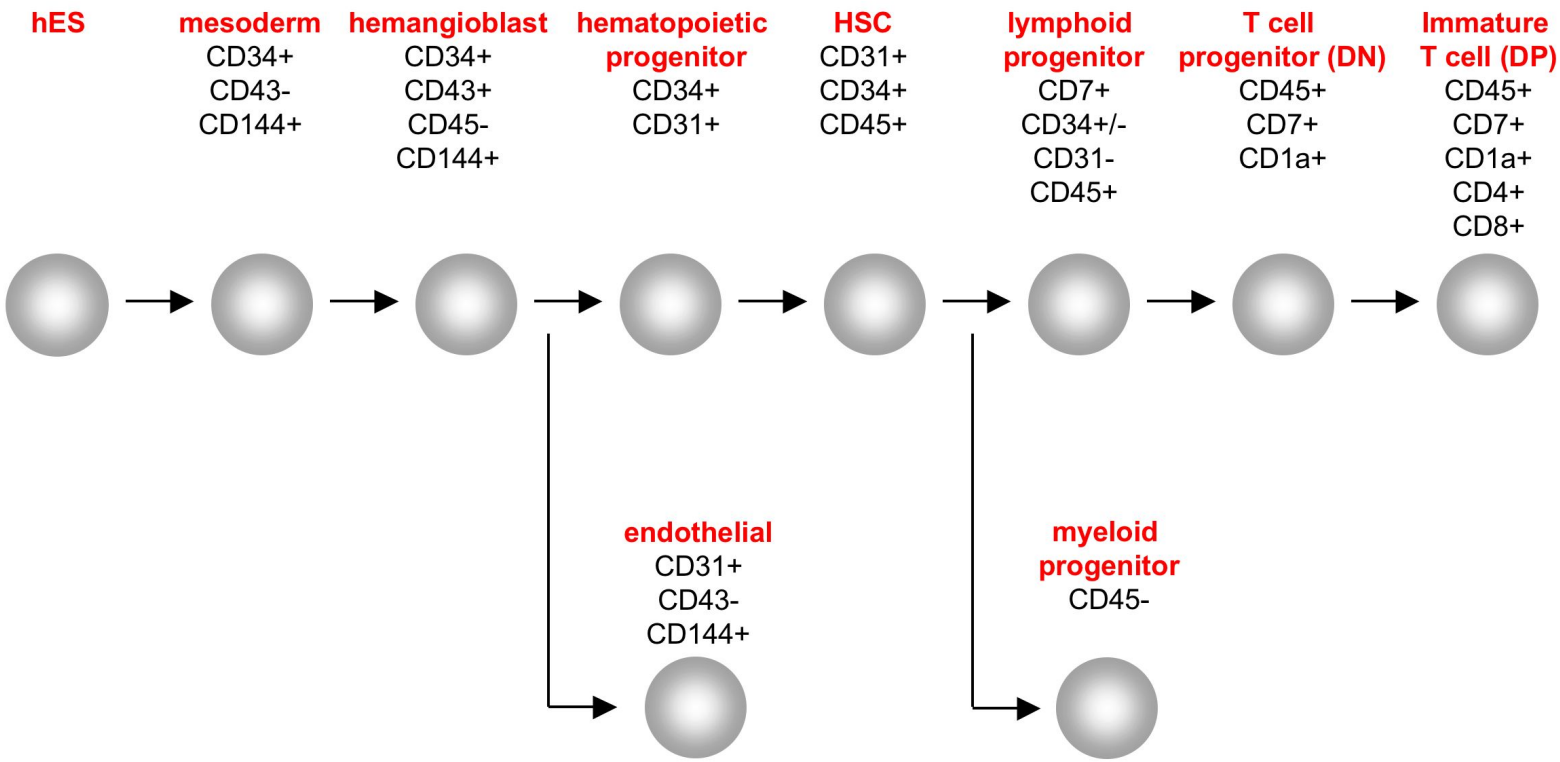
hES
mesoderm
CD34+
CD43-
CD144+
hemangioblast
CD34+
CD43+
CD45-
CD144+
hematopoietic progenitor
CD34+
CD31+
HSC
CD31+
CD34+
CD45+
lymphoid progenitor
CD7+
CD34+/-
CD31-
CD45+
T cell progenitor (DN)
CD45+
CD7+
CD1a+
Immature T cell (DP)
CD45+
CD7+
CD1a+
CD4+
CD8+
endothelial
CD31+
CD43-
CD144+
myeloid progenitor
CD45-

Figure 1.1 Hematopoiesis. The developmental stages from human embryonic stem cell to cells of the T lineage. The developmental intermediate is listed in red above each cell, with known surface marker expression just below in black. Markers listed are used to distinguish hematopoietic intermediates in chapter 2.

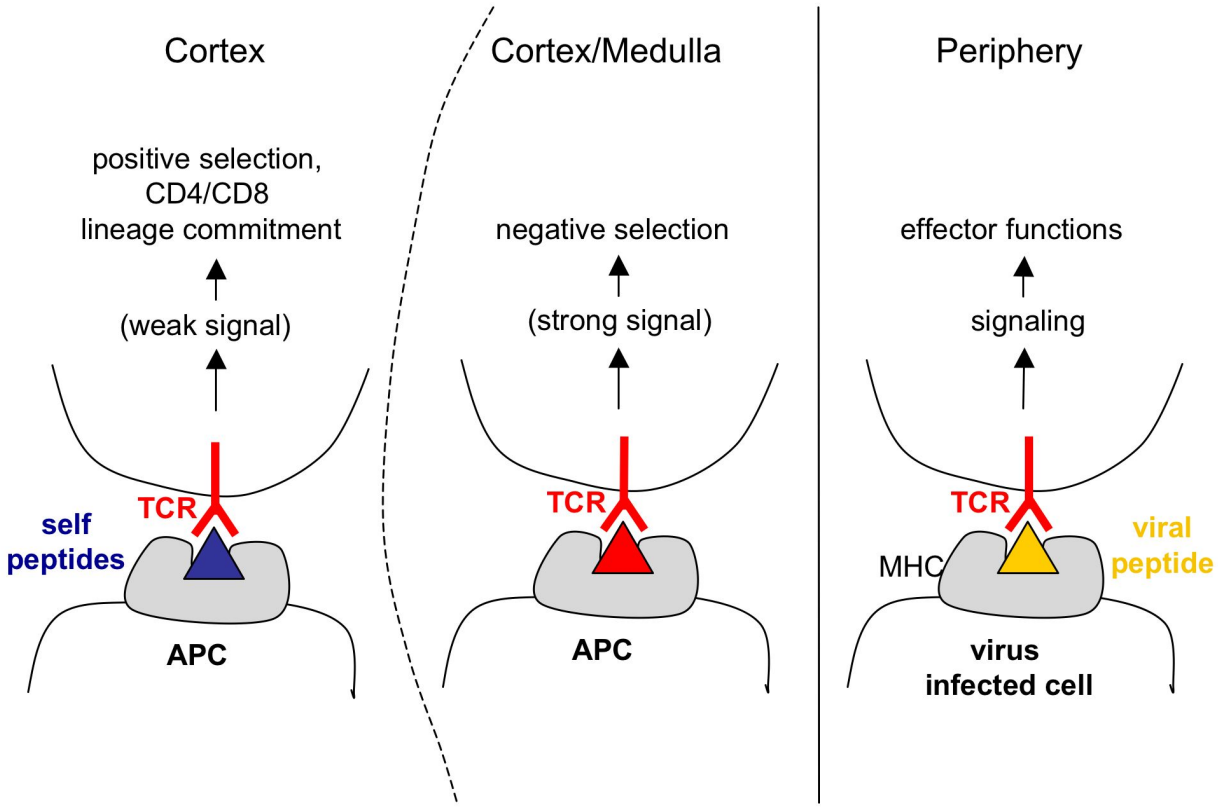
Cortex
Cortex/Medulla
Periphery
positive selection,
CD4/CD8
lineage commitment
(weak signal)
negative selection
(strong signal)
effector functions
signaling
TCR
TCR
TCR
self
peptides
MHC
viral
peptide
APC
APC
virus
infected cell

Figure 1.2 TCR interaction with self-MHC is required for selection. In the periphery, in order to be effective, a T cell must its cognate peptide antigen in the context of self-MHC. During development, individual TCRs are screened for usefulness by testing for their ability to recognize self-MHC. Specifically, those thymocytes that pass this functional test are selected for survival (positive selection), while those that do not are eliminated by death by neglect. The surviving thymocytes must be further screened to eliminate those TCRs that react too strongly with self-MHC and would therefore be auto-reactive. These cells die by the process of negative selection, thereby ensuring that a functional yet self-tolerant T cell repertoire is exported to the periphery.

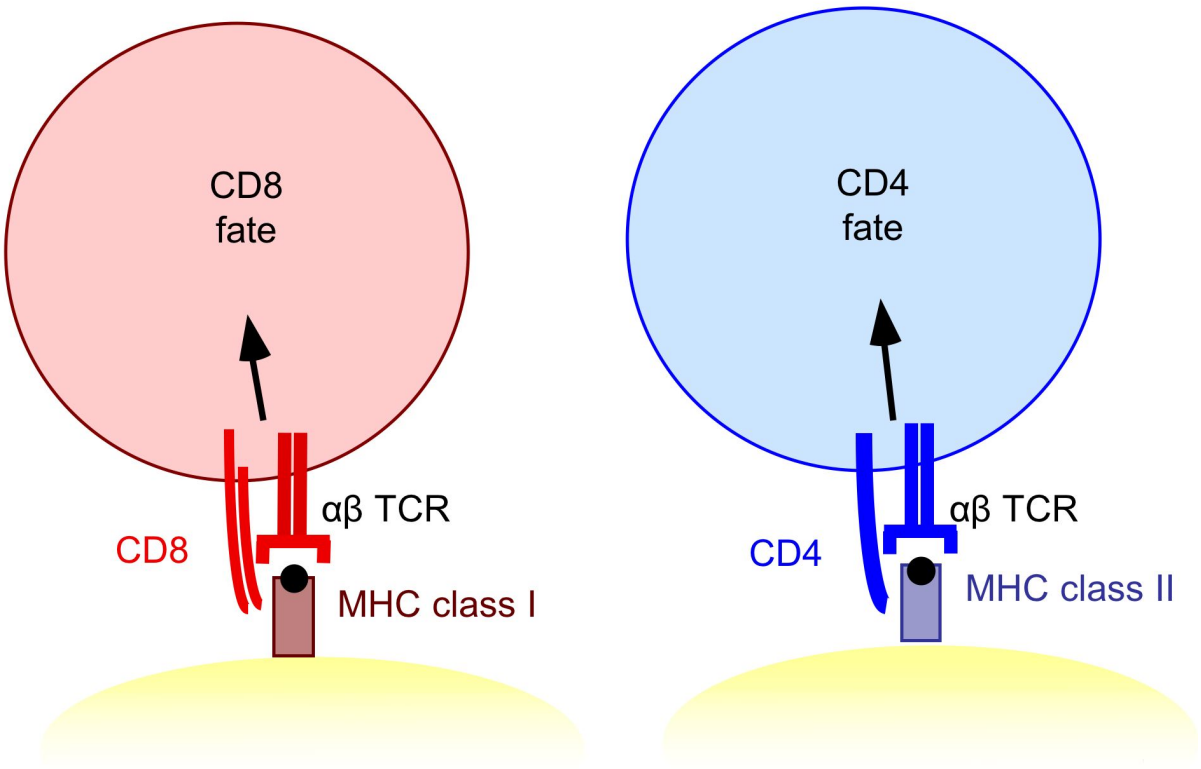

APC

Class I TCR transgenics
used in this study:

F5
OTI

Class II TCR transgenics
used in this study:

AND
OTII

Figure 1.3 Signaling through the TCR and co-receptors influences the lineage choice of precursor T cells in the thymus. Developing CD 8 T cells recognize peptide presented by class I MHC and this interaction involves signaling through the αβ TCR as well as the CD8 co-receptor (left). Similarly, developing CD4 T cells must recognize peptide presented by class II MHC via the αβ TCR and CD4 co-receptor (right). The TCR transgenics used in this study are F5 and OTI for class I, and AND and OTII for class II.

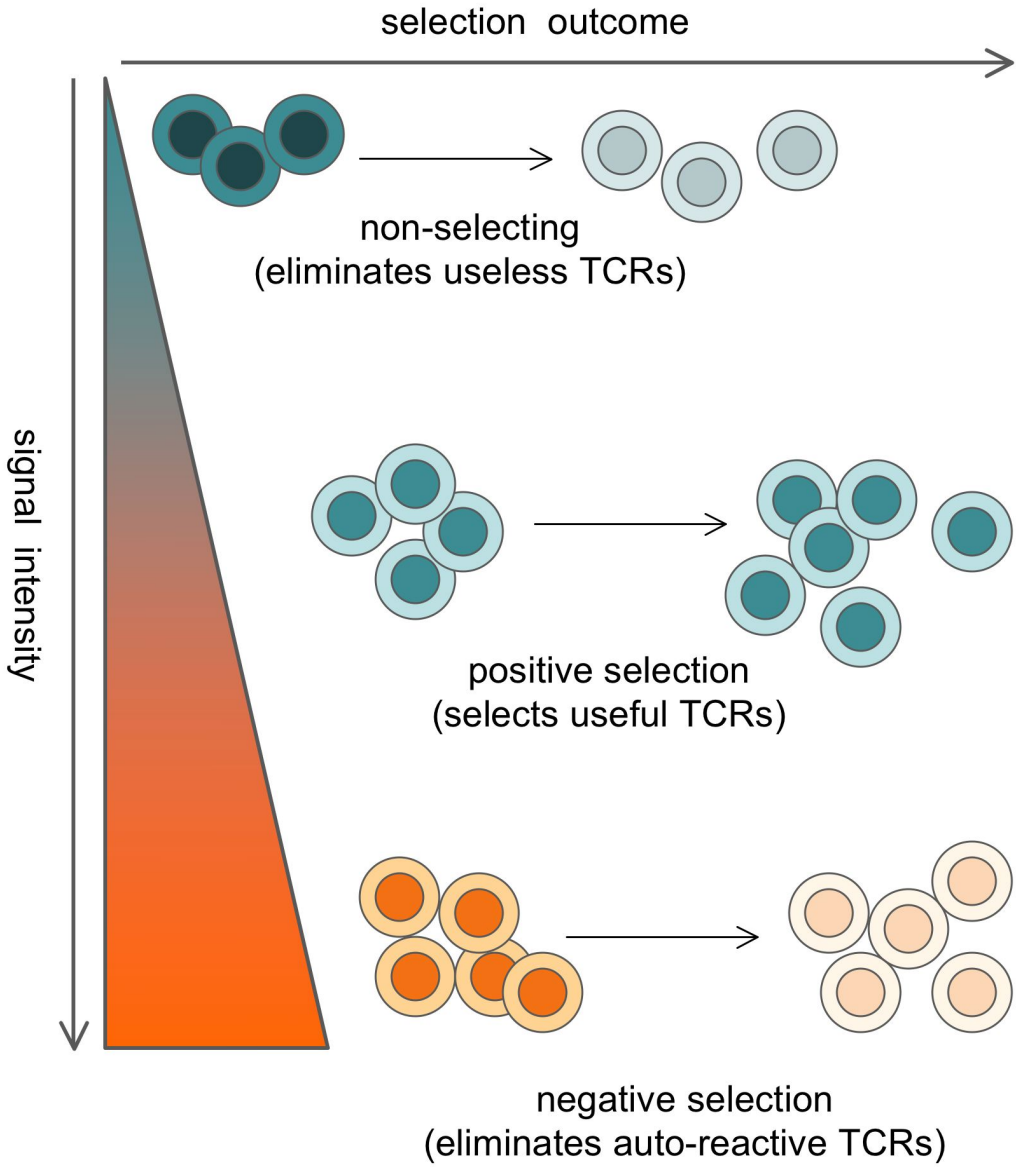
selection outcome
signal intensity
non-selecting
(eliminates useless TCRs)
positive selection
(selects useful TCRs)
negative selection
(eliminates auto-reactive TCRs)

Figure 1.4 Affinity model of selection. The affinity model of selection is based on the idea that the strength of the TCR interaction with peptide-MHC is the main determinant of T cell selection. Specifically, those thymocytes with low or no affinity for self-MHC die by neglect. Of those thymocytes that are able to interact self-MHC, there can be two fates. Intermediate affinity binding leads to positive selection in the form of a survival signal while high affinity binding leads to negative selection as a cell is induced to die by apoptosis. It is important to note that the affinity is not solely responsible for selection outcome as there are other factors that can contribute to the overall avidity of peptide/MHC interaction. These other factors include, but are not limited to the presence or absence of co-stimulatory and adhesion molecules, cytokines, chemokines, and the level of TCR expression.

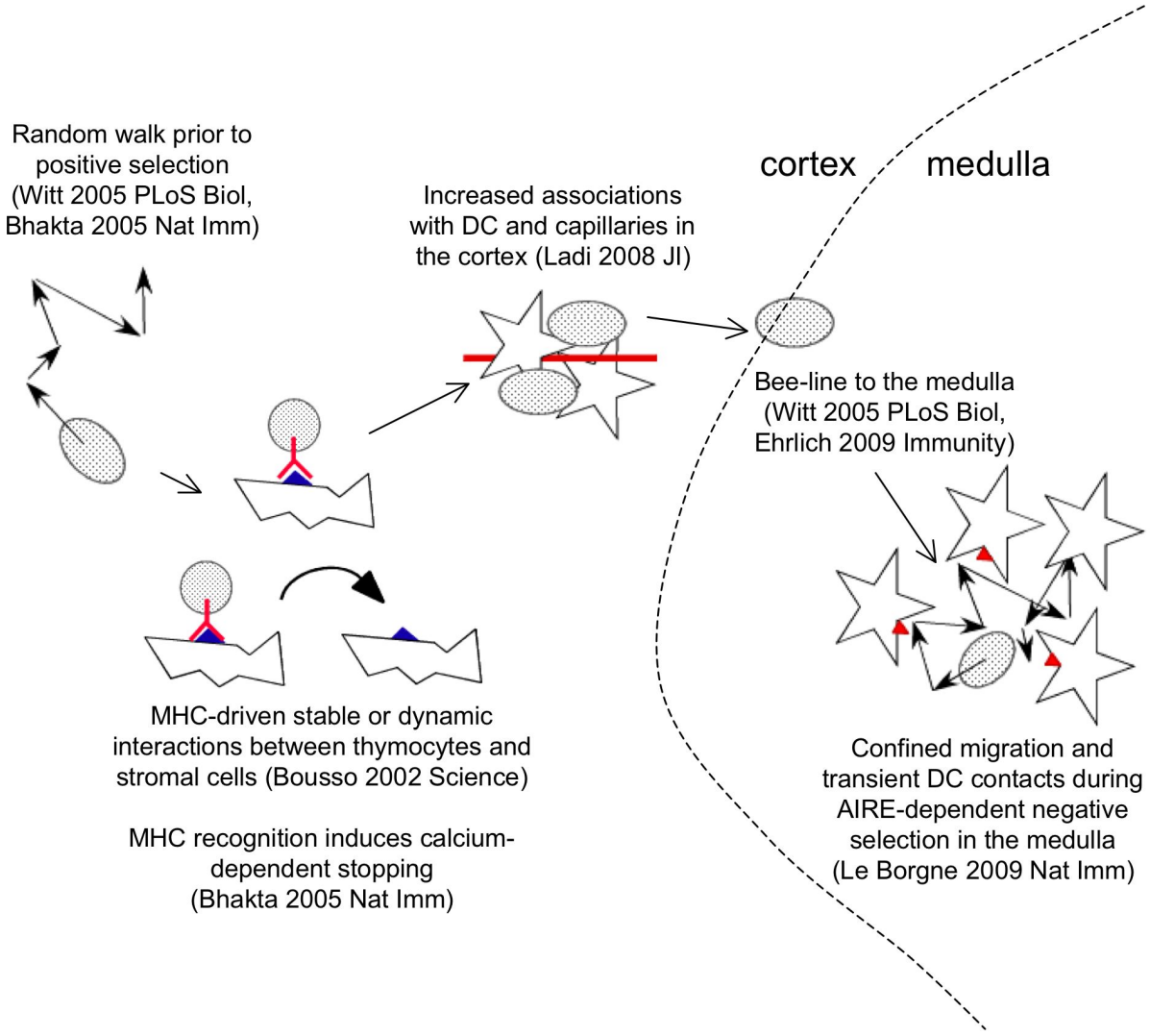
Random walk prior to positive selection (Witt 2005 PLoS Biol, Bhakta 2005 Nat Imm)
Increased associations with DC and capillaries in the cortex (Ladi 2008 JI)
cortex
medulla
Bee-line to the medulla (Witt 2005 PLoS Biol, Ehrlich 2009 Immunity)
MHC-driven stable or dynamic interactions between thymocytes and stromal cells (Bousso 2002 Science)
MHC recognition induces calcium-dependent stopping (Bhakta 2005 Nat Imm)
Confined migration and transient DC contacts during AIRE-dependent negative selection in the medulla (Le Borgne 2009 Nat Imm)

Figure 1.5 Thymocyte migration and cellular interactions during selection in the thymus. Two-photon imaging experiments have revealed the dynamic nature of thymocyte behavior during development. Prior to positive selection, thymocytes migrate slowly via random walk in the cortex (Witt). Recognition of positively selecting ligand leads to stable or dynamic interaction with thymic stromal cells (Bousso) with stopping being calcium dependent (Bhakta). There is also an increased association of thymocytes with capillaries and DCs in the cortex. Thymocytes increase their speed, and begin migration toward the medulla (Witt, Ehrlich). Ultimately, thymocytes undergo rapid migration in the medulla and confined migration with transient DC contacts during AIRE-dependent negative selection within the medulla (LeBorgne).

1.5 References

Amsen D, Kruisbeek AM. CD28-B7 interactions function to co-stimulate clonal deletion of double-positive thymocytes. Int Immunol. 1996 Dec;8(12):1927-36.

Aoki N, Inobe M, Murakami M, Abe R, Iizuka H. The functional role of B7 molecules on the induction of thymocyte activation and apoptosis. Microbiol Immunol. 1998;42(8):555-65.

Bachmann, M., McKall-Faienza, K., Schmits, R., Bouchard, D., Beach, J., Speiser, D., Mak, T., Ohasi, P. 1997. Distinct roles for LFA-1 and CD28 during activation of naive T cells: adhesion versus costimulation. Immunity. 7(4): 549-57.

Baldwin, T.A., Sandau, M.M., Jameson, S.C. & Hogquist, K.A. The timing of TCR alpha expression critically influences T cell development and selection. The Journal of experimental medicine 202, 111-121 (2005).

Becker AJ, Mc CE, Till JE. Cytological demonstration of the clonal nature of spleen colonies derived from transplanted mouse marrow cells. Nature. 1963;197:452–454.

Bhakta NR, Oh DY, Lewis RS. Nat Immunol. 2005 Calcium oscillations regulate thymocyte motility during positive selection in the three-dimensional thymic environment. Feb;6(2):143-51. Epub 2005 Jan 16.

Bousso, P., Bhakta, N., Lewis, R., Robey, E. 2002. Dynamics of Thymocyte-Stromal Cell Interactions Visualized by Two-Photon Microscopy. Science 296: 1876-1880.

Bromley SK, Peterson DA, Gunn MD, Dustin ML. 2000 Cutting edge: hierarchy of chemokine receptor and TCR signals regulating T cell migration and proliferation. J Immunol. Jul 1;165(1):15-9.

Buhlmann JE, Elkin SK, Sharpe AH. A role for the B7-1/B7-2:CD28/CTLA-4 pathway during negative selection. J Immunol. 2003 Jun 1;170(11):5421-8.

Campbell, J.J., J. Pan, and E.C. Butcher. 1999. Cutting edge: developmental switches in chemokine responses during T cell maturation. J. Immunol. 163: 2353–2357.

Carlow, D., Van Oers, N., Teh, S., Teh, H. 1992. Deletion of Antigen-Specific Immature Thymocytes by Dendritic Cells Requires LFA-1/ICAM Interactions. J. Immunol, 148: 1595-1603.

Daley, S.R., Hu, D.Y. & Goodnow, C.C. Helios marks strongly autoreactive CD4+ T cells in two major waves of thymic deletion distinguished by induction of PD-1 or NF-kappaB. The Journal of experimental medicine 210, 269-285 (2013)

Dolmetsch RE, Xu K, Lewis RS. Calcium oscillations increase the efficiency and specificity of gene expression. Nature 1998;392:933–6.

Dustin, M. 2008. T-cell Activation through Immunological Synapses and Kinapses. Immunol Reviews. 221: 77-89.

Dustin, M. Visualization of cell-cell interaction contacts-synapses and kinapses. Adv Exp Med Biol. 2008;640:164-82.

Dustin ML, Bromley SK, Kan Z, Peterson DA, Unanue ER. 1997. Antigen receptor engagement delivers a stop signal to migrating T lymphocytes. Proc. Natl. Acad. Sci. USA 94:3909–13

Evans M, Kaufman M. Establishment in culture of pluripotent cells from mouse embryos. Nature 292 (5819): 154–6. (1981).

Friedl P, Bröcker EB. TCR triggering on the move: diversity of T-cell interactions with antigen-presenting cells. Immunol Rev. 2002 Aug;186:83-9.

Friedman, R., Jacobelli, J., Krummel, M. 2006. Surface-bound Chemokines Capture and Prime T Cells for Synapse Formation. Nat. Immunol. 7: 1101-1108.

Graf, B., Bushnell, T., Miller, J. 2007. LFA-1 Mediated T Cell Costimulation through Increased Localization of TCR/Class II Complexes to the Central Supramolecular Activation Cluster and Exclusion of CD45 from the Immunological Synapse. J. Immunol. 179: 1616-1624

Gunzer, M., Schafer, A., Borgmann, S., Grabbe, S., Zanker, K., Brocker, EB., Kampgen, E., Friedl, P. 2000. Antigen Presentaation in Extracellular Matrix: Interactions of T Cells with Dendritic Cells are Dynamic, Short Lived, and Sequential. Immunity, 13: 323-332.

Hailman, E., Burack, R., Shaw, A., Dustin, M., Allen, P. 2002. Immature CD4+CD8+ Thymocytes Form a Multifocal Immunological Synapse with Sustained Tyrosine Phosphorylation. Immunity 16: 839-848.

Hailman, E and Allen, P. 2002. Inefficient Cell Spreading and Cytoskeletal Polarization by CD4+CD8+ Thymocytes: Regulation by the Thymic Environment. J. Immunol, 175: 4847–4857.

He, X., He, X., Dave, V., Zhang, Y., Hua, X., Nicolas, E., Xu W., Roe, B., Kappes, D. 2005. The Zinc Finger Transcription Factor Th-POK Regulates CD4 vs CD8 T-cell Lineage Commitment. Nature, 433: 826-833.

Hogquist KA, Tomlinson AJ, Kieper WC, McGargill MA, Hart MC, Naylor S, Jameson SC. (1997) Identification of a naturally occurring ligand for thymic positive selection. Immunity. Apr;6(4):389-99.

Jenkinson, E., Anderson, G., and Owen, J. 1992. Studies on T Cell Maturation on Defined Thymic Stromal Cell Populations *In Vitro*. J. Exp. Med. 176: 845-853.

Jones LA, Izon DJ, Nieland JD, Linsley PS, Kruisbeek AM. CD28-B7 interactions are not required for intrathymic clonal deletion. Int Immunol. 1993 May;5(5):503-12.

Kaufman, D.S., Lewis, R.L., Auerbach, R., and Thomson, J.A. 1999. Directed differentiation of human embryonic stem cells into hematopoietic colony forming cells. Blood. 94.

Kishimoto H, Cai Z, Brunmark A, Jackson MR, Peterson PA, Sprent J. Differing roles for B7 and intercellular adhesion molecule-1 in negative selection of thymocytes. J Exp Med. 1996 Aug 1;184(2):531-7.

Ladi E, Schwickert TA, Chtanova T, Chen Y, Herzmark P, Yin X, Aaron H, Chan SW, Lipp M, Roysam B, Robey EA. Thymocyte-dendritic cell interactions near sources of CCR7 ligands in the thymic cortex. J Immunol. 2008 Nov 15;181(10):7014-23.

Le Borgne M, Ladi E, Dzhagalov I, Herzmark P, Liao YF, Chakraborty AK, Robey EA.
The impact of negative selection on thymocyte migration in the medulla. Nat Immunol. 2009 Aug;10(8):823-30.

Lepesant, H., Reggio, H., Pierres, M., Naquet, P. 1990. Mouse thymic epithelial cell lines interact with and select a CD3lowCD4 + CD8 + thymocyte subset through an
LFA-1 -dependent adhesion - de-adhesion mechanism. International Immunology. 2: 1021-1032.

Lewis RS. Calcium signaling mechanisms in T lymphocytes. Annu Rev Immunol 2001;19:497–521.

Lucas B, Germain RN. Opening a window on thymic positive selection: developmental changes in the influence of cosignaling by integrins and CD28 on selection events induced by TCR engagement. J Immunol. 2000 Aug 15;165(4):1889-95.

Martin GR Teratocarcinomas and mammalian embryogenesis. *Science* 209 (4458): 768–76. (1980).

McCaughtry TM, Baldwin TA, Wilken MS, Hogquist KA, 2008. Clonal deletion of thymocytes can occur in the cortex with no involvement of the medulla. J. Exp. Med. 205(11):2575-84.

Negulescu PA, Krasieva TB, Khan A, Kerschbaum HH, Cahalan MD. 1996 Polarity of T cell shape, motility, and sensitivity to antigen. Immunity. May;4(5):421-30.

Norment, A., Becan, M. 2000. Role of Chemokines in Thymocyte Development. Seminars in Immunol. 12: 445-255.

Page DM, Kane LP, Allison JP, Hedrick SM. Two signals are required for negative selection of CD4+CD8+ thymocytes. J Immunol. 1993 Aug 15;151(4):1868-80.

Palmer, E., Naeher, D. 2009. Affinity Threshold for Thymic Selection through a T-Cell Receptor Co-Receptor Zipper. Nature Reviews 9: 207-213

Ponti A, Machacek M, Gupton SL, Waterman-Storer CM, Danuser G. 2004. Two distinct actin networks drive the protrusion of migrating cells. Science 305:1782–86

Revilla, C., Gonzalez, A., Conde, C., Lopez-Hoyos, M., Merino, J. 1997. Treatment with anti-LFA-lα monoclonal antibody selectively interferes with the maturation of CD4- 8+ thymocytes. Immunology, 90: 550-556

Scharffetter-Kochanek K, Lu H, Norman K, van Nood N, Munoz F, Grabbe S, McArthur M, Lorenzo I, Kaplan S, Ley K, Smith CW, Montgomery CA, Rich S, Beaudet AL. 1998. Spontaneous skin ulceration and defective T cell function in CD18 null mice. J Exp Med. Jul 6;188(1):119-31.

Schmitt TM, de Pooter RF, Gronski MA, Cho SK, Ohashi PS, Zuniga-Pflucker JC. Induction of T cell development and estab- lishment of T cell competence from embryonic stem cells differentiated *in vitro*. Nat Immunol. 2004;5:410–7.

Setoguchi, R., Tachibana, M., Naoe, Y., Muroi, S., Akiyama, K., Tezuka, C., Okuda, T., Taniuchi, I. 2008. Represion of the Transcription Factor Th-POK by RUNX Complexes in Cytotoxic T cell Development. Science. 319: 822-825

Siminovitch L, McCulloch EA, Till JE. The Distribution of Colony-Forming Cells among Spleen Colonies. J Cell Physiol. 1963;62:327–336.

Skokos D, Shakhar G, Varma R, Waite JC, Cameron TO, et al. 2007. Peptide-MHC potency governs dynamic interactions between T cells and dendritic cells in lymph nodes. Nat. Immunol. 8:835–44

Stritesky, G.L. et al. Murine thymic selection quantified using a unique method to capture deleted T cells. Proceedings of the National Academy of Sciences of the United States of America 110, 4679-4684 (2013).

Takahashi K, Yamanaka S. Induction of pluripotent stem cells from mouse embryonic and adult fibroblast cultures by defined factors. Cell. 2006 Aug 25;126(4):663-76. Epub 2006 Aug 10.

Tan R, Teh SJ, Ledbetter JA, Linsley PS, Teh HS. B7 costimulates proliferation of CD4-8+ T lymphocytes but is not required for the deletion of immature CD4+8+ thymocytes. J Immunol. 1992 Nov 15;149(10):3217-24.

Tavian M, Biasch K, Sinka L, Vallet J, Péault B. Embryonic origin of human hematopoiesis. Int J Dev Biol. 2010;54(6-7):1061-5.

Teh HS, Teh SJ. The affinity/avidity and length of exposure to the deleting ligand determine dependence on CD28 for the efficient deletion of self-specific CD4+CD8+ thymocytes. Cell Immunol. 2001 Feb 1;207(2):100-9.

Till JE, Mc CE. A direct measurement of the radiation sensitivity of normal mouse bone marrow cells. Radiat Res. 1961;14:213–222.

Timmermans F, Velghe I, Vanwalleghem L, De Smedt M, Van Coppernolle S, et al. (2009) Generation of T cells from human embryonic stem cell-derived hematopoietic zones. J Immunol 182: 6879–6888

Vacchio MS, Williams JA, Hodes RJ. A novel role for CD28 in thymic selection: elimination of CD28/B7 interactions increases positive selection. Eur J Immunol. 2005 Feb;35(2):418-27.

Walunas TL, Sperling AI, Khattri R, Thompson CB, Bluestone JA. CD28 expression is not essential for positive and negative selection of thymocytes or peripheral T cell tolerance. J Immunol. 1996 Feb 1;156(3):1006-13.

Williams JA, Sharrow SO, Adams AJ, Hodes RJ. CD40 ligand functions non-cell autonomously to promote deletion of self-reactive thymocytes. J Immunol. 2002 Mar 15;168(6):2759-65.

Witt CM, Raychaudhuri S, Schaefer B, Chakraborty AK, Robey EA. Directed migration of positively selected thymocytes visualized in real time. PLoS Biol. 2005 Jun;3(6):e160. Epub 2005 May 3. Erratum in: PLoS Biol. 2005 Oct;3(10):e373.

Wu AM, et al. Cytological evidence for a relationship between normal hemotopoietic colony-forming cells and cells of the lymphoid system. J Exp Med. 1968;127(3):455–464.

Yin X, Ladi E, Chan SW, Li O, Killeen N, Kappes DJ, Robey EA. CCR7 expression in developing thymocytes is linked to the CD4 versus CD8 lineage decision. J Immunol. 2007 Dec 1;179(11):7358-64.

Chapter 2: Comparative study of hematopoietic differentiation between human embryonic stem cell lines

2.1 Introduction

Directed differentiation of human embryonic stem cells (hESCs) into a variety of cell types has vast promise in the context of personalized human therapeutics and also towards understanding developmental paradigms. Specifically, hESC-derived hematopoietic subsets could theoretically be used for a variety of therapeutic purposes such as replenishment of lymphocyte deficiency due to chemotherapy, suppression of autoimmunity by regulatory T cells, or T cell mediated anti-tumor therapy. However, we first need to establish a robust and repeatable protocol for *in vitro* differentiation.

Differences in lineage potential among independently derived hESC lines has been noted for a number of downstream target cell types and at different stages of development. In addition to gene expression heterogeneity among the hESC lines themselves, lineage skewing among hESC lines has been identified as early as commitment to the three germ layers [1–6]. In other reports, lineage bias between hESC lines is detected at the latest stages of development—definitive differentiation of forebrain versus hind- brain neurons, for example [7]. For the hematopoietic lineage, the potential of hESCs to develop into blood lineage cells has primarily been addressed with a restricted number of stem cell lines and differentiation methods. Several groups have reported success in generating erythrocytes, various myeloid lineage cells, B cells, and NK cells from hESCs, albeit differentiation of B cells was based primarily on expression of lineage markers rather than functional assays [8–17]. However, generation of T lymphocytes from the same hESC lines has been difficult to achieve, despite the fact that mouse ESCs can be easily induced to differentiate toward the T cell lineage by co-culturing with Notch-1 ligand expressing stromal cells [18]. One group has verified T lineage potential from the H1 hESC line through *in vivo* passage of hESC-derived hematopoietic progenitor cells in a humanized mouse model [19,20]. Recently, another group reported generation of T cells from what they refer to as ‘‘hematopoietic zones’’ *in vitro* [21]. This is currently the sole successful report of *in vitro* T cell differentiation. However, under similar conditions, another group reported a strong lineage bias against the development of T lineage cells from hESCs, and rather an NK lineage pre-disposition [15]. These discrepancies in T lineage differentiation potential between labs using similar protocols, and the low efficiency of T cell development in successful labs highlights a need for improved understanding of hESC culture conditions and differentiation protocols before becoming clinically useful.

The basis for these differences in lineage potential among hESC lines are not completely understood but could stem from a number of variables including, but not limited to, genetic background, the quality and stage of the embryo at derivation, and the hESC isolation method. In addition, the sensitivity of hESC lines to experimental variability make it extremely difficult to compare the differentiation potential of hESC lines indirectly via published results. Here, we set out to establish the hematopoietic and lymphoid potential of a sampling of hESC lines from various sources under different culture conditions and differentiation protocols in a side-by-side comparison at different stages of differentiation. We found significant differences in hematopoietic potential among independent hESC lines, differences in blood lineage

development under different passage conditions regardless of karyotypic abnormalities, and disparities under unique directed differentiation protocols. These lineage biases were identified early in hematopoietic development and also at subsequent stages of lymphoid development. In contrast, ex vivo hematopoietic progenitors developed consistently and efficiently into lymphoid cells, specifically the T cell lineage, under the same *in vitro* differentiation conditions.

2.2 Results

We sought to compare the hematopoietic potential of several hESC lines from different sources. In this analysis we included one human ES cell line reportedly skewed toward mesoderm (HuES8), one toward endoderm (HuES14), one not described (HuES15), the two lines most prevalently used by others for hESC-hematopoietic differentiation, H1 and H9, and another independently-derived hESC cell line, HSF-6 [4,22,23].

First, we analyzed the proportion of each hESC line that gave rise to putative hemangioblasts (CD34+CD45-) and hematopoietic progenitor cells (CD34+CD45+) under various passage and differentiation parameters (Fig. 2.1). We compared the affect of enzymatic (trypsin treatment) versus manual passage on hematopoietic development. To assess the initial commitment to the hematopoietic lineage, we allowed hESCs to differentiate into embryoid bodies (EB) or co-cultured hESCs on an OP9 mouse bone marrow stromal cell monolayer in the absence of lineage skewing cytokines. Consistently, and regardless of cell line, manual passage gave rise to a higher proportion of hESCs differentiating to CD34+ cells in EB culture (Fig. 2.1A). Under the same differentiation conditions, enzymatically passaged hESCs also failed to up-regulate CD45, a marker indicative of hematopoietic commitment. In contrast, under the same differentiation conditions, CD45 was detectable on all the hESC lines maintained through manual passage (Fig. 2.1A). It has been shown that enzymatic passage of hESCs can lead to an increased frequency of karyotype abnormalities [6,24]. Therefore, we also performed karyotype analysis periodically to determine gross karyotypic changes under different culture conditions. Trypsin-passaged HuES8, HuES14, and HuES15 hESC cultures consistently displayed gross karyotype abnormalities (Fig. 2.1B). However, no significant karyotype abnormalities were observed in H1 or H9 trypsin-passaged hESC cultures, nor were any chromosomal abnormalities noted in any of the manually passaged cultures. All hESC lines used throughout the manuscript maintained normal karyotypes with the exception of the top panel of Figure 2.1A, as noted.

We next analyzed the propensity of manually passaged hESC lines to generate CD34+ and CD34+CD45+ using a complementary differentiation system. Undifferentiated hESCs were harvested and plated on a monolayer of OP9 mouse bone marrow stromal cells capable of promoting hematopoietic development. Again, CD34 and CD45 expression were monitored by flow cytometry. Overall, all hESC lines consistently gave rise to CD34- expressing cells. However, several differences in the differentiation potential were noted using the two different protocols. Cell-surface CD45 was not detected at any time point on hESCs differentiated in the OP9 co-culture system (Fig. 2.1A, bottom panel and data not shown). In addition, although the H1 line consistently had a higher proportion of CD34+ cells in both differentiation conditions, other hESC lines, specifically H9 and HSF6 generated proportionally more CD34+ cells in the OP9 co-culture system as compared with the EB condition. We also observed that the kinetics of cell-surface CD34 expression differed significantly between hESC lines and the differentiation protocols (Fig. 2.1C).

The CD34+ population contains developmental intermediates capable of giving rise to multiple lineages. To compare the potential of CD34+ cells derived from independent hESC lines, CD34+CD45- cells from EB cultures were enriched by fluorescence activated cell sorting (FACS) and placed into culture with differentiation media containing lineage-promoting

cytokines and growth factors that provide hematopoietic- or endothelial-skewing conditions. As expected, under hematopoietic skewing conditions, CD34+ cells differentiated into CD45+VE-cadherin- cells (Fig. 2.2A), whereas under endothelial skewing conditions, CD34+ cells up-regulated cell-surface expression of VE-cadherin (Fig. 2.2B) [25]. Of the lines generating CD45+ cells from CD34+CD45- populations (HuES8, HuES14, H1, and H9), the proportion of CD45+ cells is comparable (Fig. 2.2A.) Whether generation of CD45+ cells in these conditions is due to loss of non-hematopoietic committed cells remains to be seen. We also noticed that the number of CD45+ cells relative to the starting population varied among hESC lines and between experiments (Fig. 2.2C). HuES8, in particular, showed extensive variability in the generation of CD45+ cells between experiments (Fig. 2.2C). This is in contrast to the ability of CD34+ cells from different hESCs to give rise to endothelial cells, which was more consistent from line to line (Fig. 2.2D). Interestingly, H1-derived CD34+ cells generated relatively more CD45+ cells while HSF-6-derived CD34+ cells consistently gave rise to relatively more VE-cadherin+ cells as compared to other hESC lines (Figs. 2.2C and 2.2D).

It has been shown that hESC-derived hematopoietic progenitor cells differ phenotypically from their *in vivo* fetal liver or cord blood counterparts that can easily differentiate into all hematopoietic lineages, being more similar to primitive blood cell progenitors [15,26–28]. This difference might be one reason for their inability to efficiently generate all the blood lineages *in vitro*. To examine the possible differences among hematopoietic progenitors, we assessed the cell-surface expression of a cohort of markers indicative of hematopoietic differentiation state and maturity. Based on CD34, CD31, and CD45 expression, hESC-derived cells were more similar to CD34+ human fetal liver cells, whereas the majority of cord blood CD34+ cells expressed CD45+ cells (Fig. 2.3A). Since the fetal liver and cord blood CD34+ cells have similar lymphoid lineage differentiation potential, and the fetal liver CD34+ cells resemble hESC-derived CD34+ cells, these markers alone cannot distinguish the *in vitro* differentiation capacity of CD34+ cells.

Co-culture of hematopoietic progenitors on the mouse bone marrow stromal cell line, OP9, is known to support lymphocyte differentiation from a number of human hematopoietic progenitor populations [29]. Therefore, we followed the differentiation steps of hESC-derived CD34+ cells on an OP9 monolayer by analyzing the expression of a lymphocyte commitment marker, CD7, by flow cytometry. As shown in Figure 2.3C, lines HuES8, HuES14, HuES15, and H1 gave rise to a small population of CD7+ cells. In contrast, H9 or HSF6-derived CD34+ cells did not produce appreciable CD7+ cells in OP9 co-culture, and overall, lymphoid progenitor yield was low among lines (Fig. 2.3B). In addition, we analyzed the ability of hESC-derived CD34+ cells to differentiate into T cells. To test T lineage differentiation, we co-cultured hESC-derived CD34+ cells on OP9 stromal cells that express human delta-like 1 Notch ligand (OP9-DL1). This system has been shown to support T lineage differentiation from a variety of mouse and human progenitor cell sources [18,29,30]. Both human fetal liver and cord blood CD34+ cells generate a significant populations of cells co-expressing CD7 and CD1a marking T lineage commitment within 14 days of co-culture initiation (Figs. 2.3C and 2.3D). In contrast, no CD7+CD1a+ T cell progenitors were seen in cultures with hESC-derived CD34+ cells (Figs. 2.3C and 2.3D), despite the ability of the same co-culture system to support further differentiation of CD34+CD45lo and CD34+CD45hi fetal liver progenitors to CD4+CD8+-expressing T lineage cells (Fig. 2.3E).

Several groups have attempted similar differentiation of T lineage cells from hESC-derived progenitor cells with limited success *in vitro*. The only exception was a recent report that purportedly found a CD34+CD43+ population in a structurally distinct ‘‘hematopoietic zone’’, which can be differentiated into CD4+CD8+ T cells by co- culturing with OP9-DL1 cells [21]. Despite extensive search under microscopes, however, we could not detect any ‘‘hematopoietic zones’’ as described in our hESC/OP9-DL1 co-cultures. We also analyzed expression of CD43 in CD34+ cells differentiating in the presence of OP9-DL1 cells. In contrast to cord blood CD34+ cells that did generate T lineage cells and express CD43, no expression of CD43 was detected by flow cytometry on differentiating hESC-derived CD34+ cells (Fig. 2.3F).

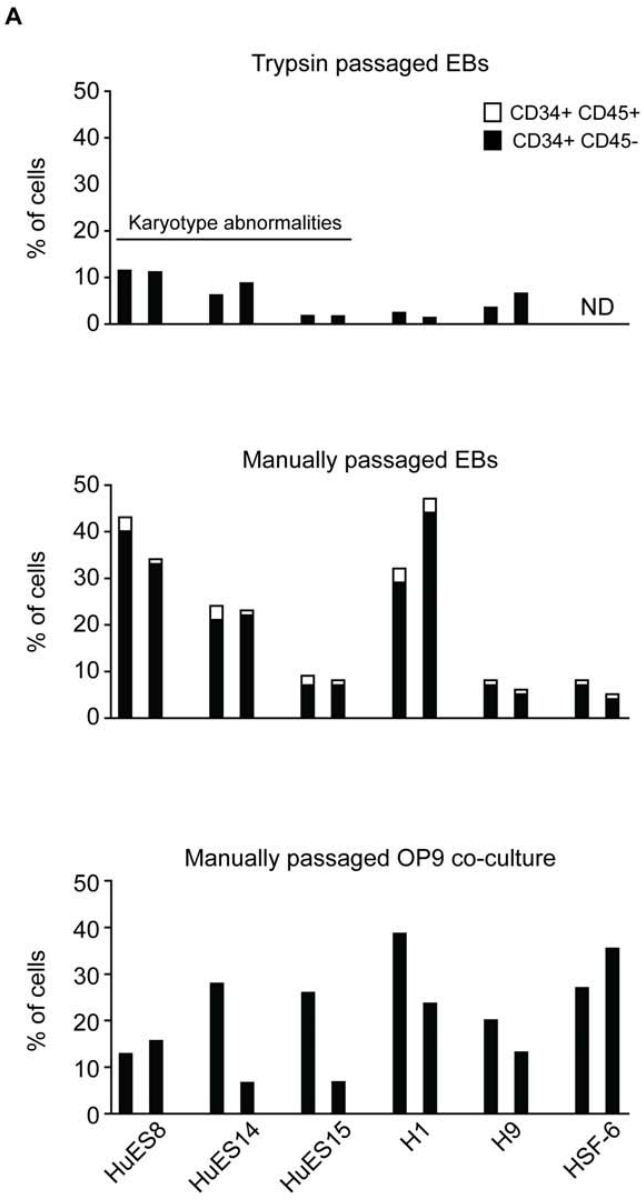

B

hESC line	abnormal karyotype [frequency]	abnormal chromosomes
HuES8	48,XY,+12,+17 [34/40]	12, 17
HuES14	46,XY,der(22)t(17;22)(q11.2;p11.2) [17/40]	22
	46,XY,add(X)(p22.3),der(22)t(17;22)(q11.2;q11.2) [23/40]	22, X
HuES15	46XX, inv(13)(q12q32) [40/40]	13

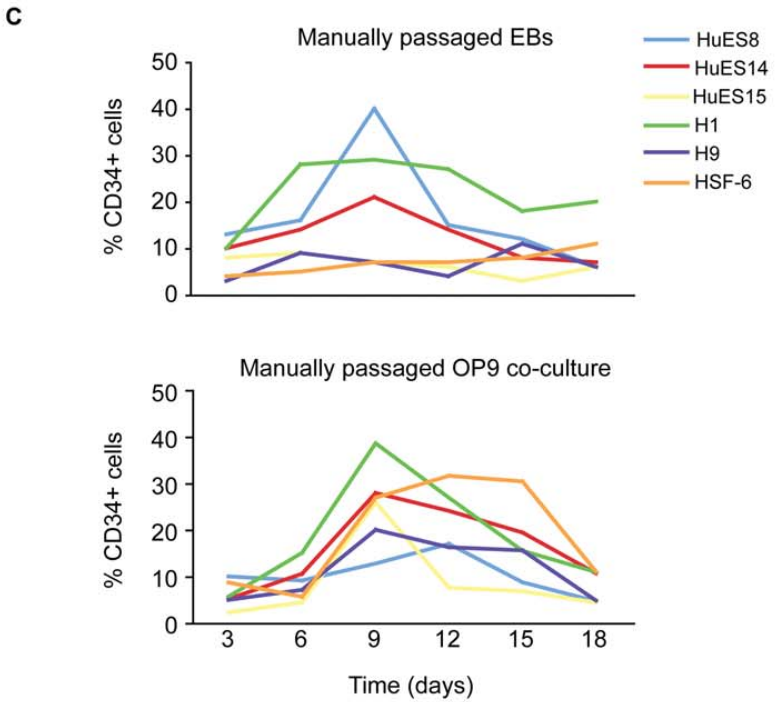

Figure 2.1. Comparative analysis of hemangioblast development from independently-derived hESC lines. Several hESC lines were differentiated as embryoid bodies (EB) for nine days after several trypsin passages (A, top panel) or after several manual passages (A, middle panel) in EB media without lineage-skewing cytokines. CD34+ and CD34+CD45+ development was determined by flow cytometric analysis of several cell surface markers indicative of differentiation state. The proportion of hESC-derived CD34+CD45- cells is presented on differentiating hESCs in black. The proportion of CD34+CD45+ progenitors is indicated in white. HuES8, HuES14, and HuES15 cell lines were highly susceptible to gross karyotypic abnormalities during trypsin passage (as indicated). H1, H9, and HSF6 manually passaged cells had previously been passaged with trypsin (.5 manual passages before differentiation). (A, bottom panel) Independently-derived hESC were differentiated on an OP9 monolayer for nine days, and CD34 and CD45 cell surface expression analyzed by flow cytometry. Two representative experiments of each condition are presented. (B) Abnormal karyotypes observed in trypsin-passaged cells. (C) Representative time course of CD34 expression on manually passaged, independently-derived hESCs differentiated as EBs or on an OP9 monolayer. CD34 expression was analyzed on days 3, 6, 9, 12, 15, 18.

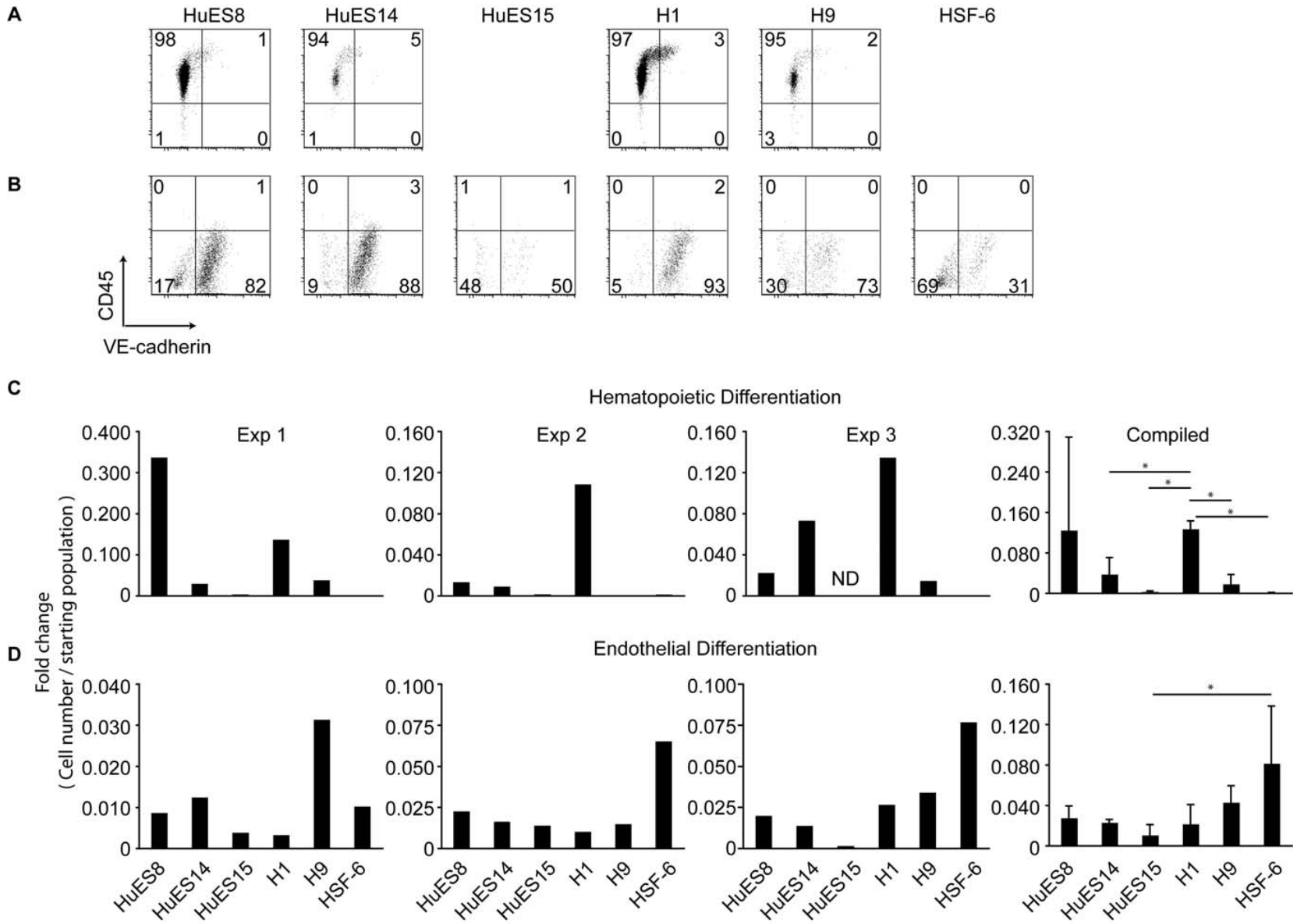
A
HuES8
HuES14
HuES15
H1
H9
HSF-6
98
1
1
0
94
5
1
0
97
3
0
0
95
2
3
0
B
0
1
17
82
0
3
9
88
1
1
48
50
0
2
5
93
0
0
30
73
0
0
69
31
CD45
VE-cadherin
C
Hematopoietic Differentiation
Exp 1
Exp 2
Exp 3
Compiled
ND
Fold change
(Cell number / starting population)
0.400
0.300
0.200
0.100
0
0.160
0.120
0.080
0.040
0.320
0.240
*
D
Endothelial Differentiation
0.040
0.030
0.020
0.010
0.100
0.075
0.050
0.025
HuES8
HuES14
HuES15
H1
H9
HSF-6

Figure 2.2. Skewed hematopoietic vs. endothelial potential from EB-derived CD34+CD45- cells. (A) The indicated hESC lines were first differentiated as EBs in EB media without lineage skewing cytokines. CD34+CD45- cells were enriched by fluorescence activated cell sorting (FACS) on day 10 of EB culture and differentiated on fibronectin-coated plates in the presence of IL-3, IL-6, SCF, G-CSF, Flt3L, and BMP4 for an additional 7 days. Representative flow cytometry plots of CD45 (hematopoietic marker) and VE-cadherin (endothelial marker) are presented. (B) Comparative analysis of endothelial potential from independently-derived hESC lines. Endothelial differentiation of hESC lines was determined by a two-step culture. hESCs were initially differentiated for 9 days as EBs as in (A), and CD34+ cells enriched by FACS. CD34+ cells were plated on fibronectin-coated plates in the presence of an endothelial growth factor cocktail containing bovine pituitary extract, heparin, and hVEGF, and analyzed after 7 additional days in culture. Representative flow cytometry plots of CD45 and VE-cadherin are presented. (C) Graphs depict the relative number of hematopoietic (CD45+) or (D) endothelial lineage (VE-cadherin+) cells as identified by flow cytometry over the starting (CD34+, CD452-, VE-cadherin-) population. Three independent experiments are shown in (C) and (D). The right panels denote the average of the three independent data sets with error bars and standard deviation between hESC lines. * denotes p,0.05.

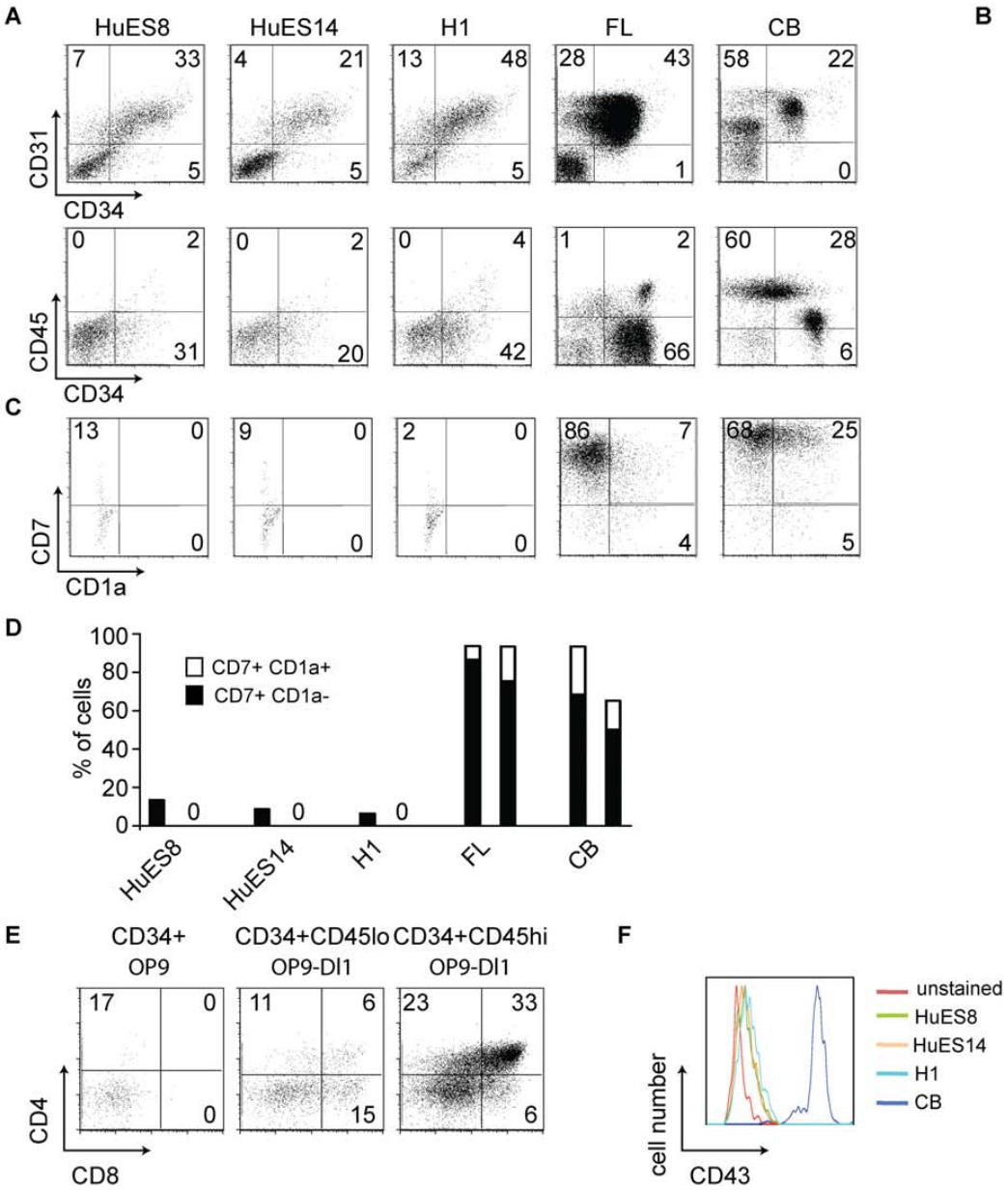
A
HuES8
HuES14
H1
FL
CB
CD31
CD34
CD45
CD34
C
CD7
CD1a
D
% of cells
CD7+ CD1a+
CD7+ CD1a-
HuES8
HuES14
H1
FL
CB
E
CD34+
OP9
CD34+CD45lo
OP9-Dl1
CD34+CD45hi
OP9-Dl1
CD4
CD8
F
cell number
CD43
unstained
HuES8
HuES14
H1
CB

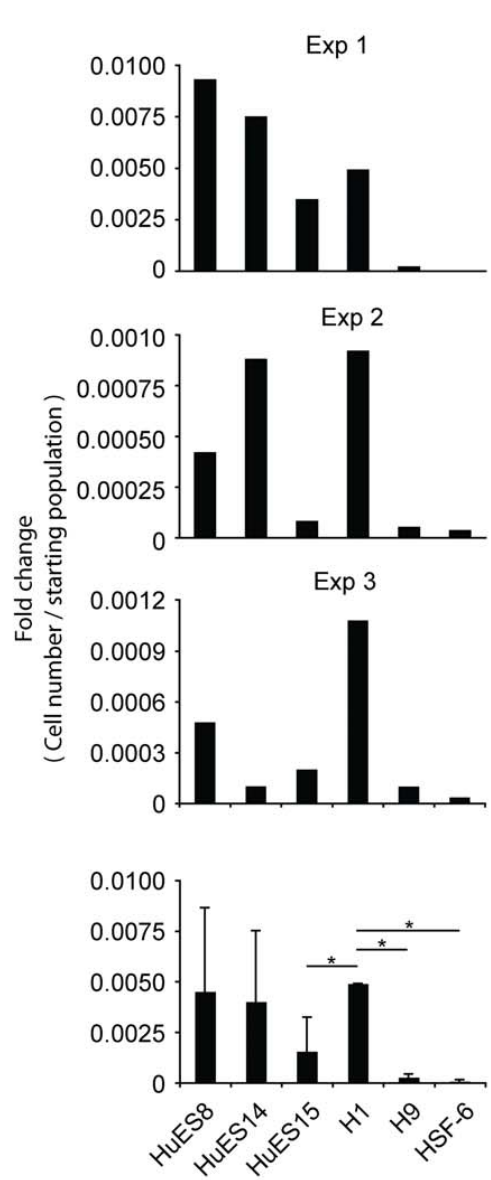
B
Exp 1
Exp 2
Exp 3
Fold change
(Cell number / starting population)
HuES8
HuES14
HuES15
H1
H9
HSF-6

Figure 2.3. hESC-derived hematopoietic progenitor cells are phenotypically and developmentally distinct from *in vivo* hematopoietic precursors. (A) Significant phenotypic differences among hESC-derived, cord blood, and fetal liver hematopoietic progenitor cells. Representative plots of cell surface expression of CD34, CD31, and CD45 on differentiated hESCs (EB culture for 9 days), and CD34+ cell enriched cord blood and fetal liver. (B) Relative number of lymphocyte committed cells (as evidenced by expression CD7) as compared to input population (CD34+ population enriched by FACS from day 9 EBs.) Three independent experiments are shown (Exp 1–3). The bottom panel denotes the average of the three independent data sets (Exp 1–3), after normalization to the fold change of the H1 sample in each experiment. Standard deviations between hESC cells with p,0.05 (*) are also indicated. (C) Analysis of CD7 and CD1a expression from FACS enriched EB-derived, fetal liver, or cord blood CD34+ cells differentiated on OP9-hDL1 co-cultures for 14 days. (D) The proportion of T lineage-committed cells was determined by flow cytometric analysis of CD7 (lymphocyte) and CD1a (T cell) expression. Duplicate experiments are shown as representative of differentiation of CD34+ cells into CD7+ cells in OP9-hDL1 co-culture conditions (Enriched CD34+ cells from HuES15, H9, and HSF6 hESC lines failed to expand/survive in co-culture with OP9-hDL1 and are thus not presented). (E) Representative flow plots of cell-surface CD4 and CD8 expression from fetal liver CD34+ subsets differentiated on OP9 (left) or OP9-hDL1 (center and right) cells for 28 days. Fetal liver cells expressing CD34 were sorted to .95% purity. Additionally, fetal liver subsets were also sorted on CD34+CD45lo or CD34+CD45hi populations due to a gradient of CD45 expression. Cells were co-cultured on either OP9 or OP9- DL1 as indicated. (F) Flow cytometric analysis of cell-surface CD43 staining on HuES8, HuES14, and H1-derived hematopoietic progenitors (EB culture, day 9) and human cord blood progenitors. Flow plots were gated on CD34+ cells.

2.3 Discussion

Successful development of directed differentiation protocols for all hematopoietic lineages from hESC lines would allow not only the possibility of generating blood cell subsets for therapeutic purposes, but would also permit research into early human blood cell development that is otherwise inaccessible to observe and manipulate. Despite the intense interest and investment in developing blood cell therapies from hESCs, we still lack adequate understanding of how culture conditions and differentiation protocols may affect lineage development. Here we present a comparison of the developmental potential of six independent hESC lines maintained and differentiated under multiple parameters.

Unlike previous studies that compare multiple cell culture conditions for one hESC line, or one differentiation protocol for multiple hESC lines, our approach was to directly compare multiple hESC lines under several culture and differentiation conditions [4,31–34]. This provides a comprehensive side-by-side analysis of important variables on *in vitro* blood cell development. Though we do observe similar lineage potential differences in some previously compared hESC lines (HuES8, HuES14, and HuES15), we note additional differences among these lines based on passage conditions and differentiation method. First, there were significant developmental differences among the same hESC lines when passaged under different conditions. Enzymatic passage of hESCs has been shown to favor karyotype instability [6,24], and as expected, three of the hESC lines displayed gross karyotype abnormalities following trypsin passage. Interestingly, H1 and H9 did not exhibit any karyotypic abnormalities under enzymatic passages. However, the differentiation potential of the enzymatically passaged H1 and H9 cultures as compared to manually passed H1 and H9 hESCs was dramatically impaired. These data highlight the need for manual passage of all hESC cell work.

We noted that differentiation into hematopoietic lineages varies between hESC lines and culture conditions. This is in contrast to endothelial lineage development, which was more similar between lines and experiments. This might be attributed to the endothelial lineage being a ‘‘default’’ pathway during lineage commitment. Using CD45 as a marker of early hematopoietic commitment, we found EB-based culture conditions superior to OP9 co-culture methods in all the hESC lines. Some of the hESC lines (HuES 8, 14, 15 and H1) consistently produced more CD34+CD45+ cells. The hESC line HuES8, for example, could produce up to 40% CD34+ cells within 10 days. Under hematopoietic skewing conditions, CD34+CD45- cells from EB cultures could differentiate into CD45+ cells. Again, in contrast to the ability of CD34+ cells from all hESC lines tested to develop into endothelial cells, only three hESC lines (HuES 8, 14 and H1) consistently differentiated into the CD45+ early hematopoietic progenitors. A similar finding was observed when EB-derived CD34+ cells were co-cultured with OP9 cells, and the lymphoid marker, CD7, was used to measure differentiation into the lymphoid lineages.

We were particularly interested in improving the efficiency of generating T cells from hESCs by co-culturing CD34+ cells with Notch-ligand expressing OP9-DL1 cells. However, despite evidence from one group that reported development of T lineage cells from hematopoietic zones in this OP9 co-culture system, we and others have not been successful in doing so [15,21]. The reasons behind this are not clear. The comparatively high expression of Id factors in hESCs and hESC-derived hematopoietic cells as compared to cord blood hematopoietic progenitors has been

noted. Id genes antagonize T lineage development and may be one of the hurdles to *in vitro* T cell generation from hESC lines [15]. An additional test of T lineage potential may be passage of hESC-derived hematopoietic progenitors through a humanized mouse model. H1 hESC cells were shown to be capable of differentiating into T cells *in vivo* [19,20]. Despite these reports concerning *in vivo* differentiation, we showed that this line was unable to differentiate into T cells *in vitro* under each of the several conditions tested.

The difficulty of differentiating hESCs into T cells is in contrast to the ease in which mouse ESCs develop into CD4+CD8+ T cells in the presence of OP9-DL1 cells. It has been suggested recently that the majority of hESCs in existence share more similarities to mouse epiblast cells than mouse ESCs derived from the blastocyst inner cell mass. Mouse epiblast stem cells are not truly pluripotent and are characterized by flattened morphology and the inability to grow from a single cell. Like hESCs, they also differentiate into teratomas. Thus, it is possible that generating new hESC lines that are more similar to mouse ESCs might be more conducive for T cell differentiation. To that end, recent studies isolating hESCs under controlled oxygen conditions or pushing existing ‘‘epiblast-like’’ hESCs back to a more pluripotent state by manipulation of the KLF transcriptional circuitry may provide more consistent stability of hematopoietic and T cell differentiation [35,36]. Rigorous comparison of independent lines derived under these conditions will be needed to determine if the more ‘‘primitive’’ hESC lines may present better starting material for robust and repeatable hESC differentiation *in vitro*.

2.4 Methods

Ethics statement

This research was reviewed and approved by the UC Berkeley Stem Cell Research Oversight Committee.

hESC Cell Culture

All hESCs have been described previously [22,23]. hESCs were maintained on irradiated mouse embryonic feeder cells derived from C57BL/6 mice (E12.5–E13.5) in knockout-DMEM media as described [4] (Invitrogen). hESCs were passaged by either enzymatic passage using 0.05% trypsin or manual passage using StemPro EZPassage (Invitrogen) and split at a ratio between 1:3 to 1:6 [4]. hESC samples were split at various time points for karyotype analysis at the Children's Hospital Oakland Research Institute.

Differentiation protocols

Embryonic bodies (EBs) from hESCs were formed essentially as described [4]. hESC colonies were dissociated by adding 1 mg/ mL collagenase IV for 10minutes at 37uC. Plates were subsequently washed with PBS and EB media was added (no cytokines or growth factors). Dissociated colonies were removed from plates using a cell scraper and transferred into six-well low- attachment plates (Corning). Half media changes were done every other day for the duration of EB culture. EBs were dissociated for flow cytometric analysis or CD34+ cell enrichment by FACS by the addition of 1 mg/mL collagenase B (Roche) for 2 hours at 37uC, following by vigorous pipetting.

For hematopoietic and endothelial two-step cultures, 24 or 48 well plates were coated with fibronectin, and sorted, day 9 EB- derived CD34+ cells were plated in differentiation media containing IL-3, IL-6, SCF, G-CSF, Flt3L (PeproTech), and BMP4 (R&D) (hematopoietic differentiation conditions) or in Medium-199 with 20% fetal bovine serum (FBS), bovine pituitary extract (Invitrogen), heparin (Leo Pharma Inc), and hVEGF (R&D) (endothelial differentiation conditions) for 7 days with media changes on days 2, 4, and 6 as described [25,37].

For co-culture experiments, hESC cells or FACS enriched EB- derived CD34+ cells were plated on OP9 or OP9-DL1 (gift from JC Zuniga-Pfluucker, University of Toronto) cells in MEM alpha media with 20% defined FBS as described [16,18,21]. Cultures were maintained with half media changes every other day up to 18 days. Differentiated cells were liberated by either vigorous pipetting (FACS enriched CD34+ cells) or by collagenase IV treatment at 37uC for 30 minutes followed by a 15 minute incubation at 37uC with 0.05% trypsin (hESC cultures).

Flow cytometry and cell sorting

CD34+ cells were initially enriched from human fetal liver (ABR Inc., Alameda, CA, USA) or human cord blood (NDRI, Philadelphia, PA, USA) using the EasySep Human CD34 Positive Selection Kit (Stem Cell Technologies, Vancouver, Canada) for cell surface marker analysis by flow cytometry. Single cell suspensions of CD34-enriched fetal liver and cord blood, or dissociated EB were incubated with fluorochrome conjugated anti- human CD34 and anti-human CD45 antibodies as indicated, and washed. Cell suspensions were sorted using a Cytopeia INFLUX Sorter (BD). For flow cytometry, single cell suspensions were stained with fluorochrome conjugated anti-human CD34, CD45, VE-cadherin, CD31, CD7, CD1a, CD4, CD8 and CD43 (R&D and eBioscience). Sample acquisitions were performed on the Beckman Coulter Cytomics FC 500 or EPICS XL flow cytometer (Miami, FL, USA), and data were analyzed with FlowJo software (Tree Star, Ashland, OR, USA).

2.5 References

1. Abeyta MJ, Clark AT, Rodriguez RT, Bodnar MS, Pera RA, et al. (2004) Unique gene expression signatures of independently-derived human embryonic stem cell lines. Hum Mol Genet 13: 601–608.

2. D'Amour KA, Agulnick AD, Eliazer S, Kelly OG, Kroon E, et al. (2005) Efficient differentiation of human embryonic stem cells to definitive endoderm. Nat Biotechnol 23: 1534–1541.

3. Kim SE, Kim BK, Gil JE, Kim SK, Kim JH (2007) Comparative analysis of the developmental competence of three human embryonic stem cell lines *in vitro*. Mol Cells 23: 49–56.

4. Osafune K, Caron L, Borowiak M, Martinez RJ, Fitz-Gerald CS, et al. (2008) Marked differences in differentiation propensity among human embryonic stem cell lines. Nat Biotechnol 26: 313–315.

5. Skottman H, Mikkola M, Lundin K, Olsson C, Stromberg AM, et al. (2005) Gene expression signatures of seven individual human embryonic stem cell lines. Stem Cells 23: 1343–1356.

6. Mikkola M, Olsson C, Palgi J, Ustinov J, Palomaki T, et al. (2006) Distinct differentiation characteristics of individual human embryonic stem cell lines. BMC Dev Biol 6: 40.

7. Wu H, Xu J, Pang ZP, Ge W, Kim KJ, et al. (2007) Integrative genomic and functional analyses reveal neuronal subtype differentiation bias in human embryonic stem cell lines. Proc Natl Acad Sci U S A 104: 13821–13826.

8. Olivier EN, Qiu C, Velho M, Hirsch RE, Bouhassira EE (2006) Large-scale production of embryonic red blood cells from human embryonic stem cells. Exp Hematol 34: 1635–1642.

9. Qiu C, Olivier EN, Velho M, Bouhassira EE (2008) Globin switches in yolk sac- like primitive and fetal-like definitive red blood cells produced from human embryonic stem cells. Blood 111: 2400–2408.

10. Takayama N, Nishikii H, Usui J, Tsukui H, Sawaguchi A, et al. (2008) Generation of functional platelets from human embryonic stem cells *in vitro* via ES-sacs, VEGF-promoted structures that concentrate hematopoietic progeni- tors. Blood 111: 5298–5306.

11. Gaur M, Kamata T, Wang S, Moran B, Shattil SJ, et al. (2006) Megakaryocytes derived from human embryonic stem cells: a genetically tractable system to study megakaryocytopoiesis and integrin function. J Thromb Haemost 4: 436–442.

12. Yokoyama Y, Suzuki T, Sakata-Yanagimoto M, Kumano K, Higashi K, et al. (2009) Derivation of functional mature neutrophils from human embryonic stem cells. Blood 113: 6584–6592.

13. Karlsson KR, Cowley S, Martinez FO, Shaw M, Minger SL, et al. (2008) Homogeneous monocytes and macrophages from human embryonic stem cells following coculture-free differentiation in M-CSF and IL-3. Exp Hematol 36: 1167–1175.

14. Woll PS, Grzywacz B, Tian X, Marcus RK, Knorr DA, et al. (2009) Human embryonic stem cells differentiate into a homogeneous population of natural killer cells with potent *in vivo* antitumor activity. Blood 113: 6094–6101.

15. Martin CH, Woll PS, Ni Z, Zuniga-Pflucker JC, Kaufman DS (2008) Differences in lymphocyte developmental potential between human embryonic stem cell and umbilical cord blood-derived hematopoietic progenitor cells. Blood 112: 2730–2737.

16. Vodyanik MA, Bork JA, Thomson JA, Slukvin II (2005) Human embryonic stem cell-derived CD34+ cells: efficient production in the coculture with OP9 stromal cells and analysis of lymphohematopoietic potential. Blood 105: 617–626.

17. Dravid G, Zhu Y, Scholes J, Evseenko D, Crooks GM (2010) Dysregulated Gene Expression During Hematopoietic Differentiation From Human Embryonic Stem Cells. Mol Ther: Dec 21, 2010, Epub ahead of print.

18. Schmitt TM, de Pooter RF, Gronski MA, Cho SK, Ohashi PS, et al. (2004) Induction of T cell development and establishment of T cell competence from embryonic stem cells differentiated *in vitro*. Nat Immunol 5: 410–417.

19. Galic Z, Kitchen SG, Kacena A, Subramanian A, Burke B, et al. (2006) T lineage differentiation from human embryonic stem cells. Proc Natl Acad Sci U S A 103: 11742–11747.

20. Galic Z, Kitchen SG, Subramanian A, Bristol G, Marsden MD, et al. (2009) Generation of T lineage cells from human embryonic stem cells in a feeder free system. Stem Cells 27: 100–107.

21. Timmermans F, Velghe I, Vanwalleghem L, De Smedt M, Van Coppernolle S, et al. (2009) Generation of T cells from human embryonic stem cell-derived hematopoietic zones. J Immunol 182: 6879–6888

22. Cowan CA, Klimanskaya I, McMahon J, Atienza J, Witmyer J, et al. (2004) Derivation of embryonic stem-cell lines from human blastocysts. N Engl J Med 350: 1353–1356.

23. Thomson JA, Itskovitz-Eldor J, Shapiro SS, Waknitz MA, Swiergiel JJ, et al. (1998) Embryonic stem cell lines derived from human blastocysts. Science 282: 1145–1147.

24. Mitalipova MM, Rao RR, Hoyer DM, Johnson JA, Meisner LF, et al. (2005) Preserving the genetic integrity of human embryonic stem cells. Nat Biotechnol 23: 19–20.

25. Wang L, Li L, Shojaei F, Levac K, Cerdan C, et al. (2004) Endothelial and hematopoietic cell fate of human embryonic stem cells originates from primitive endothelium with

hemangioblastic properties. Immunity 21: 31–41.

26. Patel E, Wang B, Lien L, Wang Y, Yang LJ, et al. (2009) Diverse T-cell differentiation potentials of human fetal thymus, fetal liver, cord blood and adult bone marrow CD34 cells on lentiviral Delta-like-1-modified mouse stromal cells. Immunology 128: e497–505.

27. Salvagiotto G, Zhao Y, Vodyanik M, Ruotti V, Stewart R, et al. (2008) Molecular profiling reveals similarities and differences between primitive subsets of hematopoietic cells generated *in vitro* from human embryonic stem cells and *in vivo* during embryogenesis. Exp Hematol 36: 1377–1389.

28. Lu SJ, Li F, Vida L, Honig GR (2004) CD34+CD382 hematopoietic precursors derived from human embryonic stem cells exhibit an embryonic gene expression pattern. Blood 103: 4134–4141.

29. La Motte-Mohs RN, Herer E, Zuniga-Pflucker JC (2005) Induction of T-cell development from human cord blood hematopoietic stem cells by Delta-like 1 *in vitro*. Blood 105: 1431–1439.

30. Schmitt TM, Zuniga-Pflucker JC (2002) Induction of T cell development from hematopoietic progenitor cells by delta-like-1 *in vitro*. Immunity 17: 749–756.

31. Chang KH, Nelson AM, Fields PA, Hesson JL, Ulyanova T, et al. (2008) Diverse hematopoietic potentials of five human embryonic stem cell lines. Exp Cell Res 314: 2930–2940.

32. Choi KD, Yu J, Smuga-Otto K, Salvagiotto G, Rehrauer W, et al. (2009) Hematopoietic and endothelial differentiation of human induced pluripotent stem cells. Stem Cells 27: 559–567.

33. Feng Q, Lu SJ, Klimanskaya I, Gomes I, Kim D, et al. Hemangioblastic derivatives from human induced pluripotent stem cells exhibit limited expansion and early senescence. Stem Cells 28: 704–712.

34. Grigoriadis AE, Kennedy M, Bozec A, Brunton F, Stenbeck G, et al. Directed differentiation of hematopoietic precursors and functional osteoclasts from human ES and iPS cells. Blood 115: 2769–2776.

35. Lengner CJ, Gimelbrant AA, Erwin JA, Cheng AW, Guenther MG, et al. Derivation of pre-X inactivation human embryonic stem cells under physiolog- ical oxygen concentrations. Cell 141: 872–883.

36. Hanna J, Cheng AW, Saha K, Kim J, Lengner CJ, et al. Human embryonic stem cells with biological and epigenetic characteristics similar to those of mouse ESCs. Proc Natl Acad Sci U S A 107: 9222–9227.

37. Bhatia M, Bonnet D, Kapp U, Wang JC, Murdoch B, et al. (1997) Quantitative analysis reveals expansion of human hematopoietic repopulating cells after short- term ex vivo culture. J Exp Med 186: 619–624.

Chapter 3: Cell type, peptide affinity, and accessory molecules contribute to unique calcium signaling profiles during positive and negative selection *in situ*

3.1 Introduction

During development, the T cell receptors (TCRs) expressed by thymocytes are screened for their ability to recognize peptide-MHC complexes at the immature $CD4^+CD8^+$ (double positive, DP) stage, a process known as positive selection. Additionally, auto-reactive DP, as well as $CD4^+$ and $CD8^+$ single positive (SP) thymocytes, are eliminated during negative selection to produce a protective, yet self-tolerant, T cell repertoire. One widely held model of thymocyte selection posits that weak TCR signals promote thymocyte survival and differentiation whereas stronger signals lead to deletion by negative selection[1]. It is unclear, however, how this difference in signal strength relates to the duration and frequency of TCR signaling events and the dynamics of contact between thymocytes and peptide-MHC bearing cells. Moreover, positive and negative selection are mediated by distinct cell types within the thymus, but the contribution of peptide presenting cell type to the temporal pattern of TCR signaling during positive versus negative selection is not known.

In a landmark study that sought to identify differences in signaling during positive and negative selection, MHC-tetramers loaded with peptide variants were used to stimulate thymocytes *in vitro*. Low, sustained increases in cytosolic calcium in response to low affinity peptides and strong, transient increases in calcium in response to high affinity peptides were observed. In addition, this group also identified a sharp affinity threshold that correlated with both these signaling differences and the ability of these peptides to induce positive versus negative selection in fetal thymic organ culture[2]. While this study provided key information about the role of peptide affinity in determining the distinct signals representative of positive and negative selection, it did not allow for the dissection of other critical factors that contribute to thymocyte selection *in vivo*, including the nature of the peptide-MHC bearing cells and the impact of thymocyte motility. This information is crucial given that thymocytes only undergo efficient positive selection when in contact with a three-dimensional stromal cell network and the observation that immature thymocytes are highly motile within this network[3-9].

Dynamic imaging of thymocytes within thymic tissue slices has revealed that TCR-induced calcium signals associated with positive selection induce migratory arrest[9]. This finding suggests that the calcium flux generated upon initial encounter with positive selecting ligands helps to prolong the interaction with peptide-MHC bearing stromal cells, which was estimated to last 15-30 minutes in this system[9]. This study examined MHC class II-restricted positive selection, and there are indications that the signals for positive selection of MHC class I-restricted thymocytes are weaker and/or of shorter duration[10, 11]. Moreover, this study focused on positive selection, and thus how the TCR signaling kinetics and thymocyte migration differ during positive and negative selection has not yet been examined.

Here, we used changes in cytosolic calcium levels and motility to monitor MHC class I-restricted TCR signaling events in thymocytes undergoing positive and negative selection *in situ*. We observed that MHC class I-restricted thymocytes undergo brief (~4 minute) and relatively infrequent (~1/hour) signaling events separated by periods of low cytosolic calcium and

migration during positive selection. In contrast, during negative selection, thymocytes experienced prolonged signaling events characterized by persistently elevated calcium, NFAT re-localization to the nucleus, and migratory arrest. We tested the role of peptide affinity and peptide-MHC bearing cell type and found that both lower affinity peptides and presentation by radiation resistant thymic stromal cells contribute to more transient signaling events associated with positive selection. These data provide the first direct comparison of the temporal pattern of TCR signaling and motility changes during positive versus negative selection within living thymic tissue, and suggest that the absence of strong stop signals and transient TCR signaling events are important features distinguishing positive from negative selection.

3.2 Results

Synchronized positive and negative selection in thymic slices

To establish the ability of the thymic slice model to support positive selection of MHC class I-restricted thymocytes, we used a relatively homogeneous population of pre-selection TCR transgenic (tg) DP cells overlaid on thymic slices in the presence or absence of positively selecting ligand. Pre-selection OT1 TCR transgenic Rag2ko DP (herein called OT1tg) cells were overlaid onto thymic slices from H2-b (wild type, WT) (positive selecting), or MHC deficient (MHCko) (non-selecting) mice, and differentiation into $CD8^+$ SP thymocytes was assessed by flow cytometry over time. OT1tg cells on WT thymic slices gave rise to a significant population of $CD8^+$ SP cells at 72 hours (Fig. 3.1a and b). In contrast, OT1tg thymocytes on MHCko slices failed to up-regulate CD69 and maintained their CD4 and CD8 expression over time (Fig. 3.1a and b). The $CD8^+$ SP cells that developed on WT slices expressed the conventional CD8αβ heterodimer and down-regulated CD24, suggesting development into mature, conventional $CD8^+$ SP cells (Fig. 3.1c and d). Addition of the negatively selecting OVA peptide (OVAp) induced more substantial CD69 up-regulation, followed by significant depletion of OT1tg DP cells by 24 hours (Fig. 3.1a). We obtained similar results using another MHC class I-restricted, HY^{CD4} TCR transgenic mouse which models negative selection to endogenous antigen[12]. Mature, $T3.70^+$ (HY TCR^+) $CD8^+$ SP thymocytes emerged in slices prepared from female WT mice (positive selecting), whereas a reduction in DP thymocytes without the generation of $CD8^+$ SP occurred on slices from male WT mice (negative selecting) (Fig. 3.1e). These data demonstrate the ability of this experimental model to support a synchronized wave of pre-selection MHC class I-restricted DP thymocytes undergoing positive and negative selection *in situ*.

Distinct TCR signaling and migration signatures associated with positive versus negative selection *in situ*

Much of our information about the TCR signaling events that influence thymic selection derives from studies of dissociated thymocytes under *in vitro* conditions that do not support positive selection and in which thymocytes are non-motile. To directly examine TCR signals and thymocyte motility during positive selection via MHC class I, we loaded OT1tg cells with a ratiometric calcium indicator dye, Indo-1 LR, and overlaid the thymocytes onto thymic slices from either WT or MHCko mice. We then imaged the labeled OT1tg thymocytes within the slices by two-photon time-lapse microscopy within 2-4 hours after thymocyte addition to the slices. Pre-selection DP thymocytes actively migrate and localize preferentially to cortical regions of thymic slices[4, 5, 9]. This allowed us to track individual thymocytes in the cortex over time and determine the ratio of fluorescent signal of calcium bound to unbound Indo-1 dye for each thymocyte at each time point. We expressed the calcium ratio as a corrected value by subtracting the average calcium ratio on non-selecting slices for all conditions and displayed the distribution of calcium values for each thymocyte at each time point (Fig. 3.2a and b). We noted a modest, but reproducible, increase in the proportion of tps in which OT1tg DP cells showed elevated cytosolic calcium levels (corrected calcium ratio >0.15) in WT compared to MHCko slices, consistent with the relatively low intensity signals predicted for positive selection.

If the increase in the frequency of tps with elevated cytosolic calcium for thymocytes on WT compared to MHCko slices is due to positive selection, we would expect it to depend on MHC class I expressed on thymic epithelial cells. To test this, we used recipient thymic slices from bone marrow chimeric mice in which MHCko hematopoietic cells developed in irradiated WT hosts (MHCko → WT). Previous studies have reported increased numbers of positively selected polyclonal thymocytes in MHCko → WT chimeras, indicative of positive selection that is relatively unopposed by negative selection[13-15]. When pre-selection OT1tg thymocytes were introduced onto thymic slices from MHCko → WT bone marrow chimeric mice, we again observed a modest increase in the frequency of cells with elevated calcium compared to those on MHCko slices, comparable to that observed when OT1tg thymocytes were introduced onto WT slices (Fig. 3.2a and b). In contrast, OT1tg thymocytes on WT slices to which OVAp was added (WT+OVA) displayed a substantial increase in the frequency of elevated cytosolic calcium (Fig. 3.2a and b), consistent with the more intense TCR signals predicted for negative selection.

A qualitatively similar pattern of intracellular calcium changes was observed for HY^{CD4} tg thymocytes. HY^{CD4} TCR tg thymocytes on thymic slices from WT female mice (positive selecting) displayed occasional, brief elevations in calcium, whereas HY^{CD4} thymocytes on slices from male mice (negative selecting) displayed more persistent calcium signals (Fig. 3.2c and d). It is noteworthy that the frequency and magnitude of the calcium changes in HY^{CD4} thymocytes were reduced compared to OT1tg thymocytes (Fig. 3.2a-d). This may be due to the fact that only ~50% of DP thymocytes are $TCRtg^{+}$ in this model[12], and/or to lower affinity or abundance of the negative selecting peptide.

Examination of cytosolic calcium in individual thymocytes revealed distinct temporal patterns of calcium changes predominating under positive versus negative selecting conditions (Fig. 3.2e-g). Whereas many OT1 and HY^{CD4} tg thymocytes in negative selecting slices showed consistently elevated calcium over the entire track (average corrected calcium for the track >0.1, and at least one time point >0.2, designated "hi"), the majority of signaling thymocytes under positive selecting conditions displayed transient elevations in calcium with the remainder of the track displaying calcium levels near background (average corrected calcium ratio of track <0.1 and at least one time point >0.2, designated "lo < > hi"). We did not observe prominent thymocyte death under negative selecting conditions, in line with evidence for a 4-12 hour lag between the initial encounter with negative selecting ligands and thymocyte death[16]. Together, these data indicate that positive selection of MHC class I-restricted thymocytes is associated with transient elevations in cytosolic calcium, whereas negative selection is associated with more sustained signals.

To explore the relationship between calcium changes and cell migration in our system, we categorized thymocyte tracks into lo, lo < > hi, and hi categories, and plotted their average speed and directionality for the different selection conditions (Fig. 3.3a). This analysis reveals that thymocytes with low calcium, which are most prominent in non-selecting MHCko slices, display the greater speeds and straighter tracks. In contrast, thymocytes displaying sustained elevated calcium, which predominate in negative selecting (WT+OVA) conditions, tend to be slower and more confined (Figure 3.3a-c). Moreover, for thymocytes in the lo < > hi category that predominate in positive selecting (WT) slices, the inverse relationship between calcium levels and speed can be seen as brief migratory pauses that coincide with transient rises in cytosolic

calcium (Fig 3.3b), consistent with previous reports.[9, 17-19]. The predominance of thymocytes with sustained calcium signaling and low motility in negative selecting WT+OVA conditions is unlikely to be an artifact from supraphysiological concentrations of agonist peptide, since similar responses were observed with HY^{CD4}tg thymocytes in response to endogenous negative selecting signals (Fig. 3.2g and data not shown). Moreover, in a study of negative selection of MHC-experienced thymocytes, very low concentrations of agonist peptide induced all-or-nothing calcium flux and migratory arrest[16]. Thus, a range of negative selecting conditions lead to migratory arrest and sustained calcium signaling, whereas positive selecting conditions are associated with brief, transient signals and continued migration.

Migratory pauses occurring with brief elevations of cytosolic calcium likely correspond to transient periods of active TCR signaling during which thymocytes engage positive selecting ligands. In addition, it is unlikely that thymocytes are engaging positive selecting ligands on immobile thymic epithelial cells while rapidly migrating and displaying low intracellular calcium. We therefore used both motility and calcium levels to define the beginning and end of transient "signaling events" in thymocytes under positive selection conditions (Fig. 3.3b, lower panel). We initially identified signaling events as portions of the cell track during which thymocytes displayed corrected calcium value of >0.2. We then defined "non-signaling" portions of the track as tps in which the interval speed was >6 microns/minute and the corrected calcium was <0.1 (Fig. 3.3b, lower panel). We considered a signaling event to have a beginning when a non-signaling portion of the track preceded it, and to have an end when a non-signaling portion of the track followed it. Based on these criteria we estimate that the average duration of transient signaling events for OT1tg thymocytes on positive selecting slices (WT or MHC → WT) is ~4 minutes (Fig. 3.3d). We also estimated the frequency of signaling events based on the total number of signaling events that began during the run, divided by the cumulative track imaging time. The number of observed signaling events during the cumulative imaging hours suggest a frequency of 1 signaling event / 62 minutes and 1 event / 73 minutes for OT1tg thymocytes on WT and MHCko → WT slices, respectively (Fig. 3.3e). The duration of the imaging runs was typically 20 minutes, and thus the majority of tracks contained one or no signaling events. However, we did occasionally observe tracks with two signaling events separated by a period of migration and low cytosolic calcium. Under non-selecting conditions (MHCko slices) thymocytes also displayed occasional calcium “events”, although these were significantly shorter duration and reduced frequency. Altogether these data indicate that brief, serial signaling events underlie positive selection.

Thymocytes arrest and signal adjacent to cortical DCs during negative selection

In contrast to the transient signals associated with positive selection, the prolonged migratory arrest of thymocytes in the presence of agonist peptide suggested a relatively monogamous interaction with a peptide-MHC bearing cell. While any MHC class I expressing cell in the thymus could potentially present OVAp in this system, we considered whether thymic DCs might play a predominant role in inducing negative selection. Thymic DCs have been implicated in negative selection and, although thymic DCs are most prominent in the medulla, there is also an extensive DC network in the cortex allowing for frequent encounters between thymocytes and DCs[6, 20]. To test whether cortical thymic DCs preferentially present negative selecting ligands, we overlaid pre-selection OT1tg DP thymocytes onto thymic slices from mice expressing a

fluorescent DC reporter, CD11c-YFP[21]. In the absence of OVAp, thymocytes migrated in the vicinity of DCs but did not form stable contacts, maintaining an average distance of ~5 microns from the nearest DC (Fig. 3.4a and b). Strikingly, addition of OVAp to the thymic slices led to the arrest of thymocytes adjacent to DCs, leading to a reduction in the average distance to the nearest DC, particularly for thymocytes with the lowest speeds (Fig. 3.4a and b).

To confirm that thymocytes arrested near cortical DCs are receiving negative selection signals, we used an NFAT-GFP fusion protein to monitor TCR signaling. NFAT relocalizes from the cytosol to the nucleus in response to TCR signaling, and an NFAT-GFP fusion protein has been previously used to monitor TCR signaling by time-lapse microscopy both *in vitro* and *in vivo*[22-25]. We also took advantage of the inherent autofluorescence of thymic DCs to simultaneously monitor thymocyte-DC contacts and the subcellular localization of NFAT in thymocytes. Two-photon microscopy of thymocytes in positive selecting slices revealed freely migrating thymocytes displaying accumulation of NFAT-GFP at the periphery of the cell, consistent with cytosolic location of the fusion protein (Fig. 3.4c, top panels). Addition of OVAp led to the appearance of a population of thymocytes displaying a more central accumulation of NFAT-GFP consistent with nuclear localization (Fig. 3.4c, bottom panels, cell #1). Thymocytes with central NFAT accumulation were typically arrested near autofluorescent cells with dendritic morphology, whereas more motile thymocytes in the same imaging volume displayed a more peripheral NFAT accumulation (Fig. 3.4c, bottom panels, cell #2). To quantify the nuclear versus cytosolic location of NFAT-GFP, we determined the volume of the cell based on a relatively high threshold of NFAT-GFP fluorescence intensity such that thymocytes with centralized accumulation of NFAT-GFP appear to occupy smaller volumes compared to thymocytes with peripheral accumulation (Fig. 3.4d). This trend was most obvious for the slowest cells (Fig. 3.4e). Thus, in response to a broadly distributed agonist peptide, thymocytes preferentially arrest and signal while in contact with cortical DCs.

Distinct responses to agonist peptide presented by cTECs versus DCs

The localization of thymocytes in close proximity to OVAp-bearing DCs suggests that thymocytes preferentially arrest in response to agonist peptide presented by DCs. This is in spite of the presence of OVAp potentially presented on other MHC class I bearing cells, including thymic epithelial cells (TECs). To determine the contributions of peptide-MHC presentation by cTECs versus DCs to thymocyte signaling and migratory arrest, we modified our experimental system to limit MHC class I expression to particular cell types. To restrict OVAp presentation to thymic stromal cells (including cTECs), we prepared thymic slices from MHCko → WT bone marrow chimeric mice and added OT1tg thymocytes and, subsequently, OVAp to the slices (stroma+OVA). Conversely, to restrict OVA presentation to DCs, we added OVAp-loaded DCs to MHCko thymic slices containing pre-selection OT1tg DP thymocytes (DC+OVA). We then assessed thymocyte activation and deletion by flow cytometry, and motility and cytosolic calcium levels by two-photon microscopy.

The presence of OVAp presented by stroma or DCs correlated with substantial up-regulation of CD69 and loss of DP thymocytes compared to either positive selecting or non-selecting conditions (Fig. 3.5a and b). However, restriction of OVAp presentation to the stromal cell

compartment reduced the extent of negative selection compared to samples in which OVAp presentation was restricted to DCs (DC+OVA), as indicated by less robust up-regulation of CD69 and depletion of DP thymocytes (Fig. 3.5a and b). This decrease in the efficiency of negative selection correlated with reduced TCR signals, with stroma+OVA samples displaying a lower proportion of tps with elevated cytosolic calcium (Fig. 3.5c-d) as well as a lower proportion of tracks in the "hi" (sustained signaling) category.

Increases in cytosolic calcium can lead to migratory arrest, thus prolonging interactions with peptide-MHC bearing cells and promoting sustained signals[9, 18]. To examine the influence of the antigen presenting cell type on migratory arrest, we compared the motility of thymocytes in the presence of OVAp presented by DCs versus the thymic stroma (Fig 3.5f). In the presence of OVAp presented by DCs, thymocytes with persistently elevated calcium ("hi" category) showed low motility, consistent with strong migratory arrest. However, when OVAp presentation was restricted to the thymic stroma, a substantial proportion of "hi" signaling thymocytes remained motile or regained motility, indicating a diminished stop signal (Fig. 3.5f).

To further compare the calcium-induced stop signal provided by DCs versus stromal cells, we defined a "typical" signaling event under different experimental conditions. To do so, we identified multiple tracks containing signaling events that began during the imaging run based on a period of elevated calcium (corrected >0.2) preceded by a non-signaling period (speed >6 microns/minute and corrected calcium <0.1). We then aligned these tracks based on the first signaling time point in each track and calculated the average calcium value and speed for all the tracks relative to the onset of the signaling event (Fig. 3.5g). OT1tg thymocytes on a positive selecting slice (MHCko → WT chimeras) displayed a rapid drop in motility coincident with the initial rise in cytosolic calcium, and a return to rapid motility and baseline calcium after several minutes. For thymocytes in the presence of OVAp-loaded DCs, the majority of signaling thymocytes in these samples had low motility and persistently elevated calcium, suggesting that they were already actively signaling at the beginning of the run (Fig. 3.5e and f). However, approximately 12% (14 out of 118 tracks) displayed high motility and low calcium at the beginning of the run and then underwent rapid arrest with increased cytosolic calcium, indicative of the beginning of a signaling event (Fig. 3.5g). Alignment and averaging of these events revealed that calcium levels in response to negative selection signals (DC+OVA) remained well above background and thymocytes remained arrested in their migration for the duration of the imaging run (Fig. 3.5g). Thymocytes in the presence of OVAp presented by radiation resistant stromal cells displayed intermediate behavior, with a detectable, but reduced stop signal. These analyses confirmed that thymic stromal cells are less effective than DCs at inducing persistent TCR signals and migratory arrest.

We also examined the stability of TCR signaling events between thymocytes engaging OVAp on DCs versus cTECs using decay analysis. For thymocytes that were signaling at the beginning of each imaging run, we determined when the signaling event ended based on both a drop in calcium (<0.1 relative calcium ratio) and an increase in motility (interval speed >6 microns/minute). We then determined the proportion of thymocytes that continued signaling over time under different conditions (Fig. 3.5h). For positive selecting samples (WT or MHCko → WT slices), approximately half of the signaling events have terminated ~6 minutes into the run. In contrast, thymocytes in the presence of OVAp-loaded DCs exhibit stable signaling events,

with 68% lasting longer than the imaging run (>20 minutes). Thymocytes on stroma+OVA slices show slightly reduced stability of signaling events relative to DC+OVA, with 52% of signaling events persisting beyond 20 minutes. This provides further indication that encounter with negative selecting peptide on thymic stromal cells provides a weaker stop signal compared to encounter with the same peptide on DCs.

One important feature of DCs that may contribute to their ability to promote migratory arrest and sustained signals is their expression of co-stimulatory molecules, such as ICAM-1 and B7. To examine the contribution of co-stimulatory molecules, we isolated DCs from B7.1 and B7.2 double knock out (B7dko) or ICAMko mice[26, 27], and tested their ability to cause migratory arrest and TCR signaling when presenting OVAp to pre-selection OT1tg DP thymocytes within MHCko thymic slices. We observed a modest, but reproducible reduction in the proportion of tps with elevated calcium with B7dko and ICAMko DCs compared to WT DCs (Fig. 3.6a and b), as well as a reduced proportion of thymocytes with consistently high calcium with some of these calcium high cell tracks remaining motile or regaining motility (Fig. 3.6c and d). In contrast to the 68% of signaling events that persisted beyond 20 minutes when WT DCs present OVAp, for B7dko and ICAM-1ko DCs, only 55% and 40% of signaling events, respectively, persisted beyond 20 minutes (Fig. 3.6e). These differences in the extent and duration of calcium signals between WT and mutant DCs correlated with reduced CD69 up-regulation (Fig. 3.6f), although B7- and ICAM-1-deficient DCs were able to induce negative selection to a similar degree as WT DCs (Fig. 3.6 g). These data suggest that B7 and ICAM-1 play a contributing, but non-essential role in promoting sustained signals during negative selection and that, in their absence, other factors are sufficient to allow for relatively efficient negative selection in this system.

Only high-affinity peptides efficiently induce migratory arrest and sustained TCR signals

The affinity of the TCR for peptide-MHC ligands is thought to be an important parameter in distinguishing positive versus negative selection. To probe the role of peptide affinity on TCR signaling *in situ*, we used a panel of altered peptide ligands (APLs) that have been previously characterized for their relative potency and ability to induce positive and negative selection of OT1tg thymocytes in fetal thymic organ cultures[2]. We overlaid pre-selection OT1tg DP cells onto MHCko thymic slices, added DCs loaded with peptides of different affinities, and examined activation and deletion using flow cytometric analysis and cytosolic calcium levels and motility using time-lapse two-photon microscopy. OVA peptide variants produce a gradient of CD69 up-regulation and DP deletion that correlated with TCR:pMHC affinity (Fig. 3.7a and b). Higher TCR:pMHC affinity also correlated with an increase in the proportion of tps displaying elevated cytosolic calcium, and an increase in the proportion of thymocytes with persistently high calcium (Fig. 3.7c and d). Moreover, higher peptide affinity was associated with more stable interactions with DCs (Fig. 3.7e). Interestingly, for peptides at or below the previously defined positive versus negative selection threshold (T4 and Q7), some calcium "hi" thymocytes remained motile, whereas for peptides with affinity above the negative selection threshold (Q4 and OVA), virtually all calcium "hi" thymocytes displayed low motility (Fig. 3.7f). In addition, whereas for Q4 and OVA peptides, 58% (Q4) and 68% (OVA) of thymocytes that were signaling at the beginning of the run remained signaling for >20 minutes, only 40 and 42% were still signaling

after 20 minutes in the presence of T4 and Q7 peptides, respectively (Fig. 3.7f). Thus, only the highest affinity peptides induced a strong, TCR-mediated stop signal in this system.

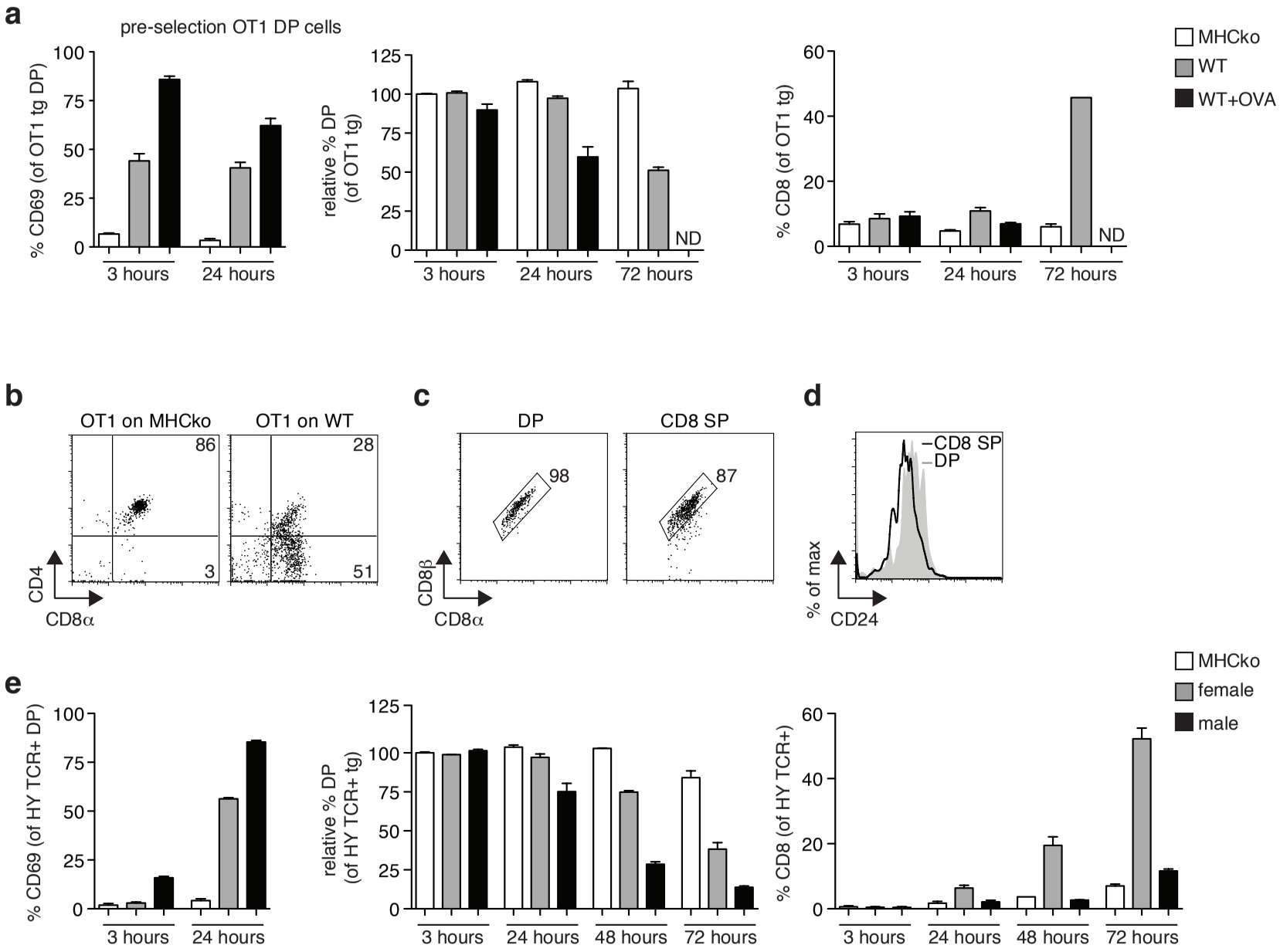
a
pre-selection OT1 DP cells
% CD69 (of OT1 tg DP)
relative % DP (of OT1 tg)
% CD8 (of OT1 tg)
3 hours
24 hours
72 hours
ND
MHCko
WT
WT+OVA
b
OT1 on MHCko
OT1 on WT
86
3
28
51
CD4
CD8α
c
DP
CD8 SP
98
87
CD8β
CD8α
d
CD8 SP
DP
% of max
CD24
e
% CD69 (of HY TCR+ DP)
relative % DP (of HY TCR+ tg)
% CD8 (of HY TCR+)
3 hours
24 hours
48 hours
72 hours
MHCko
female
male

Figure 3.1. Positive and negative selection on thymic slices. Pre-selection TCRtg DP cells were overlaid on thymic slices for 2 hours, then slices were washed, and thymocytes harvested at the times indicated for flow cytometric analysis. **(a)** Relative proportion of CD69 (on OT1 tg+ DP cells) (left panel), DP cells normalized to input DP proportion (middle panel), and $CD8^+$ SP cells (right panel). Bars indicate average of $n \geq 3$ thymic slices from 2 or more independent experiments. Error bars indicate SEM. ND, not done. **(b)** Representative flow plots of OT1tg cells from MHCko or WT thymic slices after 72 hours of incubation stained with CD4 and CD8α. **(c)** CD8αβ heterodimer expression on OT1tg DP or $CD8^+$ SP cells after 72 hours of incubation on WT thymic slices. **(d)** Representative histograms of CD24 expression on OT1tg DP (filled, gray) or $CD8^+$ SP (black, line) cells after 72 hours of incubation on WT thymic slices. **(e)** Relative proportion of CD69 (on $T3.70^+$ HY TCR tg DP cells) (left panel), DP cells normalized to input DP proportion (middle panel), and $CD8^+$ SP cells (right panel). Bar indicates average of triplicate slices from one representative experiment of at least two. Error bars indicate SEM.

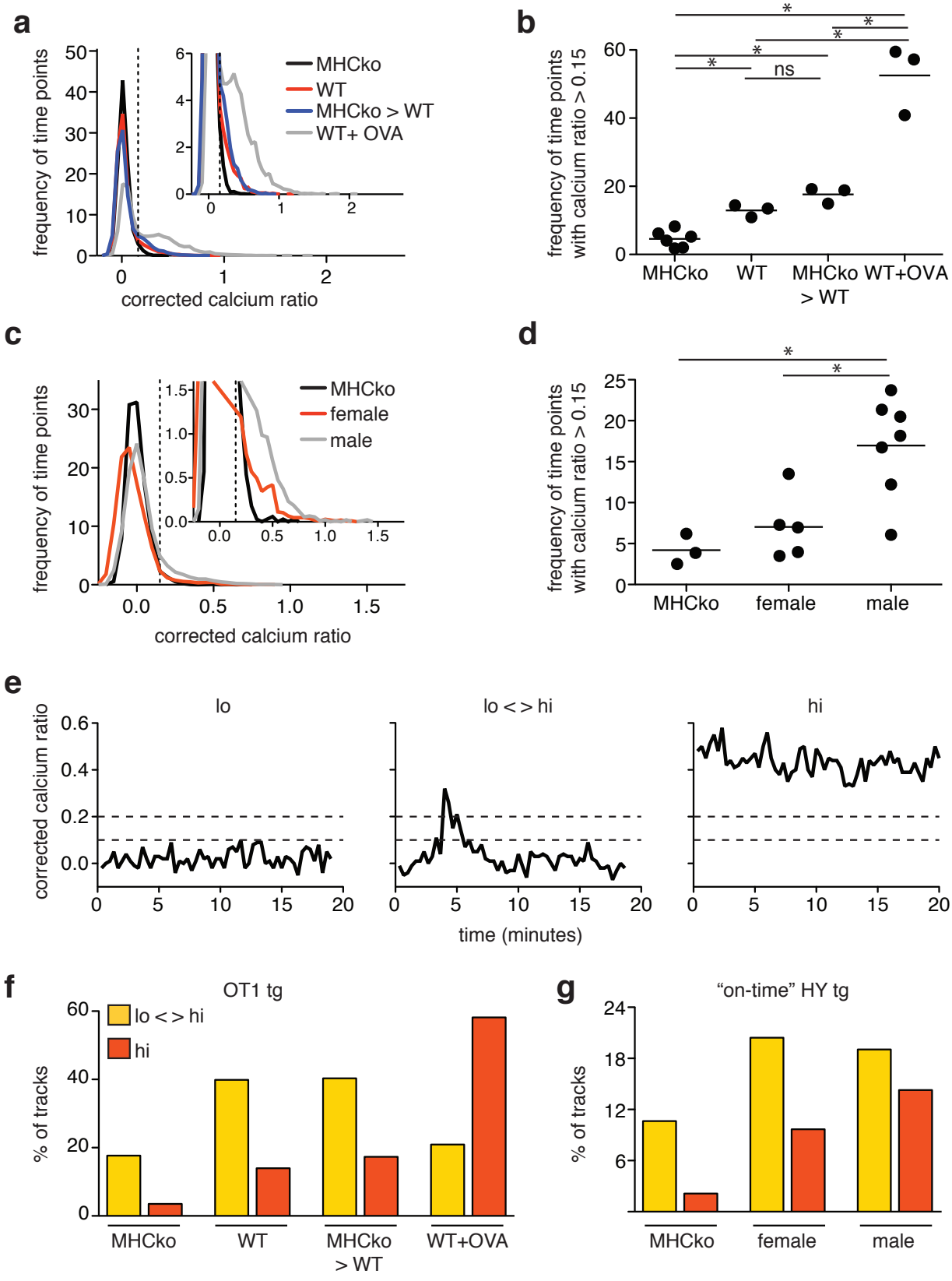
a
frequency of time points
corrected calcium ratio
MHCko
WT
MHCko > WT
WT+ OVA
b
frequency of time points with calcium ratio > 0.15
ns
MHCko
WT
MHCko > WT
WT+OVA
c
frequency of time points
corrected calcium ratio
MHCko
female
male
d
frequency of time points with calcium ratio > 0.15
MHCko
female
male
e
lo
lo < > hi
hi
corrected calcium ratio
time (minutes)
f
OT1 tg
lo < > hi
hi
% of tracks
MHCko
WT
MHCko > WT
WT+OVA
g
"on-time" HY tg
% of tracks
MHCko
female
male

Figure 3.2. Distinct calcium signals in thymocytes undergoing positive and negative selection *in situ*. Pre-selection OT1 or "on-time" HY tg thymocytes were labeled with Indo-1 and allowed to migrate into thymic slices. Two-photon time-lapse imaging was performed 2-4 hours after addition of thymocytes to slice **(a)** The frequency of time points versus the corrected calcium ratio of pre-selection OT1tg DP thymocytes on thymic slices presenting positive (WT and MHCko → WT thymic slices) or negatively (WT+OVA thymic slices) selecting peptides. Dashed line indicates the cut off used to define elevated cytosolic calcium levels. Inset shows an enlarged portion of the graph. For all imaging quantification, data is compiled from a minimum of 3 movies from 2 independent experiments for each condition throughout manuscript unless otherwise noted. For MHCko, n=5416 time points (tps) from 195 cell tracks, for WT, n=7210 tps from 195 cell tracks, for MHCko → WT, n=5896 tps from 159 cell tracks, and for WT+OVA, n=7979 tps from 197 tracks. **(b)** Frequency of time points within individual movies with a corrected calcium value over 0.15 for OT1tg cells. Each dot represents value from one movie. **(c)** The frequency of time points versus the corrected calcium ratio of pre-selection HY tg DP thymocytes on thymic slices presenting positive (female thymic slices) or negatively (male thymic slices) selecting peptides. Inset shows an enlarged portion of the graph. Inset shows an enlarged portion of the graph. **(d)** Frequency of time points within individual movies with a corrected calcium value over 0.15 for HY tg cells. Each dot represents value from one movie. **(e)** Example corrected calcium ratios of individual cells categorized as "lo" or non-signaling tracks (corrected calcium ratio remains below 0.2 for entire track, left), intermittent signaling tracks, "lo < > hi" (corrected calcium ratio goes above 0.2 at least one time point and average corrected calcium ratio for track is below 0.1, middle), or stable "hi" signaling tracks (corrected calcium ratio goes above 0.2 for at least one time point and average corrected calcium ratio for track is above 0.2, right), over the length of a movie. Corrected calcium thresholds of 0.1 or 0.2 indicated by dashed lines. **(f)** Proportion of pre-selection OT1 tg DP cell tracks (>20 time points) in the calcium signaling categories on non-selecting, MHCko slices, positively selecting, WT slices, or negatively selecting WT slices with 1nM OVAp. For MHCko, n=113, for WT, n=143, for MHCko → WT, n=119, and for WT+OVA, n=153 cell tracks. **(g)** Proportion of pre-selection "on-time" HY tg DP cell tracks (>20 time points) in the calcium signaling categories on non-selecting, MHCko slices, positively selecting, WT female slices, or positive and negatively selecting, WT male slices. For MHCko, n=113, for WT, n=143, for MHCko → WT, n=119, and for WT+OVA, n=153 cell tracks.

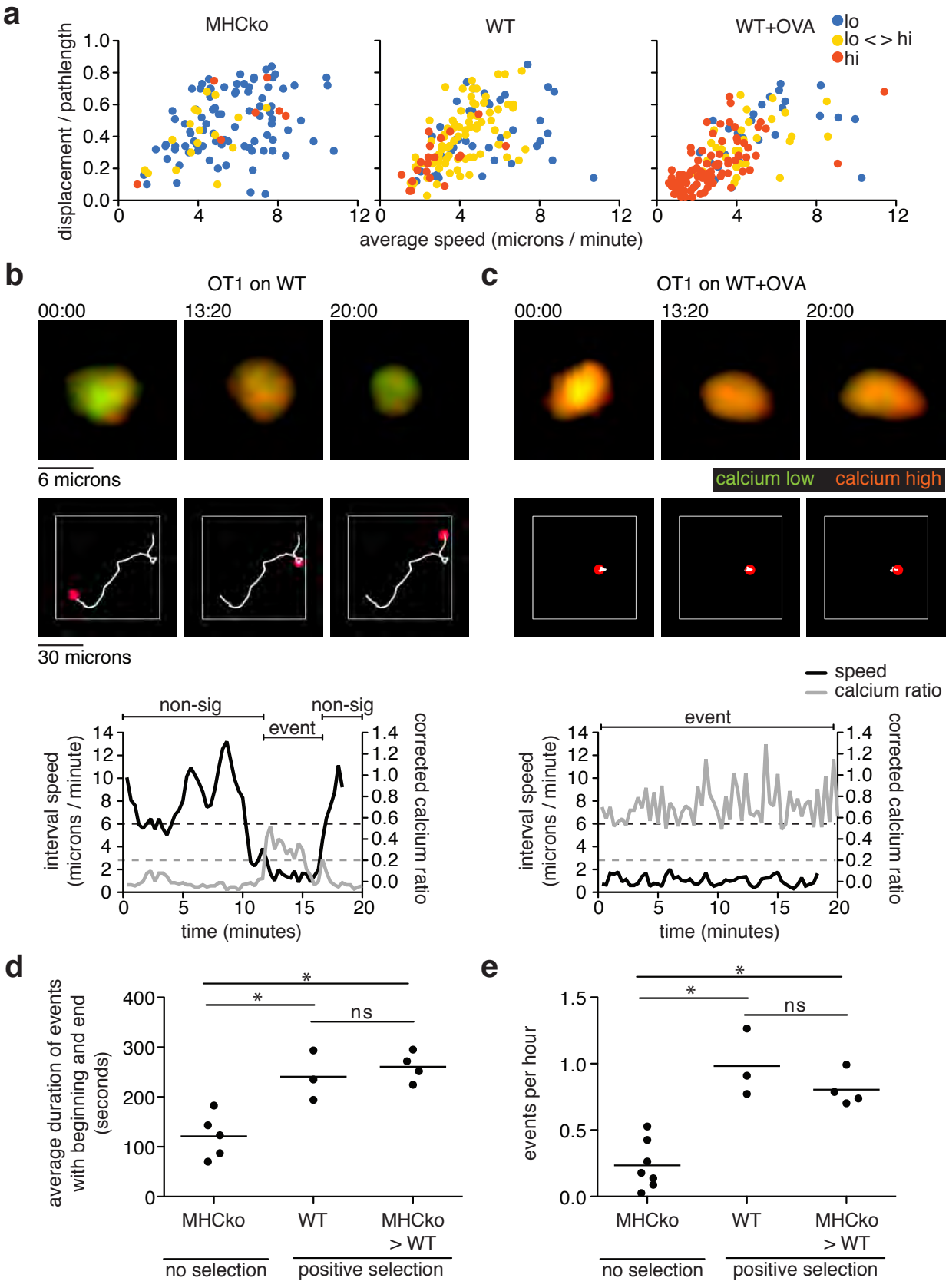
a
MHCko
WT
WT+OVA
lo
lo < > hi
hi
displacement / pathlength
average speed (microns / minute)
b
OT1 on WT
00:00
13:20
20:00
6 microns
30 microns
c
OT1 on WT+OVA
calcium low
calcium high
speed
calcium ratio
non-sig
event
interval speed (microns / minute)
corrected calcium ratio
time (minutes)
d
average duration of events with beginning and end (seconds)
ns
MHCko
WT
MHCko > WT
no selection
positive selection
e
events per hour

Figure 3.3. Inverse correlation between calcium signaling and motility. (a) Speed and straightness (displacement / path length) of pre-selection OT1 tg DP cells in non-selecting, positive selecting, and negatively selecting conditions. Each dot indicates an individual cell track (>20 time points) and is color-coded according to calcium signaling category. For MHCko, n=113, for WT, n=143, and for WT+OVA, n=153 cell tracks. **(b and c)** Representative images as well as calcium and motility plots of an OT1tg DP cell signaling on a WT, positively selecting slice (left panels) or on a WT slice in the presence of OVA (right panels). Top panels, green indicates unbound Indo-1 dye emission, and red indicates calcium bound dye emission over time as indicated. Middle panels, white line indicates cell track for the duration of the movie with red spot indicative of the location of the cell at indicated time points. Bottom panels, corrected calcium ratios are shown in gray and speed is shown in black. Dashed gray line indicates calcium signaling threshold of 0.2, and dashed black line indicates speed threshold of 6 microns / minute based on average speed over five time points (100 seconds). Regions of the cell track identified as signaling and non-signaling are indicated**. (d)** Quantification of the duration of signaling events that both began and ended within the imaging period under non-selecting and positive selecting conditions. Each dot represents average value from one movie. **(e)** Quantification of the frequency of signaling events under non-selecting and positive selecting conditions (number of signaling events that begin per hour). Each dot represents average value from one movie.

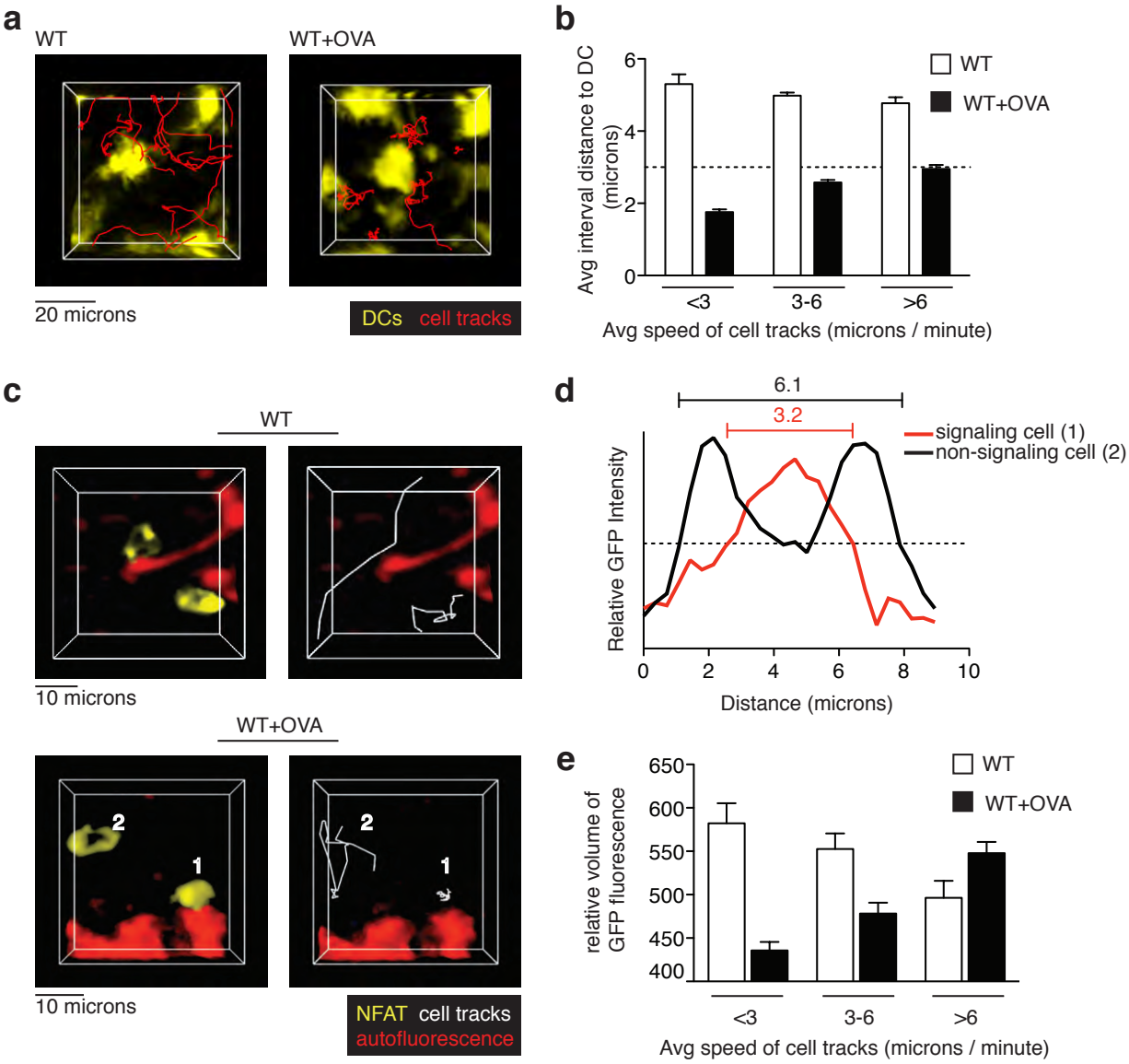
a
WT
WT+OVA
20 microns
DCs cell tracks
b
Avg interval distance to DC (microns)
WT
WT+OVA
<3
3-6
>6
Avg speed of cell tracks (microns / minute)
c
WT
10 microns
WT+OVA
2
1
10 microns
NFAT cell tracks
autofluorescence
d
6.1
3.2
signaling cell (1)
non-signaling cell (2)
Relative GFP Intensity
Distance (microns)
e
relative volume of GFP fluorescence
WT
WT+OVA
<3
3-6
>6
Avg speed of cell tracks (microns / minute)

Figure 3.4. TCR signaling predominantly occurs near DCs during negative selection. (a) Representative image of cell tracks of pre-selection OT1 tg DP cells (red) in the cortex of CD11c YFP thymic slices. **(b)** Quantification of pre-selection OT1tg DP cell interactions with CD11c YFP tg DCs versus average track speed in the presence or absence of negatively selecting OVAp. Dashed line indicates cell contact (approximately the radius of a typical DP cell.) Data quantified from 1 representative movie of 3. For WT, n= 103 and for WT+OVA, n=65 cell tracks. **(c-e)** Pre-selection OT1 tg DP thymocytes expressing NFAT-GFP overlaid on WT thymic slices or WT thymic slides with OVAp. **(c)** Representative images of NFAT-GFP pre-selection OT1 tg DP cells relative to autofluorescent signals in WT and WT+OVA slices. Examples of NFAT-GFP in the nucleus of a non-migrating (1) thymocyte and in the cytoplasm of a migrating (2) thymocyte are indicated in negatively selecting WT+OVA conditions. **(d)** Distribution of fluorescence throughout the length of a cell. **(e)** Analysis of the relative volume of NFAT-GFP fluorescence versus average track speed in the presence or absence of OVAp. Data quantified from 1 representative movie of 3. For WT, n=15 and for WT+OVA, n=31 cell tracks.

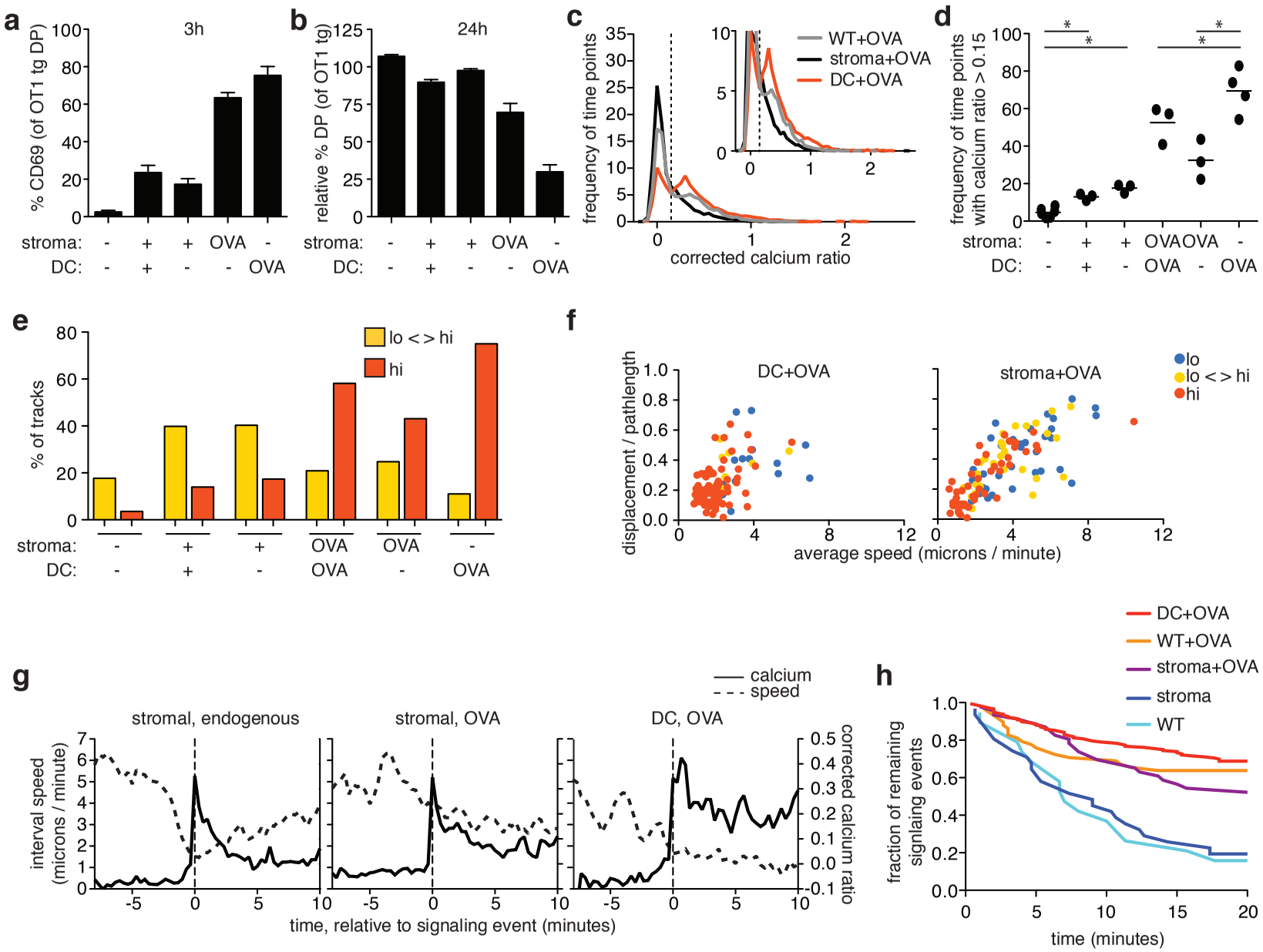
a
3h
% CD69 (of OT1 tg DP)
stroma:
DC:
b
24h
relative % DP (of OT1 tg)
c
frequency of time points
corrected calcium ratio
WT+OVA
stroma+OVA
DC+OVA
d
frequency of time points with calcium ratio > 0.15
e
% of tracks
lo <> hi
hi
f
DC+OVA
stroma+OVA
displacement / pathlength
average speed (microns / minute)
lo
lo <> hi
hi
g
calcium
speed
stromal, endogenous
stromal, OVA
DC, OVA
interval speed (microns / minute)
corrected calcium ratio
time, relative to signaling event (minutes)
h
DC+OVA
WT+OVA
stroma+OVA
stroma
WT
fraction of remaining signlaing events
time (minutes)

Figure 3.5. Radiation-resistant stromal cells do not support effective negative selection or sustained calcium signals. Pre-selection OT1 tg DP cells were overlaid on thymic slices in the presence or absence of 1nM OVAp presented by DCs or radiation resistant stromal cells (MHCko → WT BM chimeras). **(a)** Up-regulation of CD69 on DP thymocytes 3 hours after the addition of 1nM OVAp. **(b)** Relative decrease in the proportion of OT1 tg DPs 24h after the addition of 1nM OVAp. For **(a)** and **(b)**, bar indicates average of triplicate slices from one representative experiment of at least two. Error bars indicate SEM. **(c)** The frequency of time points versus the corrected calcium ratio of pre-selection OT1 tg DP thymocytes on thymic slices in the presence or absence of 1nM OVAp presented by DCs or radiation resistant stromal cells. (WT+OVA included for comparison from Fig. 3.2a) Dashed line indicates the cut off value used to define elevated cytosolic calcium levels. Inset shows an enlarged portion of the graph. For stroma+OVA, n=5348 tps from 153 cell tracks and for DC+OVA, n=5444 tps from 114 cell tracks. **(d)** Frequency of time points within individual movies with a corrected calcium value over 0.15 for OT1 tg cells overlaid on slices as indicated. Each dot represents value from one movie (data in first four conditions included from Fig 3.2b for reference.) **(e)** Proportion of pre-selection OT1tg DP cell tracks (>20 time points) on thymic slices as indicated in the calcium signaling categories. MHCko, WT, MHCko → WT, and WT+OVA conditions are included from Fig. 3.2f for comparison. For stroma+OVA, n=5348 tps from 153 cell tracks and for DC+OVA, n=5444 tps from 114 cell tracks. **(f)** Speed and straightness (displacement / path length) of pre-selection OT1 tg DP cells in encountering OVAp presented by DC or stromal cells. Each dot indicates an individual cell track and is color-coded according to calcium signaling category. For DC+OVA, n=98 and for stroma+OVA, n=109 cell tracks. **(g)** Average corrected calcium ratio and interval speed of signaling cell tracks aligned at tp=0 as signal trigger event (indicated by dashed line) over time of OT1tg DP cells overlaid on slices as indicated. For stromal, endogenous, n=37, for stroma, OVA, n=30, and for DC, OVA, n=14 averaged cell tracks. **(h)** Proportion of thymocytes that were signaling at the beginning of each imaging run that remained signaling over time in the presence or absence of OVAp presented by stromal cells or DCs. For DC+OVA, n=176, for WT+OVA, n=58, for stroma+OVA, n=46, for stroma, n=31, and for WT, n=19 signaling cells at 0 minutes.

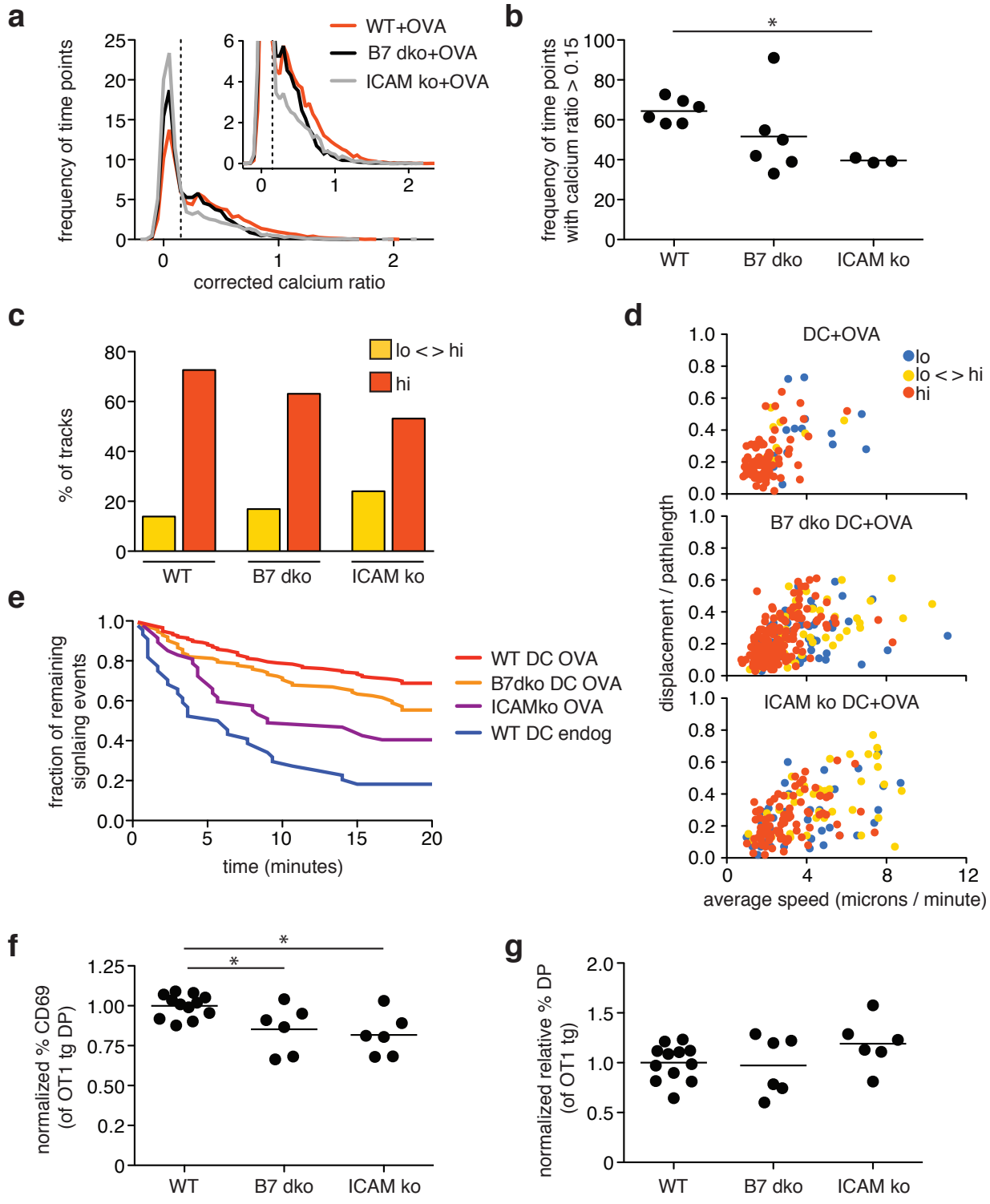
a
WT+OVA
B7 dko+OVA
ICAM ko+OVA
frequency of time points
corrected calcium ratio
b
frequency of time points with calcium ratio > 0.15
WT
B7 dko
ICAM ko
c
% of tracks
lo < > hi
hi
d
DC+OVA
B7 dko DC+OVA
ICAM ko DC+OVA
displacement / pathlength
average speed (microns / minute)
e
fraction of remaining signlaing events
time (minutes)
WT DC OVA
B7dko DC OVA
ICAMko OVA
WT DC endog
f
normalized % CD69 (of OT1 tg DP)
g
normalized relative % DP (of OT1 tg)

Figure 3.6. Co-stimulatory and adhesion molecules contribute to sustained calcium signaling during negative selection. Pre-selection OT1 tg DP cells were overlaid onto MHCko thymic slices for 2 hours, slices were washed, and WT, B7dko, or ICAMko DCs loaded with 1nM OVAp were overlaid on the slices as indicated. **(a)** The frequency of time points versus the corrected calcium ratio of pre-selection OT1 tg DP thymocytes on thymic slices with 1nM OVAp presented by WT, B7dko, or ICAMko DCs. indicates the cut-off used to define elevated cytosolic calcium levels. Inset shows an enlarged portion of the graph. For WT DCs, n= 15719 tps from 332 cell tracks, for B7dko DCs, n=13841 tps from 307 cell tracks, and for ICAMko DCs, n=8286 tps from 176 cell tracks. **(b)** Frequency of time points within individual movies with a corrected calcium value over 0.15 for OT1 tg cells overlaid on MHCko slices in the presence of WT, B7dko, or ICAMko DCs loaded with 1nM OVAp as indicated. Each dot represents value from one movie from a minimum of two independent experiments. **(c)** Proportion of pre-selection OT1 tg DP cell tracks (>20 time points) in the calcium signaling categories in the presence of 1nM OVAp presented by WT, B7dko, or ICAMko DCs. For WT+OVA, n=290, B7 dko, n=260, and for ICAM ko, n=159 cell tracks. **(d)** Speed and straightness (displacement / path length) of pre-selection OT1 tg DP cell tracks (>20 time points) in encountering OVAp presented by WT, B7dko, and ICAMko DCs. Each dot indicates an individual cell track and is color-coded according to calcium signaling category. For WT+OVA, n=290, B7 dko, n=260, and for ICAM ko, n=159 cell tracks. **(e)** Persistence of signaling over time in the presence or absence of OVAp presented by WT, B7dko, or ICAMko DCs. WT DC OVA included from Fig. 5G for comparison. For B7dko DC OVA, n=112, for ICAMko DC OVA, n=47, and for WT DC endog, n=44 signaling cells at 0 minutes. **(f)** Up-regulation of CD69 on DP thymocytes 3 hours after the addition of WT, B7dko, or ICAMko OVAp-loaded DCs. **(g)** Relative decrease in the proportion of OT1 tg DPs 24h after the addition of OVAp-loaded WT, B7dko, or ICAMko DCs. For f and g, each dot represents data from one slice that has been normalized to the average of the WT DC sample within each experiment. The bar indicates the average and data is from a minimum of two independent experiments.

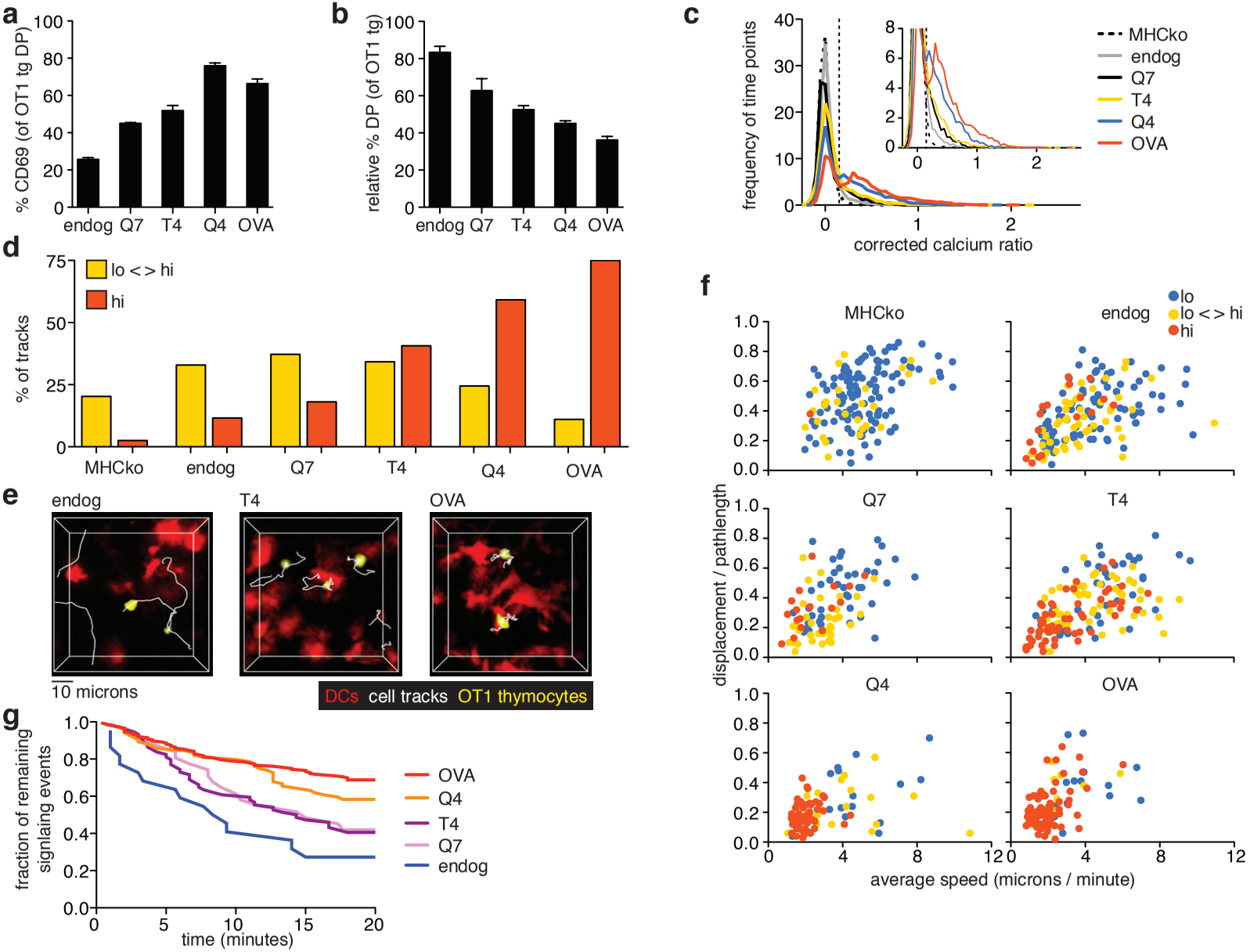
a
% CD69 (of OT1 tg DP)
endog Q7 T4 Q4 OVA
b
relative % DP (of OT1 tg)
endog Q7 T4 Q4 OVA
c
frequency of time points
corrected calcium ratio
MHCko
endog
Q7
T4
Q4
OVA
d
% of tracks
lo <> hi
hi
MHCko endog Q7 T4 Q4 OVA
e
endog
T4
OVA
10 microns
DCs cell tracks OT1 thymocytes
f
MHCko
endog
lo
lo <> hi
hi
Q7
T4
Q4
OVA
displacement / pathlength
average speed (microns / minute)
g
fraction of remaining signlaing events
time (minutes)
OVA
Q4
T4
Q7
endog

Figure 3.7. Increasing TCR:pMHC avidity correlates with a switch from intermittent to sustained signaling. Pre-selection OT1 tg DP cells were overlaid on MHCko thymic slices for 2 hours, washed, and DCs loaded with 1nM of OVAp or APLs were overlaid on the slices as indicated. **(a)** Up-regulation of CD69 on DP thymocytes 3 hours after the addition of peptide-loaded DCs. **(b)** Relative decrease in the proportion of OT1 tg DPs 24h after the addition of peptide-loaded DCs. For **(a)** and **(b)**, bar indicates average of triplicate slices from one representative experiment of at least two. Error bars indicate SEM. **(c)** The frequency of time points versus the corrected calcium ratio of pre-selection OT1 tg DP cells in the presence or absence of DCs loaded with OVAp and APLs. Dashed line indicates the cut-off used to define elevated cytosolic calcium levels. Numbers in parentheses indicate average corrected calcium ratio. Inset shows an enlarged portion of the graph. DC+OVA from Fig. 3.5c included for reference. For MHCko, n=7704 tps from 131 cell tracks, for endog, n=7671 tps from 229 cell tracks, for Q7, n=4565 tps from 104 cells tracks, for T4, n=7714 tps from 214 cell tracks, and for Q4, n=5367 tps from 110 cell tracks. **(d)** Proportion of pre-selection OT1tg DP cell tracks (>20 time points) in the calcium signaling categories in the presence of OVAp or APLs presented by WT DCs. WT+OVA included from Fig. 3.5e included for reference. For MHCko, n=149, for endog, n=155, for Q7, n=94, for T4, n=155, and for Q4, n=98 cell tracks. **(e)** Representative tracks (white) of pre-selection OT1 thymocytes (yellow) interacting with DCs (red) loaded presenting endogenous peptides, T4, or OVAp. **(f)** Speed and straightness (displacement / path length) of pre-selection OT1tg DP cell tracks (>20 time points) in the presence or absence of DCs loaded with OVAp and APLs. Each dot indicates an individual cell track and is color-coded according to calcium signaling category. WT+OVA included from Fig. 3.5f included for reference. For MHCko, n=149, for endog, n=155, for Q7, n=94, for T4, n=155, and for Q4, n=98 cell tracks. **(g)** Persistence of signaling over time in the presence of OVAp or APLs presented by WT DCs. OVA included from Fig. 3.5g and endog included from Fig. 3.6e for comparison. For Q4, n=84, for T4, n=74, and for Q7, n=31 signaling cells at 0 minutes.

3.3 Discussion

The magnitude and duration of signaling events determine downstream transcriptional programs and developmental outcome, yet little is known about the pattern of TCR signaling in thymocytes undergoing positive versus negative selection *in situ*. Here, we used two-photon microscopy to define TCR signaling during MHC class I-restricted thymocyte selection *in situ* under conditions that preserve the dynamic migration of thymocytes and their diverse cellular encounters within intact thymic tissue. We found that, whereas negative selection is associated with prolonged TCR signaling and stable cellular interactions, positive selection involved surprisingly brief and infrequent TCR signals. We also investigated the specific contribution of peptide presenting cell type, co-stimulatory signals, and affinity for pMHC ligands on the pattern of TCR signaling. We found that each of these factors contribute to generating the distinct TCR signaling and intercellular interactions characteristic of positive and negative selection. Our data shed light on how different components of the thymic microenvironment contribute to temporal TCR signaling patterns during positive versus negative selection.

The brief calcium signaling events observed during positive selection *in situ* are in sharp contrast to the sustained rise in cytosolic calcium observed when OT1tg thymocytes were stimulated *in vitro* with MHC class I tetramers loaded with low-affinity peptides[2]. While the reason for this difference is not yet clear, it is tempting to speculate that the motility of thymocytes and the dynamics of contacts with peptide-MHC bearing thymic stromal cells may contribute to the distinct temporal pattern of signaling and ultimately to the ability of thymocytes to successfully undergo positive selection. We propose that the tendency of thymocytes to migrate away from peptide-MHC bearing stromal cells may disrupt TCR engagement and thus favor transient signals. We further speculate that transient TCR engagement and dynamic contacts with peptide-MHC cells may be sufficient to allow for the generation of survival signals while avoiding negative selection, and may help to explain the requirement for a three-dimensional stromal cell network for efficient positive selection.

While positive selection is thought to involve relatively weak TCR signals, there are indications that positive selection of $CD4^+$ T cells may involve somewhat more intense and/or longer duration signals compared to positive selection of $CD8^+$ T cells[10, 11]. In this context it is interesting to compare our results using the class I-restricted OT1tg with a previous study of calcium signals during positive selection of thymocytes bearing an MHC class II-restricted TCR[9]. Although transient signals were also noted in this earlier study, the signals were estimated to last 15-30 minutes, rather than the ~4 minute events reported here. This difference in the duration of TCR signals during MHC class I versus class II positive selection is in line with the requirement for factors that prolong calcium signals in response to weak TCR ligands for $CD4^+$, but not $CD8^+$, T cell development[28]. We, and others, have previously noted that MHC expression is required to sustain low-level expression of activation markers and thymocyte motility in polyclonal DP cells suggestive of low level, tonic TCR signals[5, 6, 29, 30]. It is possible that the brief, infrequent signaling events reported here correspond to these tonic TCR signals and are sufficient to allow for positive selection of $CD8^+$ T cells.

The correlation of positive selection with continued motility and transient signals, raises the question of whether negative selection invariably involves migratory arrest and prolonged

signals. In support of this, we observed a close correlation between the prevalence of immobile, persistently signaling thymocytes and the extent of negative selection under a variety of different experimental conditions. In addition, a parallel study examining negative selection of more mature thymocytes showed that very low concentrations of agonist peptide induced all-or-nothing responses characterized by rapid migratory arrest and prolonged calcium signals, in line with evidence that agonist peptide can induce negative selection, but is ineffective at inducing positive selection, even at very low concentrations[16, 31]. On the other hand, in a steady-state model of AIRE-dependent negative selection, we observed a population of thymocytes that remained motile within confinement zones in the medulla, implying that not all thymocytes remain permanently immobile after encountering negative selecting ligands[7]. It is important to note that this study examined a steady-state population of thymocytes, and it is unclear when individual thymocytes first encountered negative selecting ligands. Indeed, we have reported that thymocyte death can occur between 4-12 hours after synchronous encounter with a negative selecting ligand, leaving an extended time window in which thymocytes could potentially integrate death and survival signals[16]. Together these observations suggest a model in which the initial encounter with a negative selecting ligand leads to migratory arrest and prolonged TCR signals, but under conditions of suboptimal negative selection signals, some thymocytes may get a reprieve. These cells may eventually recover their motility and continue to sample the thymic environment while deciding whether to die or undergo agonist selection[31].

Previous studies of mature T cells have shown that peptide ligand affinity affects the stability of DC contacts with moderate affinity ligands, such as the OVA variant, T4, leading to motile signaling contacts, termed kinapses[32-34]. Consistent with this, we observed a progressive decrease in sustained calcium signals and migratory arrest for thymocytes in the presence of DCs loaded with peptide of decreasing affinity. Interestingly, APLs with affinities above the previously defined positive/negative selection boundary tended to carry a stronger "stop signal". However, we did not observe a sharp transition in the temporal pattern of signaling, as was reported for *in vitro* stimulation with peptide-MHC tetramers[2]. It is important to note, though, that neither tetramer stimulation, nor presentation by DCs supports positive selection. For example, in our study, even low affinity, "positively selecting" APLs induced some negative selection. Additional studies will be needed to fully address the issue of how peptide affinity and peptide presenting cell type work together to allow for appropriate T cell development.

While negative selection to tissue restricted antigens occurs in the thymic medulla following positive selection, there is increasing evidence that negative selection also occurs in the thymic cortex, and that a large proportion of DP thymocytes are deleted due to negative selection[12, 20, 35, 36]. Given the unique ability of cTECs to mediate positive selection, it is of interest to determine how thymocytes respond when they encounter high affinity peptide-MHC ligands on cTECs. Here we present two lines of evidence that suggest that presentation of high affinity peptide by cTECs is much less efficient at inducing stop signals compared to the same peptide presented by DCs. First, thymocytes preferentially arrested and underwent prolonged signaling events adjacent to cortical DCs, in spite of the fact that soluble agonist peptide was added to the slice and presumably presented by all MHC class I bearing cells including cTECs. In addition, thymic slices in which MHC class I was restricted to radiation resistant thymic stromal cells (including cTECs) did not support prolonged migratory arrest and sustained signals in response to strong agonist peptide, which correlated with inefficient negative selection. There are numerous

differences between cTECs and DCs that could account for their differential ability to induce a migratory stop signal. Our evidence that mutations in B7 and other adhesion molecules impair the ability of DCs to engage thymocytes in prolonged TCR signals, indicates that expression of co-stimulatory molecules may be a contributing factor in the duration of these cellular interactions. Thymocytes also express ICAM-2, though to lower levels than ICAM-1[46], which could potentially interact with LFA-1. In the future, it will be interesting to observe signaling and development of LFA-1 deficient thymocytes in the thymic slice system.

In summary, our study is the first to compare the temporal pattern of TCR signaling during positive versus negative selection of thymocytes *in situ*, revealing the unique ability of cortical thymic epithelial cells to provide TCR-mediated signals to developing thymocytes without inducing prolonged calcium signals and strong migratory arrest. Cortical thymic epithelial cells have a number of other properties that likely contribute to their ability to induce positive selection. These include specialized machinery to generate distinct endogenous peptides and a lack of expression of co-stimulatory molecules[37-40]. Future studies combining genetic manipulation of cTECs, together with *in situ* imaging of thymocyte signaling and migration should help to address how the unique properties of cTECs allow them to deliver survival signals to thymocytes while avoiding negative selection.

3.4 Methods

Mice and bone marrow chimeras

All mice were maintained at the American Association of Laboratory Animal Care approved facility in the Life Sciences Addition at the University of California, Berkeley, CA under pathogen-free conditions. All animal procedures were approved by the Animal Care and Use Committee. CD11cYFP tg and Act-CFP tg mice were bred in-house[21, 41]. Pre-selection OT1tg Rag2KO Ly5.1 or OT1tg Rag2KO Ubi-GFP tg thymocytes were generated by transferring 1-5 x 10^6 bone marrow cells intravenously into lethally irradiated, non-selecting MHC I (B2m) or MHC I and II double knock-out (MHCko, Abb-B2m) (Taconic, Germantown, NY)[42-44]. Pre-selection HY^{CD4} tg thymocytes were maintained on a non-selecting H2-D^b knock-out background[20]. Pre-selection HY^{CD4} tg cells were depleted of cell expressing endogenous TCRs by negatively enriched with the EasySep Biotin Positive Selection Kit for depletion as directed by the manufacturer (STEMCELL Technologies, Vancouver, BC, Canada) using anti-CD69-biotin antibody (eBioscience, San Diego, CA). To generate chimeras with radiation-resistant stromal cell-restricted MHC expression, WT C57BL/6 mice were administered purified anti-NK1.1 antibody (UCSF Monoclonal Antibody Core, San Francisco, CA) by intraperitoneal injection and irradiated with two doses of 600 rads prior to intravenous injection of MHCko bone marrow. For generation of NFAT-GFP expressing pre-selection OTI tg cells, OT1 tg mice were injected with 5-fluorouracil (Sigma, St. Louis, MO, USA), and bone marrow cultured in complete DMEM with 20ng/mL rmIL-3, 50ng/mL rmIL-6, and 50ng/mL rmSCF (Peprotech, Rocky Hill, NJ, USA). Phoenix E cells were transfected with NFAT-GFP using Lipofectamine Plus according to manufacturer protocol. Supernatant containing viral particles was mixed with 4mg/mL polybrene and was used to spin infect bone marrow cells. Non-selecting recipients were irradiated with two doses of 600 rads and 0.5-5x10^6 transduced cells intravenously injected.

Thymic slices

Vibratome-cut thymic slices were prepared essentially as described[45]. Individual thymic lobes were embedded in 4% low-melt agarose dissolved in HBSS, and thymic slices at a thickness of 400 microns were used for extended culture, and 500 micron thick slices were used for two-photon imaging. Thymic slices were transferred to 0.4 micron organotypic cell culture inserts and overlaid with 0.5-2x10^6 cells in 10ml of complete DMEM. Cells were applied to slices for 2 hours, washed by gentle, indirect pipetting of PBS, and either overlaid with a second cell population or peptide, glued to cover glass for two-photon imaging, or left in culture as indicated.

Thymocyte labeling

3x10^6 cells/mL were labeled with 2uM final concentration of leakage resistant Indo-1 (TEFLabs, Austin, TX, USA) in complete RPMI for 90 minutes at 37°C, washed once with 10mL RPMI, and allowed to recover for 60 minutes in complete RPMI at 37°C. Thymocytes were labeled with 2mM SNARF-1 or 0.5mM CFDA-SE (Invitrogen, Carlsbad, CA) at a concentration of 1x10^7 cells/mL of PBS for 10 minutes at 37°C, and washed 3 times with complete DMEM before addition to thymic slices.

Flow cytometry

Thymic slices were dissociated to single cell suspensions using glass tissue grinders and filtered using nylon mesh. The following antibodies were used for flow cytometric analysis: anti-mouse CD4-PerCPefluor710, CD8α-efluor450, CD8β-APC, CD24-PE-Cy7, CD69-biotin, streptavidin-APC, and Ly5.1-FITC. Data was collected on an LSRII (BD biosciences, San Jose, CA) and analyzed using FloJo software (Tree Star, Ashland, OR).

Bone Marrow Dendritic Cells

Bone marrow was harvested from the femurs and tibias of mice and resuspended in complete RPMI supplemented with 10ng/mL recombinant murine GM-CSF (Peprotech, Rocky Hill, NJ, USA) at 5 x 10^6 cells per 10mL and plated in petri dishes. On day two of culture, another 10mL of complete RPMI with GM-CSF was added, and every other day, half media changes were performed. Semi-adherent cells were harvested on day 8 of culture.

Peptides

SIINFEKL and the Q7, T4, and Q4 variants were either purchased from AnaSpec (Fremont, CA, USA) or synthesized by Invitrogen (Carlsbad, CA). BMDCs or thymocytes were resuspended at 1 x 10^7 cells/mL and loaded with peptide at a final concentration of 1nM for 20 min at 37°C. Cells were subsequently washed three times with complete DMEM and added to slices at 1 x 10^6 cells/10mL complete DMEM. Alternatively, 1nM was added directly atop the thymic slice and in the media under the cell culture insert.

Two-photon imaging

Thymic slices were maintained at 37°C in oxygenated, phenol red-free DMEM during imaging. Images were acquired on a custom two-photon microscope using a 20X/0.95 Olympus objective and a Spectra-Physics MaiTai Laser tuned to 720nm (Indo-1 imaging) or 920nm (all other imaging). Ratiometric calcium signals were collected using 440nm and 510nm dichroic mirrors and 400/45 and 480/50 bandpass filters. CFP and CFDA-SE were separated using 495nm and 560nm dichroic mirrors, and YFP and SNARF were separated using 560nm and 650nm dichroic mirrors. Image areas of 172 x 143mm to a depth of 200mm were acquired every 20s for 20min with 3mm z steps starting from beneath the cut surface, using custom software.

Image analysis

Imaris software (Bitplane Scientific Software, Saint Paul, MN, USA) was used to process and render the two-photon movies to obtain 3D coordinates of cells for migration behavior as well as the relative intensity of Indo-1 dye for calcium analysis. Two-photon image data was analyzed using standard and custom written MATLAB scripts (Mathworks, Natick, MA, USA), Image J, and Excel. Codes available upon request. Graphing and statistical analysis was done using GraphPad Prism (La Jolla, CA, USA).

For corrected calcium values, 0.675 (the average value under non-selecting conditions for OT1tg) or 0.585 (the average value under non-selecting conditions for HY^{CD4}tg) was subtracted from raw calcium ratios values and cells were considered to be signaling when calcium values rose above 0.2 of the corrected calcium ratio for ≥ 1 time point during the duration of a cell track. Cell tracks were categorized as "lo", non-signaling, if the corrected calcium ratio did not rise over 0.2 for the duration of the track. Cell tracks were categorized as "lo < > hi", oscillating, if the corrected calcium value reached a value of ≥ 0.2 at least one over the duration of the track and the average corrected calcium ration was < 0.1. Cell tracks were categorized as "hi", stable signaling, if the corrected calcium value reached a value of ≥ 0.2 at least one over the duration of the track and the average corrected calcium ration was ≥ 0.1.

3.5 References

1. Starr, T.K., Jameson, S.C. & Hogquist, K.A. Positive and negative selection of T cells. *Annu Rev Immunol* **21**, 139-176 (2003).

2. Daniels, M.A. *et al.* Thymic selection threshold defined by compartmentalization of Ras/MAPK signalling. *Nature* **444**, 724-729 (2006).

3. Anderson, G., Moore, N.C., Owen, J.J. & Jenkinson, E.J. Cellular interactions in thymocyte development. *Annu Rev Immunol* **14**, 73-99 (1996).

4. Ehrlich, L.I., Oh, D.Y., Weissman, I.L. & Lewis, R.S. Differential contribution of chemotaxis and substrate restriction to segregation of immature and mature thymocytes. *Immunity* **31**, 986-998 (2009).

5. Halkias, J. *et al.* Opposing chemokine gradients control human thymocyte migration in situ. *J Clin Invest* (2013).

6. Ladi, E. *et al.* Thymocyte-dendritic cell interactions near sources of CCR7 ligands in the thymic cortex. *J Immunol* **181**, 7014-7023 (2008).

7. Le Borgne, M. *et al.* The impact of negative selection on thymocyte migration in the medulla. *Nat Immunol* **10**, 823-830 (2009).

8. Witt, C.M., Raychaudhuri, S., Schaefer, B., Chakraborty, A.K. & Robey, E.A. Directed migration of positively selected thymocytes visualized in real time. *PLoS Biol* **3**, e160 (2005).

9. Bhakta, N.R., Oh, D.Y. & Lewis, R.S. Calcium oscillations regulate thymocyte motility during positive selection in the three-dimensional thymic environment. *Nat Immunol* **6**, 143-151 (2005).

10. Hogquist, K.A. Signal strength in thymic selection and lineage commitment. *Curr Opin Immunol* **13**, 225-231 (2001).

11. Germain, R.N. T-cell development and the CD4-CD8 lineage decision. *Nat Rev Immunol* **2**, 309-322 (2002).

12. Baldwin, T.A., Sandau, M.M., Jameson, S.C. & Hogquist, K.A. The timing of TCR alpha expression critically influences T cell development and selection. *J Exp Med* **202**, 111-121 (2005).

13. Laufer, T.M., DeKoning, J., Markowitz, J.S., Lo, D. & Glimcher, L.H. Unopposed positive selection and autoreactivity in mice expressing class II MHC only on thymic cortex. *Nature* **383**, 81-85 (1996).

14. van Meerwijk, J.P. *et al.* Quantitative impact of thymic clonal deletion on the T cell repertoire. *J Exp Med* **185**, 377-383 (1997).

15. Bix, M. & Raulet, D. Inefficient positive selection of T cells directed by haematopoietic cells. *Nature* **359**, 330-333 (1992).

16. Dzhagalov, I.L., Chen, K.G., Herzmark, P., Robey, E.A. Elimination of self-reactive T cells in the thymus: a timeline for negative selection. *PLoS Biol* (in press).

17. Donnadieu, E., Bismuth, G. & Trautmann, A. Antigen recognition by helper T cells elicits a sequence of distinct changes of their shape and intracellular calcium. *Curr Biol* **4**, 584-595 (1994).

18. Negulescu, P.A., Krasieva, T.B., Khan, A., Kerschbaum, H.H. & Cahalan, M.D. Polarity of T cell shape, motility, and sensitivity to antigen. *Immunity* **4**, 421-430 (1996).

19. Wei, S.H. *et al.* Ca2+ signals in CD4+ T cells during early contacts with antigen-bearing dendritic cells in lymph node. *J Immunol* **179**, 1586-1594 (2007).

20. McCaughtry, T.M., Baldwin, T.A., Wilken, M.S. & Hogquist, K.A. Clonal deletion of thymocytes can occur in the cortex with no involvement of the medulla. *J Exp Med* **205**, 2575-2584 (2008).

21. Lindquist, R.L. *et al.* Visualizing dendritic cell networks *in vivo*. *Nat Immunol* **5**, 1243-1250 (2004).

22. Aramburu, J. *et al.* Affinity-driven peptide selection of an NFAT inhibitor more selective than cyclosporin A. *Science* **285**, 2129-2133 (1999).

23. Ebert, P.J., Ehrlich, L.I. & Davis, M.M. Low ligand requirement for deletion and lack of synapses in positive selection enforce the gauntlet of thymic T cell maturation. *Immunity* **29**, 734-745 (2008).

24. Marangoni, F. *et al.* The transcription factor NFAT exhibits signal memory during serial T cell interactions with antigen-presenting cells. *Immunity* **38**, 237-249 (2013).

25. Lodygin, D. *et al.* A combination of fluorescent NFAT and H2B sensors uncovers dynamics of T cell activation in real time during CNS autoimmunity. *Nat Med* (2013).

26. Borriello, F. *et al.* B7-1 and B7-2 have overlapping, critical roles in immunoglobulin class switching and germinal center formation. *Immunity* **6**, 303-313 (1997).

27. Sligh, J.E., Jr. *et al.* Inflammatory and immune responses are impaired in mice deficient in intercellular adhesion molecule 1. *Proc Natl Acad Sci U S A* **90**, 8529-8533 (1993).

28. Lo, W.L., Donermeyer, D.L. & Allen, P.M. A voltage-gated sodium channel is essential for the positive selection of CD4(+) T cells. *Nat Immunol* **13**, 880-887 (2012).

29. Azzam, H.S. *et al.* CD5 expression is developmentally regulated by T cell receptor (TCR) signals and TCR avidity. *J Exp Med* **188**, 2301-2311 (1998).

30. Merkenschlager, M. *et al.* How many thymocytes audition for selection? *J Exp Med* **186**, 1149-1158 (1997).

31. Stritesky, G.L., Jameson, S.C. & Hogquist, K.A. Selection of self-reactive T cells in the thymus. *Annu Rev Immunol* **30**, 95-114 (2012).

32. Moreau, H.D. *et al.* Dynamic in situ cytometry uncovers T cell receptor signaling during immunological synapses and kinapses *in vivo*. *Immunity* **37**, 351-363 (2012).

33. Pace, L. *et al.* Regulatory T cells increase the avidity of primary CD8+ T cell responses and promote memory. *Science* **338**, 532-536 (2012).

34. Skokos, D. *et al.* Peptide-MHC potency governs dynamic interactions between T cells and dendritic cells in lymph nodes. *Nat Immunol* **8**, 835-844 (2007).

35. Stritesky, G.L. *et al.* Murine thymic selection quantified using a unique method to capture deleted T cells. *Proc Natl Acad Sci U S A* **110**, 4679-4684 (2013).

36. Daley, S.R., Hu, D.Y. & Goodnow, C.C. Helios marks strongly autoreactive CD4+ T cells in two major waves of thymic deletion distinguished by induction of PD-1 or NF-kappaB. *J Exp Med* **210**, 269-285 (2013).

37. Murata, S. *et al.* Regulation of CD8+ T cell development by thymus-specific proteasomes. *Science* **316**, 1349-1353 (2007).

38. Honey, K., Nakagawa, T., Peters, C. & Rudensky, A. Cathepsin L regulates CD4+ T cell selection independently of its effect on invariant chain: a role in the generation of positively selecting peptide ligands. *J Exp Med* **195**, 1349-1358 (2002).

39. Nakagawa, T. *et al.* Cathepsin L: critical role in Ii degradation and CD4 T cell selection in the thymus. *Science* **280**, 450-453 (1998).

40. Degermann, S., Surh, C.D., Glimcher, L.H., Sprent, J. & Lo, D. B7 expression on thymic medullary epithelium correlates with epithelium-mediated deletion of V beta 5+ thymocytes. *J Immunol* **152**, 3254-3263 (1994).

41. Hadjantonakis, A.K., Macmaster, S. & Nagy, A. Embryonic stem cells and mice expressing different GFP variants for multiple non-invasive reporter usage within a single animal. *BMC Biotechnol* **2**, 11 (2002).

42. Grusby, M.J. *et al.* Mice lacking major histocompatibility complex class I and class II molecules. *Proc Natl Acad Sci U S A* **90**, 3913-3917 (1993).

43. Hogquist, K.A. *et al.* T cell receptor antagonist peptides induce positive selection. *Cell* **76**, 17-27 (1994).

44. Schaefer, B.C., Schaefer, M.L., Kappler, J.W., Marrack, P. & Kedl, R.M. Observation of antigen-dependent CD8+ T-cell/ dendritic cell interactions *in vivo*. *Cell Immunol* **214**, 110-122 (2001).

45. Dzhagalov, I.L., Melichar, H.J., Ross, J.O., Herzmark, P. & Robey, E.A. Two-photon imaging of the immune system. *Curr Protoc Cytom* **Chapter 12**, Unit12 26 (2012).

46. Reiss, Y., Engelhardt, B. T cell interaction with ICAM-1-deficient endothelium *in vitro*: transendothelial migration of different T cell populations is mediated by endothelial ICAM-1 and ICAM-2. *Int Immunol* **11**, 1527-1539 (1999).

Chapter 4: Kinetics of Positive Selection

4.1 Introduction

T cell precursors must be carefully screened during development to produce functional, self-tolerant T cells that make up the peripheral repertoire. As thymocytes develop within an organized and densely packed thymic tissue, these highly motile cells must undergo a screening process that involves positive selection to promote the survival of thymocytes that pass a functional test by ensuring that a T cell receptor (TCR) can recognize antigen in the context of MHC and direct them to the appropriate CD4 or CD8 lineage. Selection therefore requires that developing thymocytes make contact(s) with the stromal cells that support positive selection within the cortex.

It has been estimated that it takes 1-4 days for a "pre-selection" DP thymocyte to complete the process of positive selection (reviewed in Scollay and Godfrey, von Boehmer). We hypothesize that dynamic changes in motility, chemokine responsiveness, and tuning of TCR signaling are an important part of the process of positive selection. However the phenotypic changes, TCR signaling properties, and migratory behaviors that accompany the positive selection and lineage commitment processes are not fully understood. The study of selection events has relied primarily on *in vitro* systems that ultimately failed to support positive selection, such as TCR crosslinking (Suzuki, Hunig, Takahama), stromal cell co-cultures (Palacios, Tatsumi, Larson, Tanaka, Schmitt, Vukmanović), and peptide-MHC-tetramer stimulation (Holmberg, Daniels). While these systems allowed for observation of early signaling kinetics and phenotypic changes downstream of TCR signaling, they may not accurately reflect the nature of selection events as they occur within the 3D context of the thymus. FTOC and RTOC systems maintain a 3D thymic structure that will support positive selection (Anderson, Jenkinson) although using an FTOC system requires a DN starting population that is therefore not readily synchronized at the positive selection stage. RTOCs require up to 12 hours to reform, thereby precluding the observation of early selection events within an ordered 3D context. Additionally, both FTOC and RTOC have no separation of cortex and medulla. In contrast, two-photon imaging studies allow for the observation of migratory changes associated with selection events in their native context. From these studies, it has been inferred that prior to positive selection, DP thymocytes migrate within the cortex via random walk (Bhakta, Witt), and upon encounter with positive selecting ligands undergo calcium dependent stopping (Bhakta) that results in both dynamic and stable interactions with the stromal cell network of the thymus (Bousso). Positive selection also leads to increased, but transient interactions with dendritic cells and capillaries within the cortex (Ladi et al, 08) and ultimately to rapid, directional migration toward the medulla (Witt). However, these studies have relied on the analysis of steady state populations where the developmental status of the thymocyte must be inferred from localization or phenotype. Thus, a detailed kinetic analysis of positive selection following the phenotypic, migratory, and signaling behavior of a synchronized population of positively selecting thymocytes is lacking.

We have used the thymic slice system to characterize the properties of a synchronized wave of thymocytes undergoing positive selection and lineage commitment within their endogenous, 3D, spatiotemporal context. We found that thymocytes underwent activation as early as 3 to a6 hours, as seen by CD69 up-regulation. Over the next 24 hours, thymocytes accumulated TCR signals as

seen by accumulation of Nur77-GFP, and simultaneously decreased CXCR4 while up-regulating CCR7 as they increased their speed, and became less confined. Ultimately, by 48 hours thymocytes began to convert to SP. We also found that within the first few hours after encountering a positively selection ligand, class I-restricted TCR transgenic thymocytes, underwent serial, transient calcium signaling events that correlated with brief migratory pauses. Preliminary data suggest that after 24 hours of positive selection, thymocytes recover more quickly from a calcium dependent stop signal, perhaps reflecting a change in response to TCR signaling over time.

4.2 Results

Kinetics of class I positive selection in the thymic slice model.

It is estimated to take 1-4 days to complete the process of positive selection. Most of our knowledge about the phenotypic, migratory, and signaling behavior of positively selecting thymocytes throughout the selection process is derived from steady state thymocytes that are asynchronous in their development, thereby obscuring precisely how thymocytes are changing over time. Therefore, we set out to characterize a relatively un-manipulated and synchronized population of pre-selection thymocytes within the thymic slice model. We overlaid class I-restricted OTI TCR transgenic pre-selection thymocytes on positive selecting slices (wild type, MHC-bearing, express positive selecting ligand) or non-selecting slices (MHC class I and II deficient, do not express positive selecting ligand) and analyzed development over time by flow cytometry. Within the positively selecting slices, a decrease in the percentage of DP thymocytes and the concurrent appearance of a population of CD8 SP occurred at 48 hours followed by a more prominent population of CD8 SP at 72 hours. (Fig 4.1A and C). This corresponded with an early activation of DP as seen by CD69 up-regulation at 6 hours that was maintained until SP began to develop at 48 hours. In contrast, OT1 thymocytes that were on MHC-deficient slices failed to induce CD69 expression, and did develop into CD8SP (Fig 4.1B). Similar kinetics of activation, DP loss, and conversion to CD8 SP were observed for another class I-restricted TCR, F5 (Fig 4.2A). These kinetics are similar to the estimates reported for *in vivo* positive selection, suggesting that the inferences made from steady state thymocytes development is accurate while simultaneously validating a system that allows us to further explore the changes associated with thymic selection.

Class II positive selection in the thymic slice model.

In an effort to compare CD8 versus CD4 positive selection, we attempted to develop a comparable synchronized system using thymocytes expressing class II specific TCRs. However, when we attempted to generate pre-selection class II restricted thymocytes and observe their development on thymic slices, we encountered two problems. First, we had considerable difficulty in generating sufficient numbers of DP thymocytes using either AND or OTII class II TCR tg pre-selection thymocytes isolated from either non-selecting chimeras or when the TCR was crossed to a non-selecting background. (Yield of DP thymocytes were typically 0.25-1x10^6). Second, in the limited number of experiments that we were able to perform, there was experimental variability in CD4 SP development, with only two out of five experiments yielding CD4 SP development above background. In the two experiments in which we observed development, the two class II-restricted TCR transgenics also displayed similar kinetics, and the CD4 SP down-regulated CD24, suggesting that mature SP developed (Fig 4.2C). However, the ultimate CD4SP population was not as prominent as class I (Fig 4.2A and B). Because development was more obvious in the class I model, further studies were performed with OTI pre-selection thymocytes.

Thymocytes down-regulate CXCR4 and up-regulate CCR7 as they undergo positive selection.

Thymocytes from steady state models with ongoing positive selection are known to have a peak expression of CXCR4 at the DP stage that is down regulated by the time SP develop (Schabath, Suzuki). CCR7 is concurrently being up-regulated during positive selection (Yin), and this ultimately leads to a directed migration to the medulla (Ueno, Campbell, Kwan). Indeed, a subset of wild type DP thymocytes expresses CCR7 (Figure 4.3 A) and CD24 low DPs have higher CCR7 expression (Davalos-Misslitz) and CD69+ cells have an enhanced migration toward CCR7 ligands (Kim, Campbell). Similarly, OTI TCR transgenic steady state thymocytes have a DP population that expresses higher levels of CCR7 and lower levels of CXCR4 (Figure 4.3 C). However, the aforementioned studies looked at steady state thymocytes that were therefore in a range of developmental states so although the CXCR4 down-regulation and CCR7 up-regulation are known to be associated with positive selection, the actual kinetics with which a pre-selection thymocyte changes receptor expression levels remains unknown. In order to observe the kinetics of this process within a synchronized population, we applied pre-selection OTI DP thymocytes to selecting or non-selecting slices and analyzed chemokine receptor level expression over time by flow cytometry. Like the endogenous, wild type DP thymocytes within the slices, OTI pre-selection thymocytes expressed high levels of CXCR4 (Fig 4.3A and 4.4A and C). After 24 hours under positive selection conditions, OTIs down-regulated CXCR4 prior to the development of CD8 SP (Fig 4.4 A and B). CXCR4 was further down-regulated in DP by 48 hours and ultimately, by 72 hours, the CXCR4- population underwent positive selection to become CD8 SP (Fig 4.4 B) as can be seen by the loss of CD4 in the CXCR4- cells (Fig 4.4 A). As previously reported (Yin), positively selected OTIs also up-regulated CCR7 (Fig 4.4 C). Due to the irreproducibility of selection and low numbers of class II pre-selection cells, the chemokine kinetics of class II-restricted TCR transgenics was not performed. However, analysis of steady state TCR transgenics revealed that class I-restricted DP thymocytes down-regulated CXCR4 to a greater extent than class II-restricted DP (Figure 4.3 B). As Yin et al previously reported, CCR7 is up-regulated in a greater proportion of class I restricted DPs undergoing positive selection and the timing of its expression is linked to lineage commitment signals. CXCR4 follows a similar temporal pattern and is likely under similar regulation.

Positively selecting thymocytes become faster and less confined over time.

From previous imaging studies (Bousso, Ladi, Witt) we know that a thymocyte's localization and migratory behavior within the thymus are changing along with its developmental state. In these studies, location or developmental state are often used to infer information regarding the other and development was asynchronous, making it difficult to appreciate the kinetics and nature of the behavioral changes associated with progression through the positive selection process. Therefore, we sought to determine how migration changes over time in a pre-selection cohort of thymocytes under positive selection conditions. Pre-selection thymocytes were overlaid onto either selecting or non-selecting thymic slices for 2 hours, washed, and then imaged by two-photon microscopy at 3, 6, 12, and 24 hours. 3 dimensional volumes were collected over time and individual cells were tracked using Imaris' Bitplane software. Between 3 and 24 hours, thymocytes become less confined as can be reflected in the traces of the tracks of individual cells (Figure 5A). This corresponds with an increase in the average speed of the positively selecting thymocyte population over time relative to the non-selecting control (Figure 4.5 B). The increase

in thymocyte speed over time is accompanied by a down-regulation of CXCR4 and up-regulation of CCR7 over a 24-hour period (Figure 4.4), which is consistent with a decrease in the cortical retention signal seen in human DP (Halkias) and directed migration to the medulla seen after CCR7 up-regulation (Ueno, Campbell, Kwan).

OTI TCR transgenic, pre-selection thymocytes accumulate TCR signals over time.

Because thymocytes are altering their motility over time under positively selecting conditions, we sought to determine the kinetics and extent of TCR signal accumulation during the positive selection process. We utilized a Nur77-GFP BAC transgenic reporter system developed by Moran et al. The Nur77 GFP reporter provides a fluorescent read out for TCR signaling strength that is maintained for several hours. Therefore, we overlaid pre-selection OTI TCR tg Nur77 GFP thymocytes onto selecting or non-selecting thymic slices for 2 hours, washed, and then either analyzed thymocytes by flow cytometry or two-photon microscopy. Consistent with previously published data in steady-state thymocytes, we saw up-regulation of Nur77 GFP in DP thymocytes by flow cytometry in a time-dependent manner under positive selection conditions as compared to the non-selecting control (Figure 4.6 A and B). We also observed in increase in Nur77 GFP by two-photon microscopy over time (Fig 4.6 C and D). The accumulation of Nur77 GFP also corresponded with a loss of confinement and an increase in speed at 24 hours under positive selection conditions (Fig 4.6 D) and ultimately, confirms that migratory changes correspond to an accumulation of TCR signals over time.

Class I restricted, DP thymocytes increase basal calcium levels under positively selecting conditions.

Increased thymocyte speed and accumulation of TCR signals suggests that thymocyte signaling changes during positive selection. Therefore, we further characterized the signaling of thymocytes during development by visualizing calcium signaling over time. To do so, we overlaid pre-selection OTI TCR tg thymocytes with the ratiometric calcium indicator dye, Indo1LR for 2 hours onto selecting or non-selecting slices, washed, and then imaged slices by two-photon microscopy at either 3 or 24 hours. As we had seen before (chapter 2), after 3 hours in a positively selecting environment, thymocytes had an increased level of calcium (Fig 4.7 A) over the non-selecting control. Furthermore, this increase in calcium was maintained at 24 hours. There may have been a greater shift at 24 hours in the positive over non-selecting samples, though reproducibility was an issue (Fig 4.7 A). Of note, there was a dye-dependent shift that occurred over time that is reflected in a basal shift in calcium in the non-selecting slices as well (Fig 4.7 A and B). Temporary spikes in intracellular calcium are associated with a migratory arrest as we and others have previously seen (chapter 2, Bhakta). To determine if thymocytes are changing their responsiveness to a TCR induced stop signal, we performed a bootstrap analysis of calcium ratios to interval speeds. Pooled imaging data revealed that there was a 60% greater increase in the dynamic range of calcium levels experienced by positively selecting thymocytes at 3 compared to 24 hours (Fig 4.7 B and 4.8 A). The trend towards reduced correlation between calcium and speed was observed in individual imaging runs (Figure 4.7 C). Furthermore, aligned signaling events suggest diminished stop signal at 24 hours (Figure 4.8 A). Thus, preliminarily, it

appeared that thymocytes became faster with a less pronounced stop signal and overall higher level of basal calcium. This is perhaps surprising given the inverse relationship between calcium and speed. Ultimately, it appears as though there are two effects of positive selection on calcium levels, the first being transient spikes that are correlated with stopping and the second reflected as a basal increase in calcium levels over time that corresponds to an increase in thymocyte motility over time.

Selection kinetics of an MHC-experienced, semi-mature thymocyte population in the thymic slice model.

Indo1LR dye is slowly eliminated from thymocytes over time. As such, it makes imaging the signaling kinetics of positive selection a challenge as, after 24 hours, the fluorescence signal intensity is greatly reduced. To study any signaling events that occur later than 24 hours, we would ideally load an MHC-experienced, semi-mature population of thymocytes that is still MHC-dependent for selection with Indo dye before overlaying thymocytes onto selecting and non-selecting slices. We tried two depletion models in an effort to isolate an MHC-dependent yet experienced population from steady state OTI TCR transgenic thymocytes. The first depletion we performed was removal of lineage lineage-committed thymocytes from steady state OTIs by sorting the RFP negative population of OTI Rag-/- TCR tg Runx3 RFP thymocytes. Second, we performed a ß7 integrin depletion as post-selection thymocytes are known to up-regulate the α(4)β(7) integrin (Mintern). Both depletions enriched for immature cells as seen by an increase the proportion of DP and CD4 intermediates (these are a transitional population that is characteristic to OTI (Hogquist)) (Fig 4.9 A) as well as an enrichment for CD24 high thymocytes (Figure 4.9 B). β7 integrin depleted thymocytes underwent a robust conversion to CD8 SP (Figure 4.9 C and E) and down-regulation of CD24 (Figure 4.9 D) in positively selecting slices and to a lesser degree in non-selecting slices suggesting that thymocytes were a mixture of MHC-dependent and independent developmental states. The Runx3 RFP depleted thymocytes developed into CD8SP independently of MHC expression in the thymic slice (Figure 4.9 E). Ultimately, depletion of the most mature subsets, through integrin or lineage reporter depletion yielded a population that gave rise to CD8 SP with faster kinetics than pre-selection thymocytes (compare to Fig 4.1 A and C), Because the β7 integrin depleted thymocytes were generally MHC-dependent, they will be the most useful population for future imaging studies.

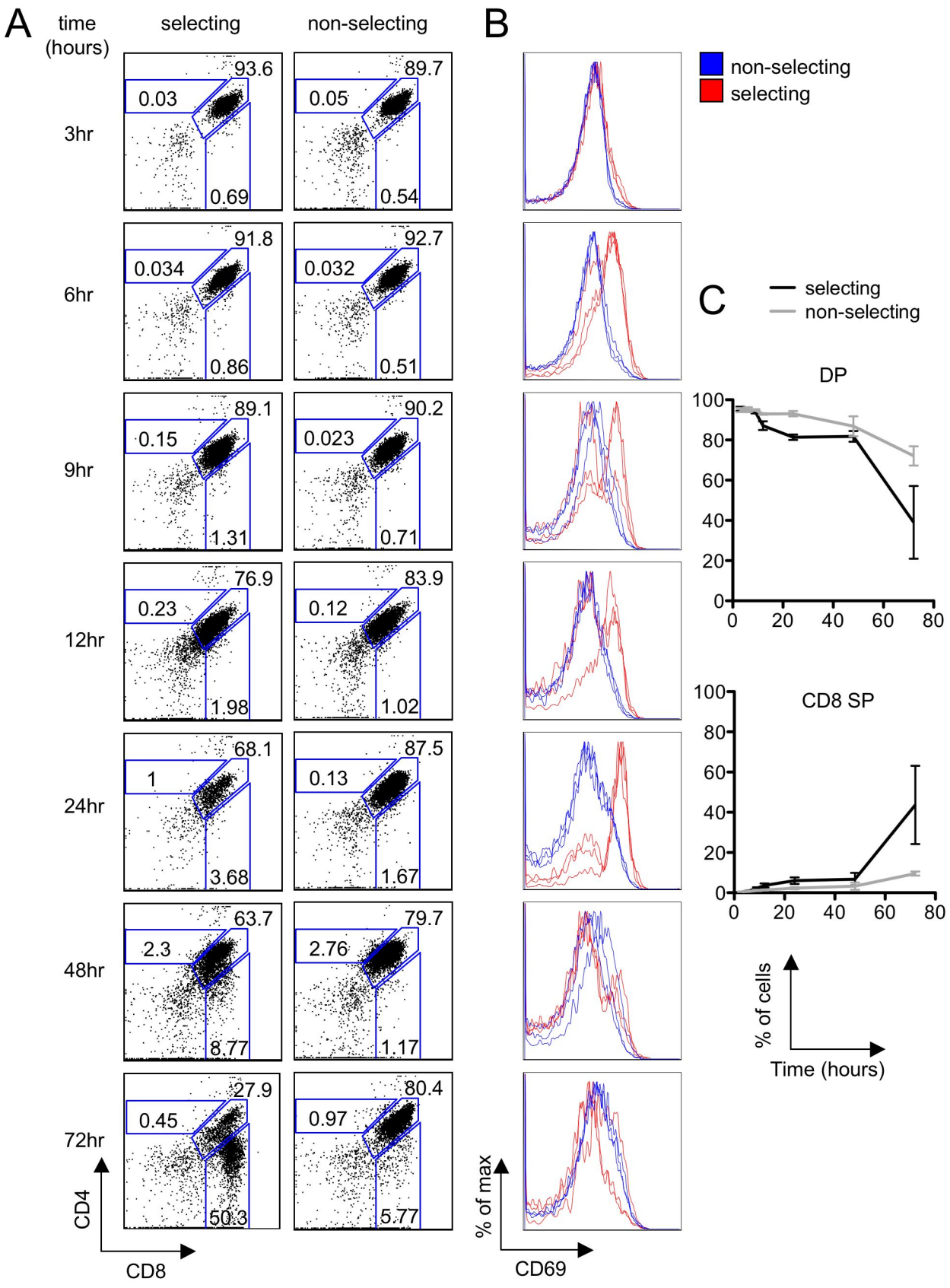
A
time (hours)
selecting
non-selecting
3hr
6hr
9hr
12hr
24hr
48hr
72hr
93.6
0.03
0.69
89.7
0.05
0.54
91.8
0.034
0.86
92.7
0.032
0.51
89.1
0.15
1.31
90.2
0.023
0.71
76.9
0.23
1.98
83.9
0.12
1.02
68.1
1
3.68
87.5
0.13
1.67
63.7
2.3
8.77
79.7
2.76
1.17
27.9
0.45
50.3
80.4
0.97
5.77
CD4
CD8
B
non-selecting
selecting
% of max
CD69
C
selecting
non-selecting
DP
CD8 SP
% of cells
Time (hours)

Figure 4.1. Positive selection kinetics on thymic slices. Pre-selection OTI TCR tg DP cells were overlaid onto thymic slices for 2 hours, rinsed, and harvested at the times indicated for flow cytometric analysis. **A**. Representative flow plots of OT1 tg cells on selecting or non-selecting thymic slices at the times indicated. **B.** Representative histograms of CD69 expression on OT1 tg DP in selecting (red) or non-selecting (blue) slices at the times indicated. Experimental triplicates are shown. **C**. Percentage of DP (top panel) or $CD8^+$ SP cells (bottom panel). Error bars indicate SD of triplicate slices from one representative experiment of at least two.

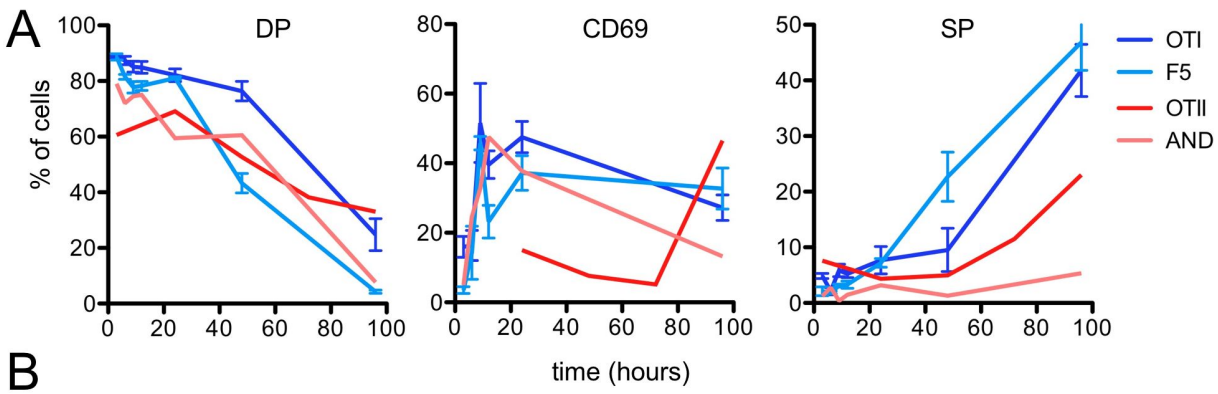
A
DP
CD69
SP
% of cells
time (hours)
OTI
F5
OTII
AND

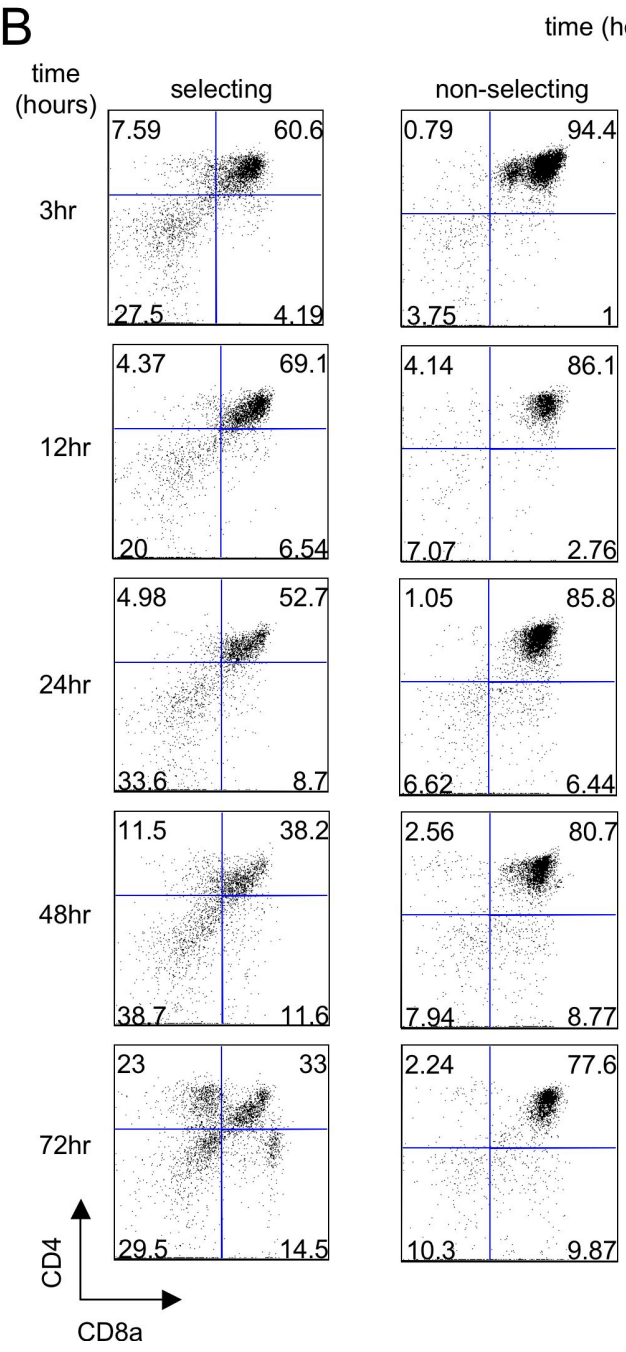
B
time (hours)
selecting
non-selecting
3hr
12hr
24hr
48hr
72hr
7.59
60.6
27.5
4.19
0.79
94.4
3.75
1
4.37
69.1
20
6.54
4.14
86.1
7.07
2.76
4.98
52.7
33.6
8.7
1.05
85.8
6.62
6.44
11.5
38.2
38.7
11.6
2.56
80.7
7.94
8.77
23
33
29.5
14.5
2.24
77.6
10.3
9.87
CD4
CD8a

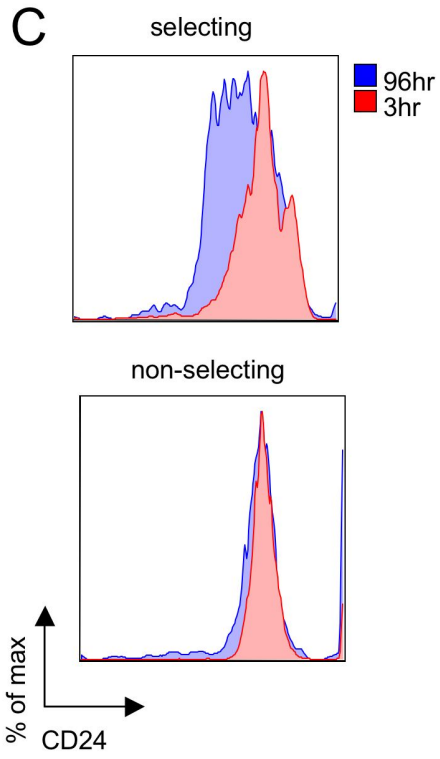
C
selecting
96hr
3hr
non-selecting
% of max
CD24

Figure 4.2. Positive Selection Kinetics of Several TCR Transgenics on Thymic Slices. Pre-selection TCR tg DP cells were overlaid onto thymic slices for 2 hours, rinsed, and harvested at the times indicated for flow cytometric analysis. **A**. Percentage of DP (left), CD69 (middle) or SP cells (right). Error bars indicate SD of triplicate slices from one representative experiment of at least two. AND values are averages of slice replicates. OTI values represent individual slices. **B**. CD4 vs. CD8 representative flow plots of OTII tg cells on selecting (left) or non-selecting (right) thymic slices at the times indicated. **C**. Representative histograms of CD24 expression on OTII tg DP in selecting (top) or non-selecting (bottom) slices at 3 (red) and 96 (blue) hours. Note: Figure 2. Class II Gated on Ly5.1 (in B6) or Vα2+ (in MHC-).

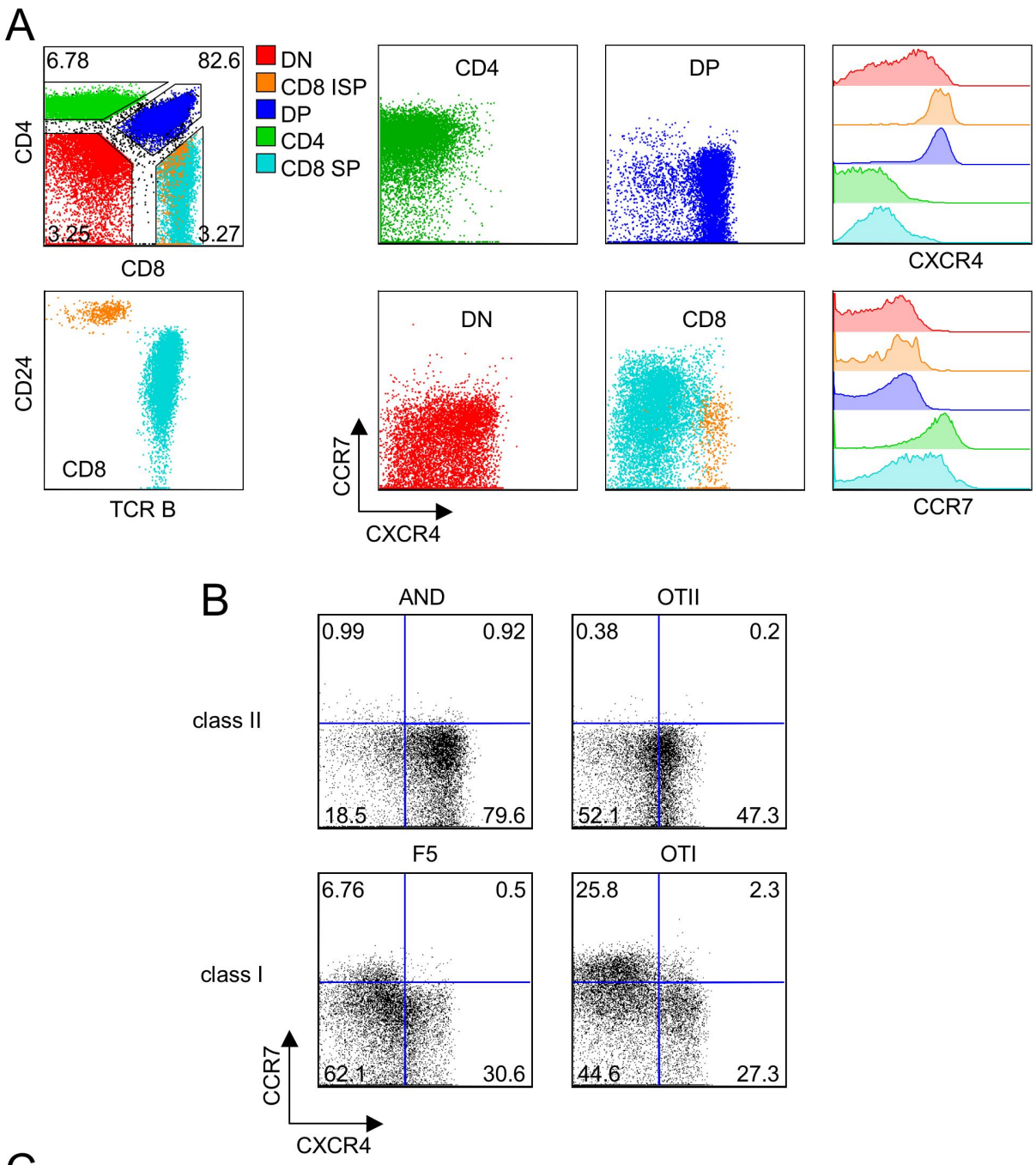
A
6.78
82.6
3.25
3.27
CD4
CD8
DN
CD8 ISP
DP
CD4
CD8 SP
CD4
DP
CXCR4
CD24
CD8
TCR B
DN
CD8
CCR7
CXCR4
CCR7
B
AND
OTII
0.99
0.92
18.5
79.6
0.38
0.2
52.1
47.3
class II
F5
OTI
6.76
0.5
62.1
30.6
25.8
2.3
44.6
27.3
class I
CCR7
CXCR4
C
6.84
38.7
21.8
22.4
CD4
CD8
% of max
CXCR4
% of max
CCR7
DN
CD8 ISP
DP
CD8 SP

Figure 4.3. Chemokine receptor expression on wild type and steady state TCR transgenic thymocytes. **A**. Total wild type thymocytes gated into DN, DP, CD4 SP, and CD8 SP populations (left) stained for CCR7 versus CXCR4 (middle two panels) and the corresponding histogram for expression levels of CXCR4 (top right) or CCR7 (bottom right). **B.** CXCR4 and CCR7 expression in DP thymocytes from steady state class II (top row, AND and OTII) vs. class I (bottom row F5 and OTI) TCR transgenics. **C**. OTI $Rag^{-/-}$ TCR transgenic steady state thymocytes (left) with CXCR4 (middle) and CCR7 (right) expression in DN, DP, CD8 ISP, and CD8 SP populations.

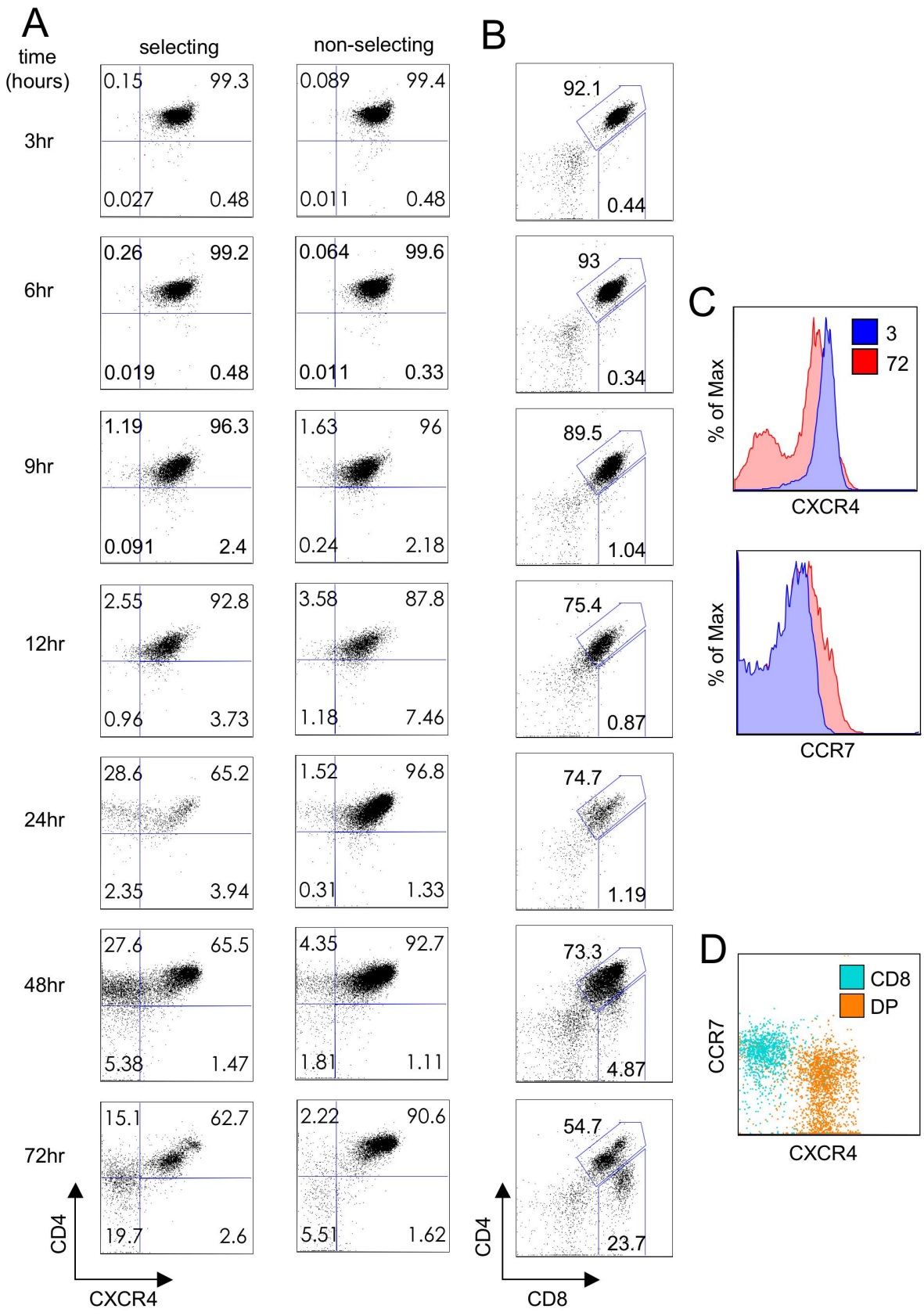
A
time (hours)
selecting
non-selecting
3hr
0.15
99.3
0.027
0.48
0.089
99.4
0.011
0.48
6hr
0.26
99.2
0.019
0.48
0.064
99.6
0.011
0.33
9hr
1.19
96.3
0.091
2.4
1.63
96
0.24
2.18
12hr
2.55
92.8
0.96
3.73
3.58
87.8
1.18
7.46
24hr
28.6
65.2
2.35
3.94
1.52
96.8
0.31
1.33
48hr
27.6
65.5
5.38
1.47
4.35
92.7
1.81
1.11
72hr
15.1
62.7
19.7
2.6
2.22
90.6
5.51
1.62
CD4
CXCR4
B
92.1
0.44
93
0.34
89.5
1.04
75.4
0.87
74.7
1.19
73.3
4.87
54.7
23.7
CD4
CD8
C
% of Max
3
72
CXCR4
% of Max
CCR7
D
CD8
DP
CCR7
CXCR4

Figure 4.4. Chemokine receptor expression kinetics during positive selection on thymic slices. OTI tg pre-selection thymocytes were overlaid onto selecting or non-selecting thymic slices, allowed to migrate in for 2 hour, washed, and dissociated and analyzed by flow cytometry at the time-point indicated. **A**. Representative flow plots of CD4 vs. CXCR4 expression in CD8+ gated OTI tg thymocytes in a positively selecting slice (left) versus non-selecting slice (right) at the time-point indicated. B. Representative CD4 vs. CD8 profiles for total OTI TCR tg thymocytes in a selecting slice at the time-points indicated. Data are representative of two experiments. **B**. Representative CXCR4 (top) and CCR7 (bottom) expression in total OTI TCR tg thymocytes in a positively selecting slice at 3 (blue) vs. 72 hours (red). **C**. Representative flow plot of the contribution of DP (orange) and CD8 SP (blue) to the CCR7 and CXCR4 populations at 72 hours in a positively selecting slice.

A

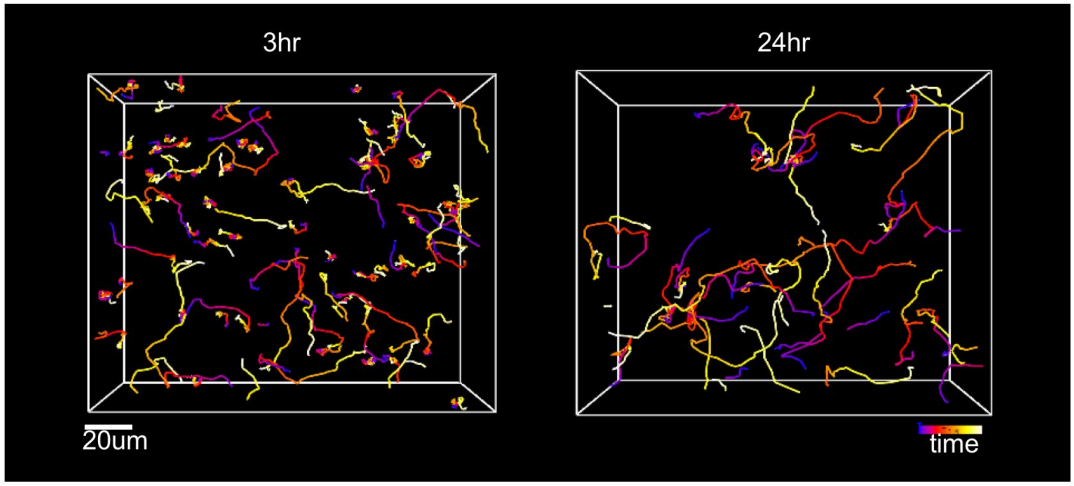
3hr
24hr
20um
time

B

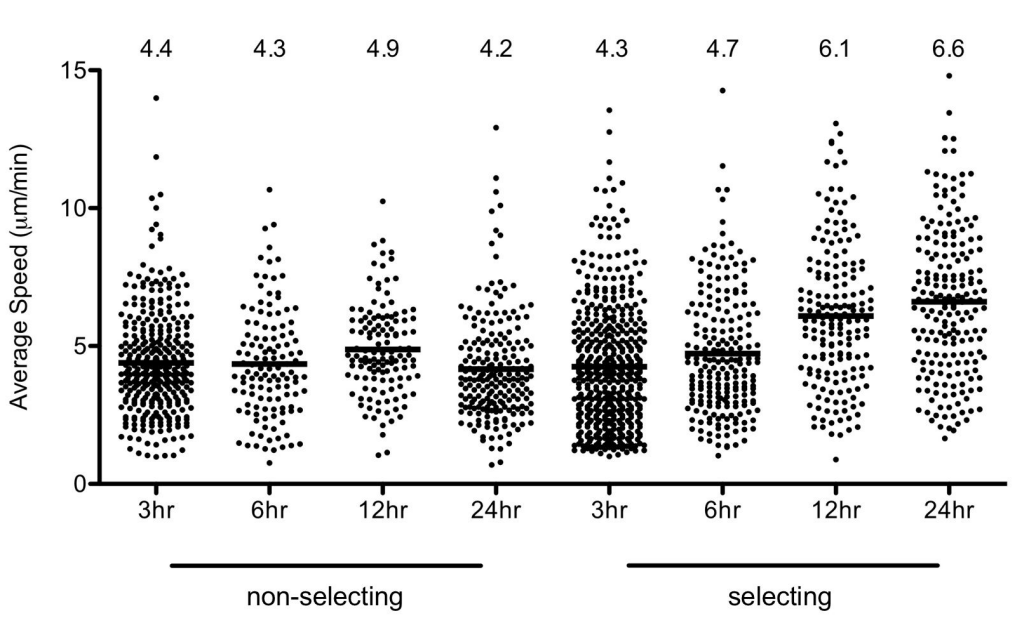
4.4
4.3
4.9
4.2
4.3
4.7
6.1
6.6
15
10
5
0
Average Speed (μm/min)
3hr
6hr
12hr
24hr
3hr
6hr
12hr
24hr
non-selecting
selecting

Figure 4.5. OTI TCR transgenic, pre-selection thymocytes increase their speed and become more directional over time under positive selection conditions. Class I (OTI) restricted TCR transgenic DP cells were applied to selecting thymic slices and allowed to migrate in for 2 hours. Thymic slices were imaged by 2P imaging at the times indicated and the x,y, and z coordinates were tracked using Bitplane's Imaris program. **A**. Individual OTI thymocyte speeds in a positive selecting slice at the times indicated. Bar and number above the plots indicate the average. **B**. Representative cell tracks from a positively selecting slice at 3 (left) versus 24 (right) hours.

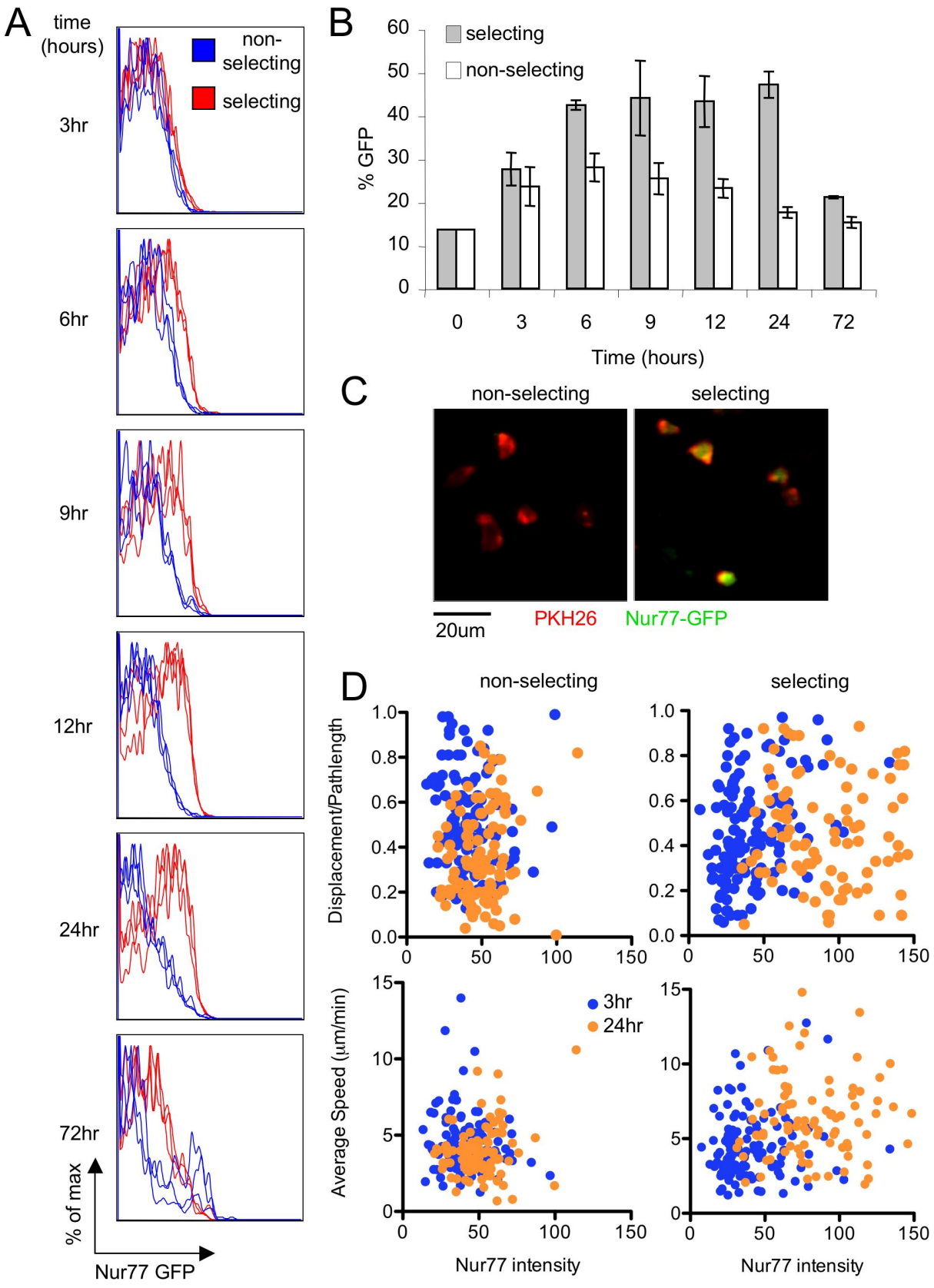
A
time (hours)
non-selecting
selecting
3hr
6hr
9hr
12hr
24hr
72hr
% of max
Nur77 GFP
B
selecting
non-selecting
% GFP
60
50
40
30
20
10
0
0
3
6
9
12
24
72
Time (hours)
C
non-selecting
selecting
20um
PKH26
Nur77-GFP
D
non-selecting
selecting
Displacement/Pathlength
1.0
0.8
0.6
0.4
0.2
0.0
0
50
100
150
Average Speed (µm/min)
15
10
5
0
3hr
24hr
Nur77 intensity
Nur77 intensity

Figure 4.6. OTI TCR transgenic, pre-selection thymocytes accumulate TCR signals over time. Class I (OTI) restricted TCR transgenic Nur77-GFP DP cells were applied to selecting or non-selecting thymic slices and allowed to migrate in for 2 hours. Thymic slices were either dissociated for analysis for flow cytometry or imaged by 2P imaging at the times indicated and cells x,y, and z coordinates were tracked using Bitplane's Imaris program. **A**. Flow cytometric histograms of Nur77 GFP expression at the time-points indicated in selecting (red) and non-selecting (blue) thymic slices. Triplicates are shown. **B.** Percent of GFP+ DP thymocytes at the times indicated. Average from triplicates from one representative experiment are shown. Error bars represent standard deviation. **C.** 2P images at 6 hours from a positive selecting slice (right panel) or non-selecting slice (left panel). PKH26 membrane dye in red and Nur77-GFP in green. **D.** The straightness (displacement/pathlength) versus relative Nur77 GFP intensity for individual thymocytes in a positive (top right) or non-selecting (top left) environment at 3 (blue) and 24 (orange) hours. Each dot represents the average value of a track. Interval speed across 100 seconds of imaging time vs. Nur77 GFP intensity in positive (bottom right) versus non-selecting (bottom left) thymic slices at 3 (blue) and 24 (orange) hours. Each dot represents a 100 second interval.

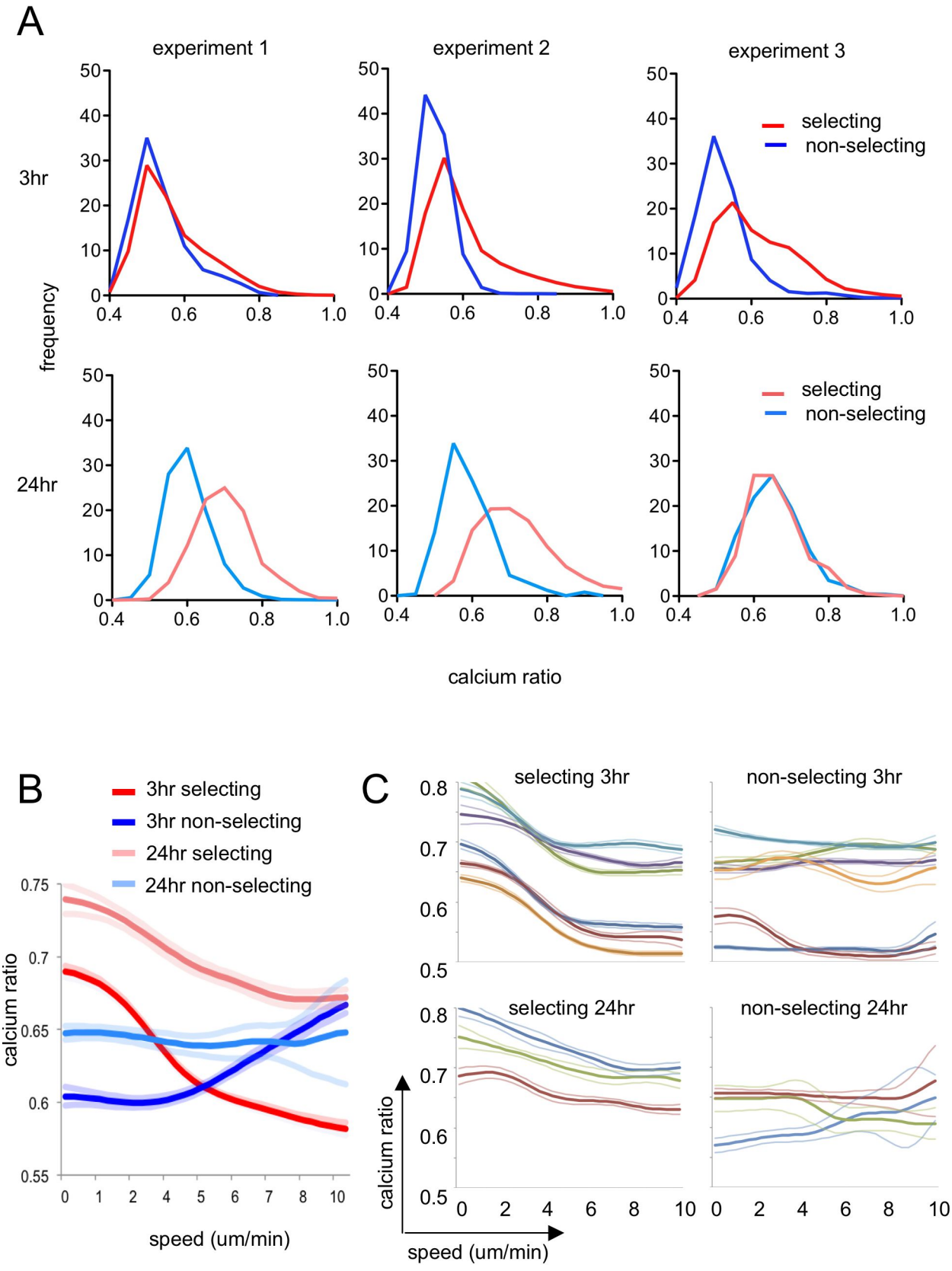
A
experiment 1
experiment 2
experiment 3
3hr
24hr
frequency
selecting
non-selecting
calcium ratio
B
3hr selecting
3hr non-selecting
24hr selecting
24hr non-selecting
calcium ratio
speed (um/min)
C
selecting 3hr
non-selecting 3hr
selecting 24hr
non-selecting 24hr
calcium ratio
speed (um/min)

Figure 4.7. Class I restricted, DP thymocytes increase basal calcium levels under positively selecting conditions. OTI DP thymocytes were loaded with the ratiometric calcium indicator dye, Indo1LR and allowed to migrate into selecting or non-selecting thymic slices for 2 hours and imaged by 2-photon microscopy at the times indicated. **A**. Average thymocyte speeds over a 100 second interval and calcium ratios at 3 (top left) vs. 24 (bottom left) hours in a positively selecting slice as well as 3 (top right) vs. 24 (bottom right) hours in a non-selecting slice. Fainter lines indicate the 95% confidence interval as determined by bootstrap analysis. Individual imaging runs are shown. **B.** Average thymocyte speeds over a 100 second interval and calcium ratios at 3 (dark red) vs. 24 (light red) hours in a positively selecting slice as well as 3 (dark blue) vs. 24 (light blue) hours in a non-selecting slice. Fainter lines indicate the 95% confidence intervals determined through bootstrap analysis. Data pooled from at least three independent imaging runs. **C**. Frequency of calcium ratios at 3 hours (top) versus 24 hours (bottom) in selecting (red) or non-selecting (blue) slices. Three independent experiments are shown.

A

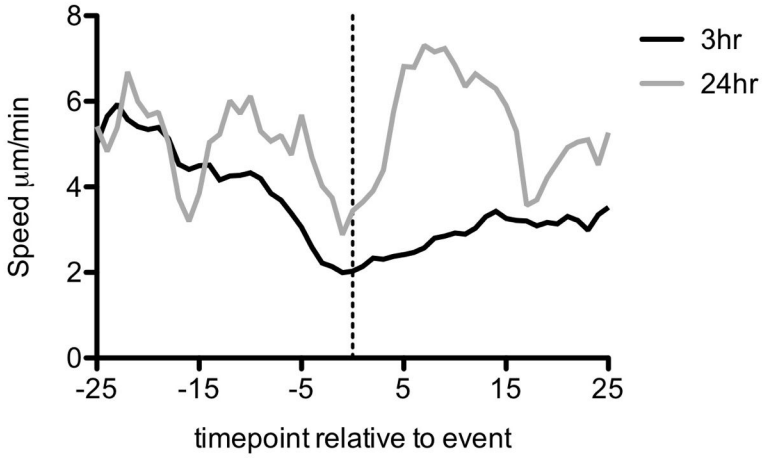
8
6
4
2
0
Speed μm/min
-25
-15
-5
5
15
25
timepoint relative to event
3hr
24hr

B

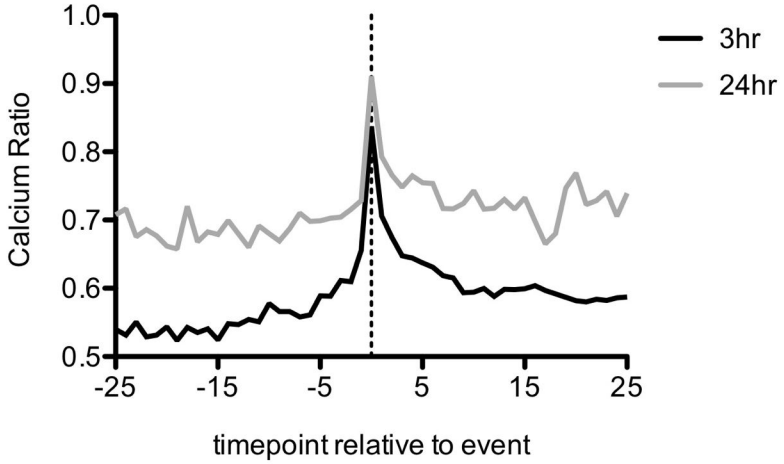
1.0
0.9
0.8
0.7
0.6
0.5
Calcium Ratio
-25
-15
-5
5
15
25
timepoint relative to event
3hr
24hr

Figure 4.8. The change in calcium levels decreases over time and is associated with less pronounced stop signals. Signaling tracks were aligned relative to the first time-point of a signaling event as described (Chapter 2) and plotted for either speed (A) or calcium ratio (B). Data is representative of one imaging experiment.

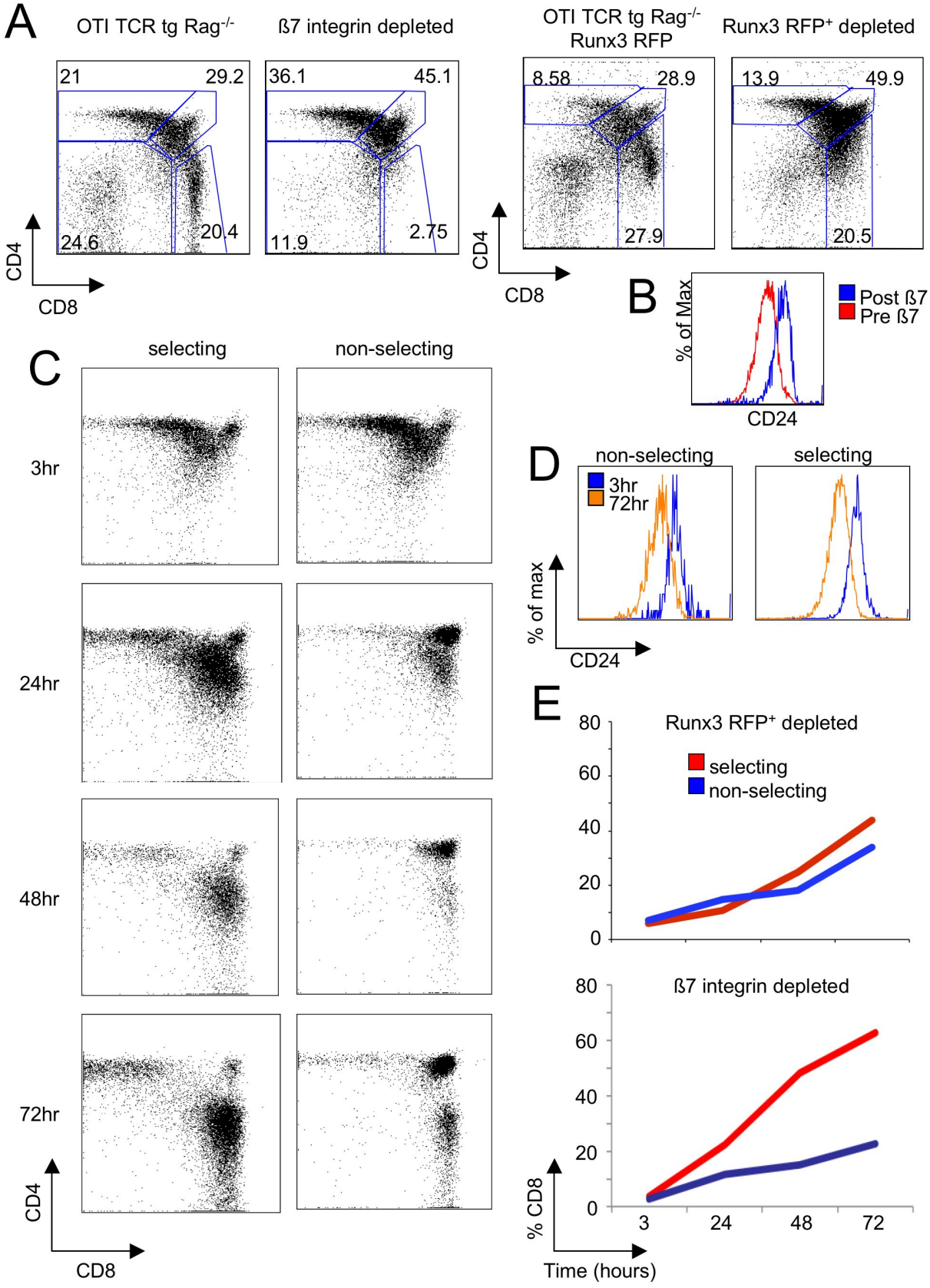
A
OTI TCR tg Rag-/-
ß7 integrin depleted
OTI TCR tg Rag-/-
Runx3 RFP
Runx3 RFP+ depleted
21
29.2
24.6
20.4
36.1
45.1
11.9
2.75
8.58
28.9
27.9
13.9
49.9
20.5
CD4
CD8
B
% of Max
CD24
Post ß7
Pre ß7
C
selecting
non-selecting
3hr
24hr
48hr
72hr
D
non-selecting
selecting
3hr
72hr
% of max
CD24
E
Runx3 RFP+ depleted
selecting
non-selecting
ß7 integrin depleted
% CD8
Time (hours)
0
20
40
60
80
3
24
48
72

Figure 4.9. Selection kinetics of an MHC-experienced, semi-mature thymocyte population. OTI TCR tg Rag-/- total thymocytes were negatively enriched for beta-7 integrin or OTI TCR tg Rag-/- Runx3 RFP total thymocytes were sorted to remove the most mature lineage committed Runx3 RFP+ cells. Either the ß7 integrin depleted or RFP- fractions were overlaid onto selecting or non-selecting thymic slices and then slices were dissociated and analyzed by flow cytometry at the timepoints indicated. **A**. CD4 vs. CD8 profiles of total thymocytes before (left) and after (middle) enrichment to deplete beta 7 integrin with the corresponding CD24 expression for the pre (red) and post (blue) enrichment (right). **B**. Representative CD4 vs. CD8 of beta 7 integrin depleted thymocytes on selecting (left) vs. non-selecting slices (right) at the time-points indicated. **C**. Representative CD4 vs. CD8 of beta 7 integrin depleted thymocytes on selecting (left) vs. non-selecting slices (right) at the time-points indicated. **C**. CD24 expression in the ß7 integrin depleted thymocyte's CD8 population at 3 (blue) vs. 72 (orange) hours in selecting (top) vs. non-selecting (bottom) slices. **D**. Kinetics of CD8 SP development within selecting (red) vs. non-selecting (blue) slices over time for the RFP depleted (top) or ß7 integrin depleted thymocytes (bottom).

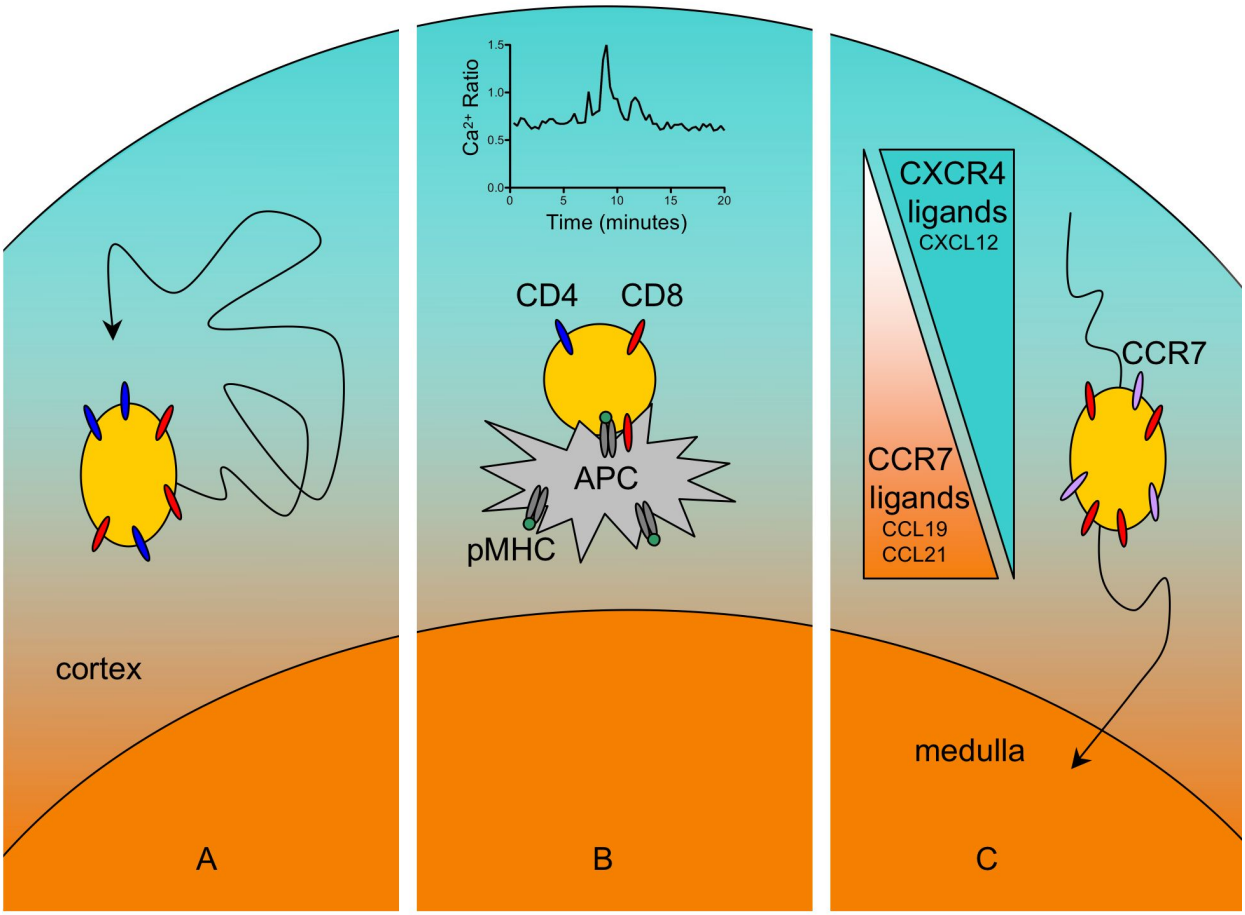
1.5
1.0
0.5
0.0
Ca2+ Ratio
0
5
10
15
20
Time (minutes)
CD4
CD8
APC
pMHC
CXCR4
ligands
CXCL12
CCR7
CCR7
ligands
CCL19
CCL21
CCR7
cortex
medulla
A
B
C

Figure 4.10. Thymocyte motility during positive selection. A. Pre-selection DP thymocytes migrate throughout the cortex via random walk. **B.** Upon encounter with self-MHC (pMHC), thymocytes arrest their migration and undergo transient intracellular calcium elevations. **C.** During selection, thymocytes up-regulate CCR7 and down-regulate CXCR4, leading to their directed migration to the medulla. Of note, a population of DP thymocytes undergoes this chemokine receptor switch, potentially attenuating TCR signaling by limiting thymocyte/APC dwell time.

4.3 Discussion

Most of what we know about the process of positive selection is derived from studies that either removed thymocytes from their native spatiotemporal context of development and/or relied on observation of a mixed population. The product/precursor relationship must be inferred from phenotypic changes, making it difficult to fully understand the dynamics of behavioral and phenotypic changes that occur in thymocytes undergoing positive selection. We have employed a thymic slice model that allowed us to follow the activation, selection, migration, and signaling of a synchronized population of pre-selection thymocytes over time, thereby allowing for a kinetic analysis of the migration and signaling properties that accompany positive selection.

We found that positive selection of thymocytes for class I restricted TCRs in a thymic slice model was robust and CD8 SP appeared as early as three days after recognition of positively selecting ligand and more prominently by four days. Between 2 to 4 hours after thymocyte addition to a positive selecting environment, signaling thymocytes underwent transient serial pausing associated with a temporary elevation in intracellular calcium (3-5 minutes). Over the next 24 hours, thymocytes increased their speed and activation state. In addition, the population started to down-regulate CXCR4 and up-regulate CCR7 during that same time period. This is consistent with our finding of increasing speed and decreasing confinement over a 24-hour period, as thymocytes are likely reading simultaneous localization and migratory cues, one from CXCR4 retaining them in the cortex as is the case for human DP (Halkias), and one for CCR7 directing them to migrate to the medulla (Ueno, Kwan, Campbell) (Figure 4.10). Additionally, chemokine gradients can help to tune TCR signaling in mature T cells. A CCR7 (but not CXCR4) gradient can overcome a TCR induced stop signal and inhibit activation by preventing the formation of an immunological synapse (Bromley). Therefore, by up-regulating CCR7 during positive selection, a thymocyte is likely making itself less sensitive to the TCR induced stop signal.

Given that positive selection takes several days and requires ongoing TCR signaling, it is of interest to compare calcium signaling and motility throughout the process of positive selection. The increase in calcium high time-points experienced in a selecting environment over a non-selecting environment observed at 3 hours was maintained at 24 hours, however, the duration of the migratory arrest as well as the magnitude of the change in calcium levels during transient signaling decreased at 24 hours. Perhaps this reflects an altered responsiveness to a calcium-dependent stop signal or a dynamic tuning of TCR sensitivity. Indeed, in mature T cells, there are both positive and negative feedback mechanisms downstream calcium signaling that are responsible for maintaining the TCR sensitivity. For example, it is known that calcium itself can regulate TCR activation via a positive feedback that sustains CD3 phosphorylation (Shi), which could sensitize a thymocyte to more transient TCR signals. Conversely, calcium flux correlates with the degree of TCR internalization (Mariathasan) reflecting a potential mechanism of dampening the signaling by limiting the number of TCR available at the cell surface. Although the mechanism(s) by which thymocytes are altering signaling over time is unknown, it seems likely that thymocytes are changing either the way they recognize or respond to positively selecting ligand throughout the selection process.

In the future, we would like to confirm the preliminary result of signaling differences over time by comparing an immature (pre-selection) versus MHC-experienced, semi-mature (ß7 integrin depleted) population in a positively selecting slice. Additional reporters of signaling such as the genetically encoded calcium reporters like TNXXL (Heider) would also allow us to confirm the 24 hour data and follow signaling events out beyond 24 hours of development. It will be interesting to test if a thymocyte's sensitivity changes over. Furthermore, although we did not observe a re-localization of NFAT under positive selection conditions for the class I-restricted OTI TCR transgenic (chapter 2), it will be important to look in a class II-restricted model, as class II lineage commitment is though to require a stronger signal. Bhakta et al only describe the early signaling events associated with positive selection in a thymic slice model. Thus, a detailed kinetic analysis of both the phenotypic and behavioral changes associated with class II is still lacking. In our hands, class II development was highly variable compared to class I. Why the generation of class I restricted pre-selection thymocytes was so much more robust than class II is unclear. Thus, it will be important to establish a robust class II selection system to compare how phenotypic changes, migration behavior, and signaling occur for class II restricted TCRs.

Another important future direction will be to test the hypothesis that stronger and/or more prolonged signals promote CD4 over CD8 fate by modulating TCR and/or chemokine signals and determining the impact on selection and/or lineage commitment events. Additionally, through the use of TCR signaling inhibitors, we hope to be able to determine the amount and or duration of TCR signaling required to commit a thymocyte to positive selection. Inhibition or attenuation of the TCR-dependent stop signal through manipulation of adhesion molecules (via ICAM-1 deficient slices or the use of antibodies or small molecule inhibitors to LFA-1 such as CD18 Fab' fragments or levostatin) or chemokines (by inhibitors such as pertussis toxin or by adding exogenous chemokine to alter existing chemokine gradients and/or increase general chemokinesis) could also potentially allow us to uncover their roles in the direction of CD4 versus CD8 lineage commitment.

4.4 Methods

Mice and bone marrow chimeras

All mice were maintained at the American Association of Laboratory Animal Care approved facility in the Life Sciences Addition at the University of California, Berkeley, CA under pathogen-free conditions. All animal procedures were approved by the Animal Care and Use Committee. Non-transgenic C57Bl/6 mice were obtained from Jackson Laboratory, Bay Harbor, Maine. Pre-selection OTI, F5, or OTII Rag-/- TCR tg thymocytes were generated by crossing OTI Rag-/- TCR tg onto a non-selecting background. Specifically, The TCR transgenics were crossed to the MHC-I deficient background (B2M) for OTI and F5 or the MHC-II deficient background for OTIIs (Abb) (Taconic, Germantown, NY). AND pre-selection thymocytes were generated by transferring $1x10^6$ bone marrow cells intravenously to MHC-I and MHC-II deficient lethally irradiated (900 rads) recipients (Abb B2M) (Taconic, Germantown, NY). For enrichment of semi-mature cells, OTI tg Rag-/- were crossed to Runx3-RFP. For the Nur77 GFP imaging studies, $1\text{-}5x10^6$ OTI Nur77 GFP (SOURCE?) bone marrow cells were injected intravenously into MHC-I and MHC-II deficient hosts that were irradiated with two doses of 600rads.

Cell enrichments

MHC-experienced, semi-mature OTI cells were obtained either by negative enrichment with the EasySep Biotin Positive Selection Kit for depletion as directed by the manufacturer (STEMCELL Technoloies, Vancouver, BC, Canada) using anti-beta-7 integrin-biotin antibody (eBioscience, San Diego, CA) or sorting on an influx (BD biosciences, San Jose, CA) to remove the Runx3-RFP^+ population of OTI Rag-/- Runx3-RFP thymocytes.

Thymic Slices

Vibratome-cut thymic slices were generated as described (Appendix 1).

Thymocyte labeling

Indo-1LR (TEFLabs, Austin, TX, USA) labeling was performed as previously described (CHAPTER 2 REF). $4x10^6$ thymocytes were labeled with the membrane dye kit PKH26 1:500 v/v for 5 minutes at 37°C, and washed 3 times with complete DMEM before addition to thymic slices. Sigma-Aldrich, St. Louis, MO).

Flow cytometry

Thymic slices were dissociated to single cell suspensions using tissue grinders then filtered through nylon mesh. The following antibodies were used for flow cytometric analysis: anti-mouse CD4-PerCPefluor710, CD8a-efluor450, CD24-PE, CD69-PECy7, CD69-biotin streptavidin-PE, and Ly5.1-FITC, CCR7-PE-Cy7, CXCR4-APC. Analysis was done using an LSRII (BD biosciences, San Jose, CA) and analyzed using FloJo software (Tree Star, Ashland, OR). Cells were stained at 4ºC for 20 minutes in 24G2 supernatant. Chemokine stains were

performed at 37ºC for 1 hour; cells were then stained for the remaining surfaces markers as usual.

Two-photon imaging

Imaging was performed as described previously for Indo-1LR (Chapter 2). GFP and PKH26 were imaged with the MaiTai laser at wavelength 920nm and separated using 560nm and 650nm dichroic mirrors.

Image analysis

Imaris (Bitplane Scientific Software, Saint Paul, MN, USA) was used to analyze the 2-photon movies to obtain x, y, and z coordinates of cells for migration behavior as well as the ratiometric Indo-1 intensities for calcium analysis. Imaging data was analyzed with MATLAB scripts (Mathworks, Natick, MA, USA) and Excel. Graphing and statistical analysis was performed with GraphPad Prism (La Jolla, CA, USA) or Excel. Bootstrap analysis was performed using MATLAB scripts (Mathworks, Natick, MA, USA) Matlab codes available upon request.

4.5 References

Anderson, G., Partington, K. M., and Jenkinson, E. J. (1998) Differential effects of peptide diversity and stromal cell type in positive and negative selection in the thymus. J. Immunol. 161, 6599–6603.

Bhakta, NR, Oh DY, Lewis RS. 2005 Calcium oscillations regulate thymocyte motility during positive selection in the three-dimensional thymic environment. Nat Immunol. Feb;6(2):143-51. Epub 2005 Jan 16.

Bousso P, Bhakta NR, Lewis RS, Robey E. 2002 Dynamics of thymocyte-stromal cell interactions visualized by two-photon microscopy. Science. Jun 7;296(5574):1876-80.

Bromley SK, Peterson DA, Gunn MD, Dustin ML. 2000 Cutting edge: hierarchy of chemokine receptor and TCR signals regulating T cell migration and proliferation. J Immunol. Jul 1;165(1):15-9.

Campbell, James J, Pan, Junliang, and Butcher, Eugene C. Cutting Edge: Developmental Switches in Chemokine Responses During T Cell Maturation. The Journal of Immunology. 1999 Sept 1 vol 163 no. 5 2353-2357.

Daniels MA, Teixeiro E, Gill J, Hausmann B, Roubaty D, Holmberg K, Werlen G, Holländer GA, Gascoigne NR, Palmer E. Thymic selection threshold defined by compartmentalization of Ras/MAPK signalling. Nature. 2006 Dec 7;444(7120):724-9

Davalos-Misslitz, A. C., Worbs, T., Willenzon, S., Bernhardt, G. & Forster, R. Impaired responsiveness to T-cell receptor stimulation and defective negative selection of thymocytes in CCR7-deficient mice. Blood 110, 4351–4359 (2007).

Ehrlich LI, Oh DY, Weissman IL, Lewis RS. 2009 Differential contribution of chemotaxis and substrate restriction to segregation of immature and mature thymocytes. Immunity. Dec 18;31(6):986-98.

Halkias J, Melichar HJ, Taylor KT, Ross JO, Yen B, Cooper SB, Winoto A, Robey EA 2013 Opposing chemokine gradients control human thymocyte migration in situ. J Clin Invest. Apr 15

Heider B, Nathanson JL, Isacoff EY, Callaway EM, Siegel RM. 2010 Two-photon imaging of calcium in virally transfected striate cortical neurons of behaving monkey. PLoS One. 2010 Nov 4;5(11)

Hogquist KA, Jameson SC, Heath WR, Howard JL, Bevan MJ, Carbone FR. T cell receptor antagonist peptides induce positive selection. Cell. 1994 Jan 14;76(1):17-27.

Holmberg K, Mariathasan S, Ohteki T, Ohashi PS, Gascoigne NR. TCR binding kinetics measured with MHC class I tetramers reveal a positive selecting peptide with relatively high affinity for TCR. J Immunol. 2003 Sep 1;171(5):2427-34.

Hunig,T.,and K.Mitnacht. T cell receptor-mediated selection of functional rat CD8 T cells from defined immature thymocyte precursors in short-term suspension cultures. J. Extx Med. 173:561. 1991.

Itano A, Salmon P, Kioussis D, Tolaini M, Corbella P, Robey E. 1996 The cytoplasmic domain of CD4 promotes the development of CD4 lineage T cells. J Exp Med. Mar 1;183(3):731-41.

Jenkinson, EJ, Anderson G, and Owen, John J. T.Studies on T Cell Maturation on Defined Thymic Stromal Cell Populations *in vitro*. J. Exp.Med. Volume176 September1992 845-853

Kwan J, Killeen N. CCR7 directs the migration of thymocytes into the thymic medulla. J Immunol. 2004 Apr 1;172(7):3999-4007.

Ladi E, Schwickert TA, Chtanova T, Chen Y, Herzmark P, Yin X, Aaron H, Chan SW, Lipp M, Roysam B, Robey EA. Thymocyte-dendritic cell interactions near sources of CCR7 ligands in the thymic cortex. J Immunol. 2008 Nov 15;181(10):7014-23.

Larsson, L., E. Timms, K. Blight, D.E. Restall, P.S.Jat, and A.G. Fisher. Characterisation of murine thymic stromal- cell lines immortalised by temperature sensitive simian virus 40 large T or adenovirus 5 Ela. Dev. Iramunol. 1:279. 1991.

Mariathasan S, Bachmann MF, Bouchard D, Ohteki T, Ohashi PS. Degree of TCR internalization and Ca2+ flux correlates with thymocyte selection. J Immunol. 1998 Dec 1;161(11):6030-7.

Mintern JD, Maurice MM, Ploegh HL, Schott E. Thymic selection and peripheral activation of CD8 T cells by the same class I MHC/peptide complex. J Immunol. 2004 Jan 1;172(1):699-708.

Palacios, K., S. Studer, J. Samardis, and J. Pelkonen. Thymice pithelial cells induce *in vitro* differentiation of PRO-T lymphocyte clones into TCR alpha beta/T3+ and TCR gamma delta T3+ cells. EMBO (Eur. Mol. Biol. Organ.) J. 8:4053. 1989

Schabath, R., Muller, G., Schubel, A., Kremmer, E., Lipp, M., Forster, R. The murine chemokine receptor CXCR4 is tightly regulated during T cell development and activation J. Leukoc. Biol., 66 (1999), pp. 996–1004

Schmitt, T. M. and Zuniga-Pflucker, J. C. (2002) Induction of T cell development from hematopoietic progenitor cells by delta-like-1 *in vitro*. Immunity 17, 749–756.

Scollay R, Godfrey DI. Thymic emigration: conveyor belts or lucky dips? Immunol Today. 1995;16:268-273.

Shi X, Bi Y, Yang W, Guo X, Jiang Y, Wan C, Li L, Bai Y, Guo J, Wang Y, Chen X, Wu B, Sun H, Liu W, Wang J, Xu C. Ca2+ regulates T-cell receptor activation by modulating the charge property of lipids. Nature. 2013 Jan 3;493(7430):111-5.

Suzuki H, Guinter TI, Koyasu S, Singer A. Positive selection of CD4+ T cells by TCR-specific antibodies requires low valency TCR cross-linking: implications for repertoire selection in the thymus. Eur J Immunol. 1998 Oct;28(10):3252-8.

Suzuki G, Nakata Y, Dan Y, Uzawa A, Nakagawa K, Saito T, Mita K, Shirasawa T. Loss of SDF-1 receptor expression during positive selection in the thymus. Int Immunol. 1998 Aug;10(8):1049-56.

Takahama Y, Suzuki H, Katz KS, Grusby MJ, Singer A. Positive selection of CD4+ T cells by TCR ligation without aggregation even in the absence of MHC. Nature. 1994 Sep 1;371(6492):67-70.

Tatsumi, Y., A. Kumanogoh, M. Saitoh, Y. Mizushima, K. Kimura, S. Suzuki, H. Yagi, A. Horiuchi, M. Ogata, T. Hamaoka, and H. Fujiwara. Differentiation of thymocytes from CD3- CD4- CD8 through CD3- CD4- CDS+ into more mature stages induced by a thymic stromal cell clone. Proc. Natl. A_cad.Sci. USA. 87:2750. 1990.

Ueno, T. et al. CCR7 signals are essential for cortex–medulla migration of developing thymocytes. J. Exp. Med. 200, 493–505 (2004).

von Boehmer H. 1990. Developmental biology of T cells in T cell-receptor trans- genic mice. Annu. Rev. Immunol. 8:53 1- 56

Vukmanović S, Stella G, King PD, Dyall R, Hogquist KA, Harty JT, Nikolić-Zugić J, Bevan MJ.A Positively Selecting Thymic Epithelial Cell Line Lacks Costimulatory Activity. J Immunol. 1994 Apr 15;152(8):3814-23.

Witt CM, Raychaudhuri S, Schaefer B, Chakraborty AK, Robey EA. Directed migration of positively selected thymocytes visualized in real time. PLoS Biol. 2005 Jun;3(6):e160. Epub 2005 May 3. Erratum in: PLoS Biol. 2005 Oct;3(10):e373.

Yujiro Tanaka, Owen Williams, Raquel Tarazona, Andreas Wack, Trisha Norton and Dimitris Kioussis. *In vitro* positive selection of αβ TCR transgenic thymocytes by a conditionally immortalized cortical epithelial clone. International Immunology, Vol. 9, No. 3, pp. 381–393 1997.

Appendix 1: Thymic Slices as an *in situ* Model of Positive and Negative Selection

5.1 Introduction

The thymic slice model is a relatively new system that was developed to study the potential use of *ex vivo*-cultured tissue for transplantation to correct thymic dysfunction (Markert). It has since been adapted for the study of T cell development (Bhakta, Ehrlich, Le Borgne, Dzhagalov, Halkias) and importantly, bypasses many potential pitfalls of other current *in vitro* systems. Here we describe the method of preparing, embedding, and vibratome slicing thymic lobes for the study of thymocyte development *in situ*. Ultimately, the ability to manipulate and interchange the developing thymocyte population as well as the stromal source makes the thymic slice system highly versatile and an ideal model for studying the processes of thymocyte development.

Thymocytes develop within the highly organized, complex 3D microenvironment of the thymus, which the current *in vit*ro systems used for studying signaling and selection fail to fully recapitulate. As a result, methods such as antibody crosslinking, peptide-MHC-tetramer stimulation, or stromal cell co-culture do not support efficient positive selection. Until the recent adaptation of the thymic slice system (Bhakta), the only culture systems that fully supported the processes of positive and negative selection were fetal thymic organ cultures (FTOC) or reaggregate thymic organ cultures (RTOC) as developed by Anderson and Jenkinson. Although these systems are useful, they are limiting in several ways. First, the RTOC requires the dissociation and reformation of the stromal network, thereby eliminating the structural integrity of the thymic environment. Second, FTOC precludes the observation of synchronized positive selection events. Even in the FTOC, where the original structural properties of the stromal network are maintained, there is no well-defined medulla (Dooly, Fontenot). Thymic slices allow for a relatively synchronized cohort of purified thymic subsets to be followed throughout development. Because the thymic structure is maintained, the slices do not require hours to reform the stromal network as they do in the RTOC system, thus allowing for the observation of signaling and activation within a few hours after overlay. Additionally, defined thymocyte populations can be labeled with fluorescent dyes to read out calcium, cell death, etc.

We have expanded the slice model to include methods for observing negative selection, further characterization of class I positive selection, and human thymocyte development. This model can be extended to any thymic development event, including alternate lineage fate decisions, beta selection, and agonist selection. Additionally, the thymic slices are ideal for both flow cytometric analysis as well as imaging studies due to the abundance of tissue, at least relative to other culture systems. Here, we outline the processes of generating thymic slices (including thymic harvest, embedding lobes in agarose, and vibratome-sectioning of embedded tissue), overlaying thymocytes, and dissociating slices for flow cytometric analysis of development.

5.2 Materials

1.2.1 Harvesting a mouse thymus for the generation of thymic slices.

1. Mouse (see **Note 1**).
2. 70% ethanol spray
3. Styrofoam board
4. Tissue pins
5. Paper towels
6. 6-cm tissue culture dishes
7. 1X Phosphate-buffered saline
8. Small scissors (Roboz, cat. no. RS-5912)
9. Sharp forceps (Roboz, cat. no. RS-5047)
10. Micro-dissection scissors (Roboz, cat. no. RS-5602)

1.2.2 Embedding and vibratome sectioning a thymic lobe in agarose.

1. A thymus to be embedded (from 1.2.1 or human thymus (see **Note 2**))
2. Low-melting temperature agarose (NuSieve GTG Agarose; Lonza, cat no. 50080)
3. HBSS
4. 500-mL beakers
5. 4% low-melting temperature agarose in HBSS: Add 2 g low-melting-point agarose per 50 mL HBSS in a 200mL Erlenmeyer flask. Microwave on a low setting until the agarose is completely dissolved, about 2 minutes. Cover with foil and move to a 55ºC water bath until needed. The 4% agarose solution can be stored in a 55ºC water bath for a couple of days.
6. Ice
7. 1X Phosphate-buffered saline
8. 6-cm tissue culture dishes
9. Tissue molds (Polysciences, cat. no. 18986-1)
10. Vibratome (1000 Plus Sectioning System)
11. Vibratome blades, 2 (feather blades; Leica Biosystems, cat. no. 39053234)
12. Paper towels
13. Tissue glue (3M Vetbond tissue adhesive, cat. no. 1469SB)
14. 1X Phosphate-buffered saline
15. Spatula, bent

1.2.3 Overlay of thymocytes onto thymic slices.

1. Purified thymocyte population of interest at $1x10^6$ cells/10uL complete RPMI (see **Note 3**).
2. 1X Phosphate-buffered saline
3. Complete RPMI
4. Thymic slices (from 1.2.2)
5. 6-well plates
6. 0.4-µm pore-size organotypic cell culture inserts (BD Biosciences, cat. no. 353090)
7. 200- and 20-µl pipet tips 200- and 20-µl pipets
8. 37ºC incubator
9. Spatula, bent

10. 6-cm tissue culture dishes

1.2.4 Dissociation of Thymic Slices for Flow Cytometric Analysis

1. Thymic slices (as generated in 1.2.3)
2. Eppendorf tubes (2 / slice)
3. 1X Phosphate-buffered saline
4. Tissue grinders
5. Nylon mesh filter
6. 200-µL pipet tips 200-µL pipets
7. 96-well plate

5.3 Methods

1.3.1 Harvesting a mouse thymus for the generation of thymic slices.

1. Euthanize the mouse by your institution's approved method.
2. Soak the mouse with 70% ethanol.
3. Using tissue pins, fix the mouse to a tissue paper-covered Styrofoam board.
4. Expose the thymus. To do this, grasp the skin below the sternum, making a small cut parallel to the bottom of the ribcage. Then make one long cut up to the throat and two smaller cuts down the legs. Peel back the skin to expose the ribcage. Grasp the sternum with the forceps and cut along the bottom of the diaphragm. Cut through the ribs up toward the head on both sides and flip up the now-cut ribcage toward the head of the mouse and secure it with a pin.
5. Using the sharp forceps, carefully separate the thymus from the connecting tissue above. Then grasp the aorta below the thymus and above the heart with the blunt forceps and using the micro-dissection scissors, cut through the attachments below and behind the thymus, cutting the aorta above the heat last. It is important not to grasp the thymic tissue itself as tears compromise the tissue and therefore, the thymic slice quality
6. Place the thymus into a 6-cm dish full of PBS.
7. Place the thymus on a paper towel wet with PBS. Using the blunt and sharp forceps, separate the lobes and remove any remaining connective tissue. Again, it is important not to grasp the thymus itself.
8. Put the individual lobes back into the 6-cm dish while you prepare to embed them.

1.3.2 Embedding and vibratome slicing a thymic lobe in agarose.

1. Make an ice water bath: fill a 500mL beaker with ice and add water until the ice barely begins to float.
2. Fill a tissue mold halfway with 4% agarose solution and wait about 30 seconds to allow the agarose to cool and solidify slightly.
3. Grasp the thymic lobe (as isolated in 1.3.1) by any remaining connective tissue and blot it on a dry paper towel to remove excess liquid. (see **Note 4**).
4. Carefully insert the lobe into the agarose using the blunt forceps either vertically to maximize slice number or horizontally to maximize slice area (figure 5.1 A). (see **Note 5** and **Note 6**).
5. Place the mold in the ice-water bath until the agarose is set (~5 minutes, agarose will be opaque and firm to the touch) (figure 5.1A) (see **Note 7**).
6. While the agarose solidifies, set up the vibratome by inserting a vibratome blade. The following settings should be used for sectioning thymic tissue: cutting angle 5º, maximum amplitude, minimum speed.
7. To release the agarose embedded tissue, press on the center of the inverted mold.
8. Using a sharp blade (see **Note 8**), trim the agarose block. Make sure to leave about 0.5cm of excess agarose below the thymic lobe as the vibratome can only cut to 0.5cm above the stage (figure 5.1B).
9. Place the trimmed agarose-embedded tissue into a 6-cm dish filled with PBS for transport to the vibratome.
10. Dry the agarose embedded tissue block on a paper towel.
11. Using a pipet tip, apply a small amount of tissue glue to the vibratome stage, directly in

front of the blade and place the agarose embedded lobe on top (figure 5.2C). (see **Note 9**).
12. Align the vibratome blade with the top of the tissue (figure 5.2 C).
13. Add about 50mLs PBS to fill the vibratome stage and submerge the agarose blocks and blade (figure 5.2D).
14. Section thymus at the desired thickness (see **Note 10**).
15. Retract the blade 200µm after each slice to prevent dragging along the surface of the tissue.
16. Transfer slices after each cut using a bent spatula (figure 5.2 D).

1.3.3 Overlay of thymocytes onto thymic slices

1. Set up the tissue culture plates by adding 1-2mLs complete RPMI to each well of a 6-well plate and then adding a cell culture insert (see **Note 11**).
2. Transfer sections generated in 3.2 to the cell culture plates by using a pipet tip to gently slide the slice off the spatula and onto the cell culture insert.
3. Remove all excess liquid on the top of the insert (any accumulated PBS and/or medium), surrounding the thymic slices by pipetting (see **Note 12**).
4. Pipet 10µL of thymocytes of interest on top of each slice. (We generally add $1x10^6$ cells/slice).
5. Incubate slices at 37ºC for 2 hours.
6. Rinse the slices with 1mL/well PBS to wash off any cells that have not yet migrated in.
7. Continue to incubate slices at 37ºC for the desired length of time (see **Note 13**). Thymic slices have good viability over a 24-hour period, but there is a significant decline thereafter (Figure 5.2).

1.3.4 Dissociation of Thymic Slices for Flow Cytometric Analysis

1. Add 150µL of PBS to an eppendorf tube (1 tube/sample).
2. Add 1mL of PBS to tissue culture insert containing the thymic slice.
3. Transfer thymic slice to eppendorf tube using the bent spatula (see **Note 14**).
4. Dissociate slice using tissue grinder.
5. Add another 150µL PBS.
6. Filter the 300µL volume of cells through a mesh filter into a new eppendorf tube.
7. Transfer the filtered cells into a 96-well plate for staining.

5.4 Notes

1. Plan on obtaining about 10-12 slices from a vertically embedded lobe of a 1-2 month old wild type or MHC-deficient mouse.
2. Part of a lobe of a human thymus can be embedded the same way a mouse thymus is, however, extra cake must be taken to remove the connective tissue, as it tends to cause the thymus to be either crushed or pulled from the agarose block during vibratome slicing.
3. Use thymocytes that are either congenic or fluorescently labeled (genetic such as ubiquitin GFP or vital dye such as CFSE or SNARF) to distinguish endogenous thymocytes from the overlaid population and/or visualize thymocytes during imaging.) Additionally, other cell populations can be added to thymic slices, such as BMDCs, which will migrate in well (figure 5.3).
4. If there is excess liquid surrounding the thymus, the lobe has a greater tendency to be pulled out of the agarose block during sectioning.
5. Up to three individual lobes can be embedded into one block simultaneously if they are inserted vertically although this makes trimming the blocks a bit more challenging later. Two lobes can be easily trimmed, however.
6. Ensuring that the lobe touches the bottom of the mold when you insert it generally means that you have at least an extra 0.5cm of agarose below your tissue, which you will want for sectioning later.
7. There is about a 30 second window once you place the mold into the top of the water bath where you can adjust the lobes. Use the blunt forceps to move the thymus into the positioning you desire.
8. Reuse vibratome blades from the previous sectioning.
9. We have had success with sectioning up to three embedded tissue blocks simultaneously. Ensure that they are roughly equivalent in height for best results.
10. We typically use 400μm thick slices for tissue culture and 500μm thick slices for imaging.
11. We typically place three slices per insert, which is convenient for the analysis of triplicate samples.
12. If the slices are not well dried, the overlaid cells tend to spill off. Additionally, if there are any tears or chunks of agarose missing from the tissue slice, overlaid thymocytes tend to spill off. Drying the slices well allows you to visually inspect the slice quality best. It is a good idea to cut extra slices and replace any as needed.
13. We typically harvest a time-point at 3 hours to establish a baseline of the cells that migrated into the slices. To observe thymocytes selection, kinetic studies must be performed for the TCR transgenic of interest but we have typically used 24 hours as a readout of negative selection and 72 hours as a readout for positive selection. After 96 hours, the quality of the thymic slices significantly deteriorates. We have successfully cultured slices out to 96 hours. Human slices have been cultured for weeks.
14. Over time, thymocytes leak out of the slices due to the absence of a fully enclosed capsule. We have noted slight differences in the populations of thymocytes within or leaking out over time, and thus, it is a good idea to collect both during long-term culture of slices.

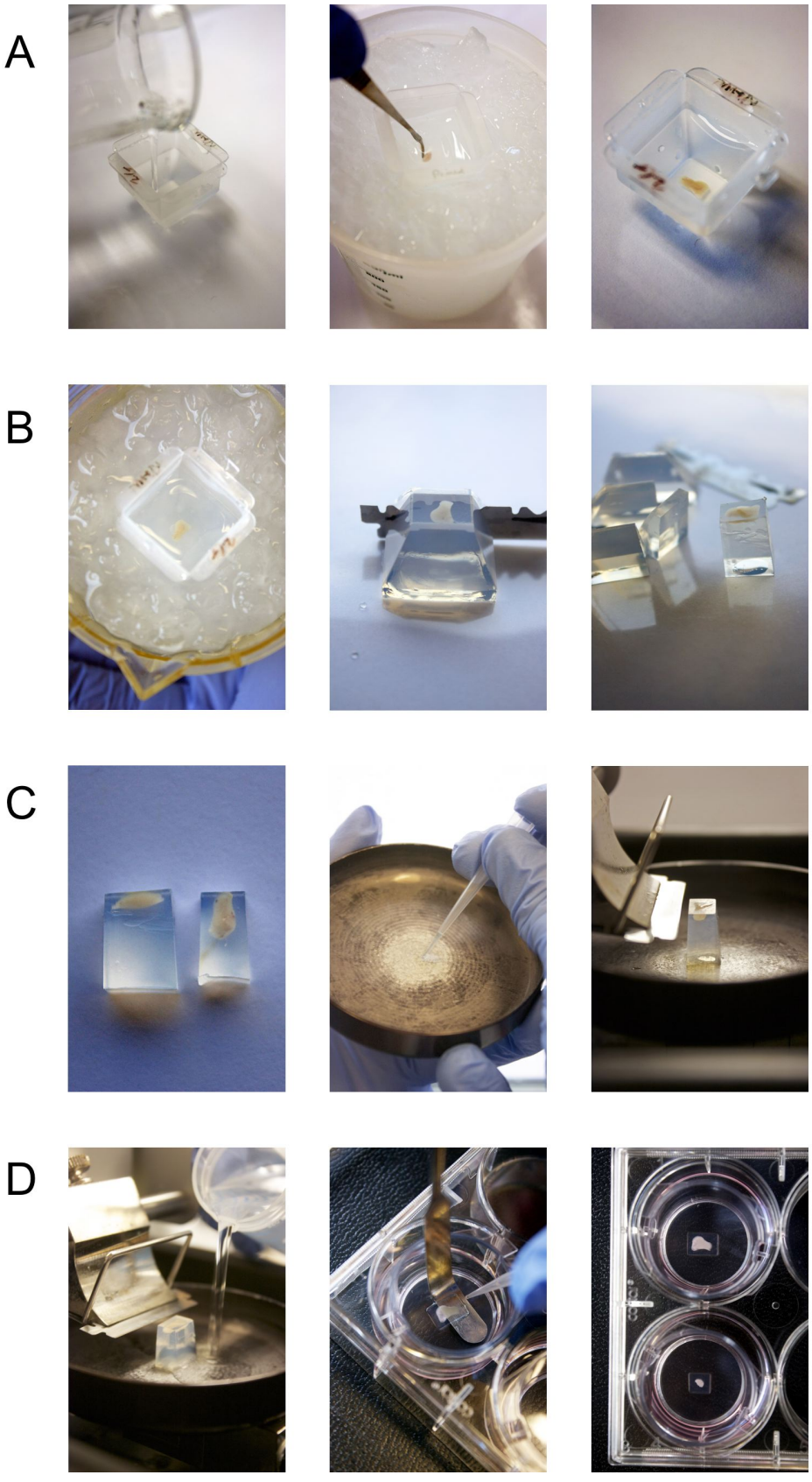
A
B
C
D

Figure 5.1 Preparation of thymic slices. A. Tissue molds are filled halfway up with agarose (left) and a lobe is inserted using forceps (center) at the bottom of the well (right). **B**. The agarose is allowed to set in an ice water bath (left) and the embedded tissue block is gently removed by pressing it out of the mold. Trimming of the agarose embedded lobe to remove excess agarose (left and center). **C**. Example of horizontal versus vertical embedding (left). Attaching the embedded block is achieved by applying tissue glue to the vibratome stage (center) and setting the block on top of the glue, in front of the vibratome blade (right). **D**. The stage is then filled with PBS in preparation for slicing and as thymic slices are generated, they are caught using a bent spatula. Thymic slices are transferred to cell culture inserts using a bent spatula (center). At right is shown thymic slices on cell culture inserts that have been cut from a horizontally embedded lobe (top well) versus vertically embedded lobe (bottom well).

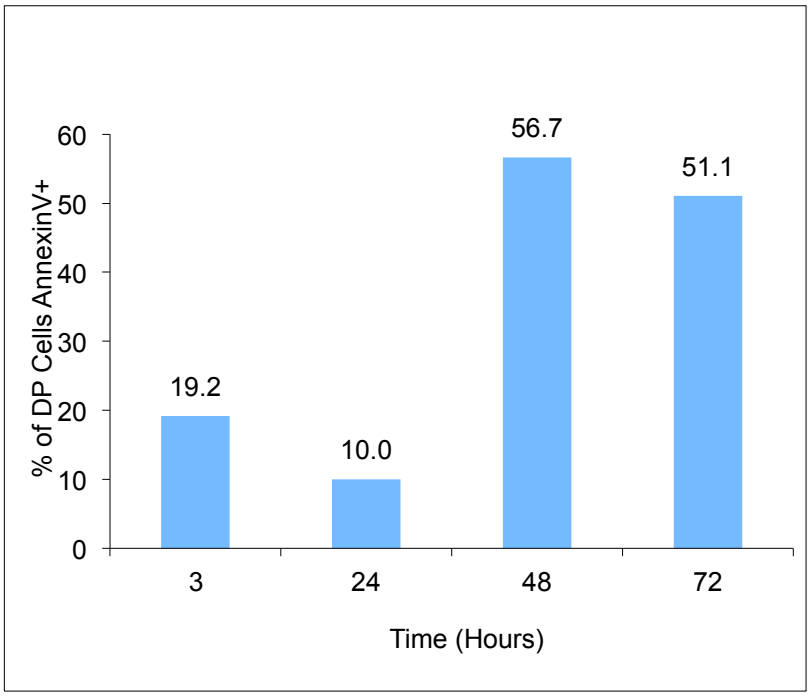

Figure 5.2 Thymic slice viability decreases over time. Thymic slices were dissociated at the time-points indicated and stained with Annexin V to determine viability over time. Viability is maintained over 24 hours but declines thereafter.

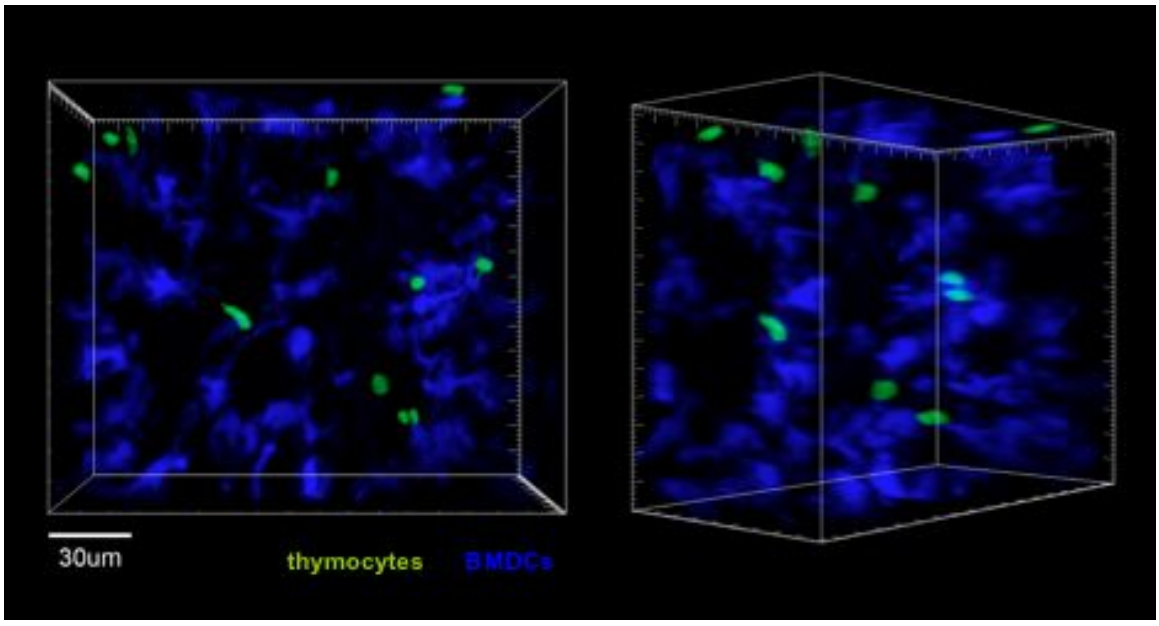

Figure 5.3 BMDCs migrate into cut thymic slices. GFP thymocytes (green) were overlaid onto thymic slices for 2 hours, excess thymocyte that had not migrated in were rinsed off and then CFP BMDCs (blue) were overlaid onto the same slices for an additional 2 hours. The slices were then rinsed and imaged by two-photon microscopy. The image on the left is looking down through z. The same imaging volume rotated at right to demonstrate that the BMDCs have become evenly distributed within the tissue.

5.5 References

1. Anderson, G., Partington, K. M., and Jenkinson, E. J. (1998) Differential effects of peptide diversity and stromal cell type in positive and negative selection in the thymus. J. Immunol. 161, 6599–6603.

2. Bhakta NR, Oh DY, Lewis RS. (2005) Calcium oscillations regulate thymocyte motility during positive selection in the three-dimensional thymic environment. Nat Immunol. Feb;6(2):143-51.

3. Dooley J, Erickson M, Farr AG. (2005) An Organized Medullary Epithelial Structure in the Normal Thymus Expresses Molecules of Respiratory Epithelium and Resembles the Epithelial Thymic Rudiment of Nude Mice. J Immunol. Oct 1;175(7):4331-7.

4. Ehrlich LI, Oh DY, Weissman IL, Lewis RS. (2009) Differential contribution of chemotaxis and substrate restriction to segregation of immature and mature thymocytes. Immunity. Dec 18;31(6):986-98.

5. Fontenot JD, Dooley JL, Farr AG, Rudensky AY (2005) Developmental regulation of Foxp3 expression during ontogeny J. Exp. Med. J Exp Med. Oct 3;202(7):901-6.

6. Jenkinson, EJ, Anderson G, and Owen, John J. T. (1992) Studies on T Cell Maturation on Defined Thymic Stromal Cell Populations *In Vitro*. J. Exp.Med. Volume176 September 845-853.

7. Le Borgne M, Ladi E, Dzhagalov I, Herzmark P, Liao YF, Chakraborty AK, Robey EA. (2009) The impact of negative selection on thymocyte migration in the medulla. Nat Immunol. 2009 Aug;10(8):823-30.

8. Markert ML, Watson TJ, Kaplan I, Hale LP, Haynes BF. The human thymic microenvironment during organ culture. Clin Immunol Immunopathol. 1997 Jan;82(1):26-36.